12-2010

Use of a Press-Fit Grip Sleeve for Cable-In-Conduit Superconductor Integration: Effects of Tensile and Fatigue Loading

Paul Michael Hayes
University of Tennessee - Knoxville, phayes4@utk.edu

To the Graduate Council:

I am submitting herewith a thesis written by Paul Michael Hayes entitled "Use of a Press-Fit Grip Sleeve for Cable-In-Conduit Superconductor Integration: Effects of Tensile and Fatigue Loading." I have examined the final electronic copy of this thesis for form and content and recommend that it be accepted in partial fulfillment of the requirements for the degree of Master of Science, with a major in Mechanical Engineering.

Madhu S. Madhukar, Major Professor

We have read this thesis and recommend its acceptance:

Don W. Dareing, John D. Landes

Accepted for the Council:
Carolyn R. Hodges

Vice Provost and Dean of the Graduate School

(Original signatures are on file with official student records.)

To the Graduate Council:

I am submitting herewith a thesis written by Paul Michael Hayes entitled "Use of a Press-Fit Grip Sleeve for Cable-In-Conduit Superconductor Integration: Effects of Tensile and Fatigue Loading." I have examined the final electronic copy of this thesis for form and content and recommend that it be accepted in partial fulfillment of the requirements for the degree of Master of Science, with a major in Mechanical Engineering.

Madhu S. Madhukar, Major Professor

We have read this thesis
and recommend its acceptance:

Don W. Dareing

John D. Landes

Accepted for the Council:

Carolyn R. Hodges
Vice Provost and Dean of the Graduate School

(Original signatures are on file with official student records.)

Use of a Press-Fit Grip Sleeve for Cable-In-Conduit Superconductor Integration: Effects of Tensile and Fatigue Loading

A Thesis Presented for the
Master of Science Degree
The University of Tennessee, Knoxville

Paul Michael Hayes
December 2010

ABSTRACT

Presently, one of the most promising sources for a future of abundant, low-emission, and efficient energy comes in the form of nuclear fusion. However, in order for it to become a reality, fusion technology must overcome the obstacle of plasma confinement. Utilizing the tokomak based design for magnetic plasma confinement; ITER is currently developing a fusion reactor to prove its commercial viability.

The purpose of this research was to determine the feasibility of pulling superconducting cable with a press-fit grip sleeve that utilizes friction to generate a gripping force. Such a design is being considered by ITER to integrate (join) 800 m long sections of superconducting cable and conduit for use in toroidal field plasma confinement coil construction. In order to see if friction alone had the potential to withstand the required pulling load, eight grip sleeve samples were subjected to monotonic tensile loading until failure (sleeve slippage) occurred. It was also important that the grip could withstand the variable loading that will likely occur during the pulling process due to friction between the cable and conduit. Therefore, a period of cyclic loading, prior to tensile loading, was incorporated into the testing regimen. Based on the results of each experiment, additional modifications were made until the sleeve's gripping strength exceeded that of the weld joint used in the design, meaning the physical limitations of the grip sleeve had been reached. Once the design was optimized, additional samples were tested under identical conditions to establish repeatability. In addition, Finite Element Analysis was used to obtain better insight into the deformation behavior of the cable.

Based on the findings of this research, it was determined that a 300 mm long press-fit sleeve with a 25.4 mm long reinforcement grip ring is capable of supporting a 116 kN (26,000 lbf) to 126.5 kN (28,500 lbf) tensile load, with little to no adverse effects from fatigue testing. Since this value exceeds the 8,000 lbf load used by a Russian team to perform this same task, it can be concluded that the press-fit grip design is capable of performing the required cable pull with a generous safety factor.

TABLE OF CONTENTS

Chapter **Page**

1. Introduction....1
1.1. Energy Crisis....1
1.2. Nuclear Power....2
1.2.1. ITER....3
1.3. Magnetic Confinement of Plasma....4
1.4. Construction of Toroidal Field Magnetic Coils....6
1.4.1. Why an 800 meter Cable Pull?....9
1.5. Modeling Toroidal Field Conductor as Wire Rope....10
1.6. Methods of Cable Termination....12
1.6.1. Cable Pull Requirements....21

2. Review of Literature....23
2.1. Overview....23
2.2. Mechanics of Wire Rope....23
2.2.1. Wire and Strand Lay Variations....24
2.2.1. End Supports of Twisted Rope and Torque....27
2.2.2. Influence of Wire and Strand Lay on Torque....28
2.2.3. Torque Balanced Rope....29
2.3. Press Fit Analysis....30
2.3.1. Stick Slip Condition....31
2.4. Related Studies....31

3. Methodology....33
3.1. Overview....33
3.2. Experimental Testing....33
3.2.1. Test Sample Materials....34
3.2.2. Types of Test samples....35
3.2.3. Sample Construction and Preparation....36
3.2.4. Method of Attachment to Test Fixture....43
3.2.5. Testing Descriptions....44
3.3. Finite Element Analysis....45
3.3.1. Geometric Modifications....46
3.3.2. Solver Settings....50

4. Results and Discussion....52
4.1. Experimental Test Results....52
4.1.1. Preliminary Tests....52
4.1.2. Full Scale Testing....63
4.1.3. Modified Grip Design....85
4.1.4. Fatigue Testing....100
4.2. Finite Element Analysis Results....120

4.3. Welding Metallurgy Results....120

5. Conclusions and Recommendations....122
5.1. Conclusions....122
5.2. Recommendations....123

References....124

Appendix....130

LIST OF FIGURES

Figure **Page**

1.1 Conceptual cutaway view of the ITER tokomak....4
1.2 Schematic of the current and magnetic fields within a tokomak....5
1.3 Rendering of the ITER tokomak highlighting the key components of the magnet system....6
1.4 Rendering of Toroidal Field Coil design....7
1.5 Assembled cable-in-conduit conductor....8
1.6 Cross section of TF coil to show the layering strategy of the cable windings....8
1.7 Illustration of problem statement....9
1.8 Proposed TF cable-in-conduit integration site at airport in Florida....10
1.9 Schematic illustrating wire rope construction....11
1.10 Schematic illustrating superconducting cable construction....11
1.11 Loop termination with ferrule....13
1.12 Eye splice rope termination....13
1.13 Loop termination with wire rope clips....14
1.14 Schematic of wedge socket termination....15
1.15 Installation of Lace-up grip....16
1.16 Rendering of various spelter socket designs....16
1.17 Stages of assembly of dry spelter socket termination....17
1.18 Rendering of non-swage fitting....18
1.19 Stages of assembly of non-swage end fitting....19
1.20 Grip sleeve and cable prior to swaging....20
1.21 Grip sleeve and cable after swaging....20
1.22 Rendering of loop socket auxiliary coupling....21
1.23 Rendering of tensile Lug auxiliary coupling....21

2.1. Wire rope featuring Left hand Lay strand orientation....24
2.2. Wire rope featuring Right hand lay strand orientation....24
2.3. Comparison of the most common wire and strand lay combinations....25

2.4. Illustration of strand length measurement of a wire rope.....25
2.5. Forces acting on straight lay rope under tensile load.....26
2.6. Force decomposition of straight laid wire rope.....26
2.7. Forces acting on helically laid rope under tensile load.....27
2.8. Force decomposition of helically laid wire rope.....27
2.9. Cross-section of Single Layer Rope.....29
2.10. Cross-section of Two Layer Rope.....29
2.11. Schematic of rope layer cross sections to illustrate torque balancing……...30
2.12. Schematic of a press fit grip illustrating interference and contact pressure.....31

3.1 Cross-section of conductor showing its 6 strand single layer construction.....34
3.2 Side view of conductor showing its right laid Lang lay wire orientation.....34
3.3 Rendering of full scale TF sample configuration.....36
3.4 Proposed grip sleeve design with tensile lug.....37
3.5 Actual pre-crimped grip sleeve with tensile lug.....37
3.6 Pre-crimped grip sleeve compared to nominal cable diameter.....38
3.7 Hose clamps positioned around cut to prevent unwinding.....38
3.8 Insertion of solid rod into core tube of TF cable.....39
3.9 Grip sleeve positioned on TF cable prior to compaction.....39
3.10 Val Power material crimping machine used during test sample fabrication.....40
3.11 Initial stages of TF grip sleeve compaction.....40
3.12 Jaws of crimping machine fully compressed around grip sleeve.....41
3.13 Grip sleeve exiting from crimping machine.....41
3.14 Fully assembled full scale TF pull test sample.....42
3.15 Work hardened region on pre-crimped sleeve.....43
3.16 Bottom view of threaded tensile lug.....44
3.17 Side view of threaded tensile lug.....44
3.18 Contact area of circular strands with circular grip sleeve.....47
3.19 Contact area of octagonal strands with dodecagon grip sleeve.....47
3.20 Displacement of square sleeve and strands subjected to tensile loading.....48
3.21 Displacement of octagonal sleeve and strands subjected to tensile loading.....48

3.22 Cross-section of FEA model showing single layer 6 strand construction with octagonal strands and dodecagonal core and sleeve.....49
3.23 FEA model without grip sleeve to show combination of coiled and straight strand geometry.....50
4.1 Equipment Setup for Preliminary Pull Tests.....52
4.2a TF – WC1 Schematic.....53
4.2b TF – WC1 cross-section.....53
4.3a TF-WOC1 Schematic.....54
4.3b TF-WOC1 Cross section.....54
4.4 Threaded stud connected to tensile lug.....55
4.5 Extensometer set-up used in preliminary testing.....55
4.6 Axial Force vs. Displacement for TF-WOC1 and TF-WC1.....56
4.7 Axial Force vs. Time for TF-WOC1 and TF-WC1.....57
4.8 TF-WC1 grip sleeve position before testing.....58
4.9 TF-WC1 grip sleeve position after testing.....58
4.10 TF-WOC1 grip sleeve position before testing.....59
4.11 TF-WOC1 grip sleeve position after testing.....59
4.12 Axial Strain for TF-WC1 and TF-WOC1 measured by extensometer.....60
4.13 TF – WOC1 Copper Cable Exposure from grip sleeve slippage.....61
4.14 TF-WC1 Copper Cable Exposure from grip sleeve slippage.....61
4.15 Indentions of cable strands on grip sleeve due to contact pressure.....62
4.16 Base component of static coupling attached to hydraulic actuator.....64
4.17 All-thread rod to mate test sample and fixture.....64
4.18 Fully assembled static coupling mounted to hydraulic actuator.....65
4.19 Main anchor component for upper dynamic coupling.....66
4.20 Hemispherical nut for upper sample support.....66
4.21 Unthreaded attachment rod to join sample and test fixture.....67
4.22 Assembled upper sample attachment rod.....67
4.23 Assembled dynamic coupling to illustrate attachment rod clearance.....68
4.24 Fully assembled dynamic coupling installed on cross head.....68
4.25 Contrasting colored band to indicate sleeve slippage.....69

4.26 Dynamic coupling connected to upper tensile lug....70
4.27 Test specimen mounted to fixture's cross head....70
4.28 All-thread rod installed in lower tensile lug....71
4.29 All-thread rod contacting lower coupling....72
4.30 Test specimen mounted to fixture's hydraulic actuator....72
4.31 TF-WC2-FS mounted to Interlaken testing machine....73
4.32 Vertical markings to monitor displacement due to rotation....74
4.33 Schematic of TF-WOC1 specimen....75
4.34 Schematic of TF-WC2-FS specimen....75
4.35 Comparison of axial force vs. time for TF-WOC1 and TF-WC2-FS....76
4.36 Comparison of axial force vs. displacement for TF-WOC1 and TF-WC2-FS....76
4.37 Indention of cable strands on inner surface of TF-WOC1 grip sleeve without the protective foil – This sample did have sub-cable foil on it....78
4.38 Conductor cable showing sub-cable foil wrap....79
4.39 Indention of cable strands on inner surface of TF-WC2 grip sleeve with the protective foil – This sample also had sub-cable foil on it....79
4.40 Dimensions of TF-WC2-FS upper grip sleeve before pull test....80
4.41 Dimensions of TF-WC2-FS upper grip sleeve after pull test....80
4.42 Dimensions of TF-WC2-FS lower grip sleeve before pull test....80
4.43 Dimensions of TF-WC2-FS lower grip sleeve after pull test....80
4.44 First occurrence of stick-slip mechanism for TF-WC2-FS....82
4.45 Second occurrence of stick-slip mechanism for TF-WC2-FS....82
4.46 Third occurrence of stick-slip mechanism for TF-WC2-FS....83
4.47 Fourth occurrence of stick-slip mechanism for TF-WC2-FS....83
4.48 Close-up of fourth occurrence of stick-slip for TF-WC2-FS to show constant magnitude of oscillation....84
4.49 Wrap end of cable with tape to prevent foil from unwrapping....86
4.50 Slide uncompacted sleeve over end of cable....86
4.51 Reference lines marked to indicate where to cut foil....86
4.52 Protective foil being removed, revealing sub-cable foil....86
4.53 End of cable with foil removed showing 0.5" foil band for grip sleeve overlap...87

4.54 Schematic of modified TF grip sleeve design....88
4.55 Reinforcement grip rings prior to install....89
4.56 Uncompacted grip ring compared to partially compacted sleeve....89
4.57 Grip ring positioned on compacted grip sleeve....89
4.58 Grip ring taped in place in preparation for swaging....89
4.59 Reinforcement grip ring after compaction around grip sleeve....89
4.60 Smooth grip sleeve surface due to incremental compaction....90
4.61 Deformed grip sleeve surface due to compaction in one step....90
4.62 Single accent band for samples without reinforcement grip ring....91
4.63 Double accent band for samples with reinforcement grip ring....91
4.64 Tensile lug flush with lower coupling to prevent rotation....92
4.65 Reference lines to monitor specimen rotation....92
4.66 Comparison of axial force vs. time for TF-WC2-FS, TF-WC3-FS, and TF-WC4-FS....93
4.67 Comparison of axial force vs. displacement for TF-WC2-FS, TF-WC3-FS, and TF-WC4-FS....93
4.68 Grip sleeve failure due to sleeve slippage....96
4.69 Grip sleeve failure due to seam weld fracture....96
4.70 Grip sleeve failure due to seam weld fracture....96
4.71 First occurrence of stick-slip mechanism....97
4.72 Second occurrence of stick-slip mechanism....97
4.73 Load drop due to sample rotation....99
4.74 Sample rotation responsible for load drop with respect to fixed coupling....100
4.75 Jam nut installed against upper tensile lug to prevent rotation....101
4.76 Lower tensile lug tightened flush with coupling to prevent rotation....101
4.77 Reference marks to monitor sample rotation....102
4.78 Initial 100 sec. interval of TF-WC5-FS fatigue test....104
4.79 Intermediate 100 sec. interval of TF-WC5-FS fatigue test....104
4.80 Final 100 sec. interval of TF-WC5-FS fatigue test....105
4.81 Initial 100 sec. interval of TF-WC6-FS fatigue test....105
4.82 Intermediate 100 sec. interval of TF-WC6-FS fatigue test....106

4.83 Final 100 sec. interval of TF-WC6-FS fatigue test.....106
4.84 Initial 100 sec. interval of TF-WC7-FS fatigue test.....107
4.85 Intermediate 100 sec. interval of TF-WC7-FS fatigue test.....107
4.86 Final 100 sec. interval of TF-WC7-FS fatigue test.....108
4.87 TF-WC5-FS displacement increase with increasing time/# cycles.....109
4.88 TF-WC6-FS displacement increase with increasing time/# cycles.....109
4.89 TF-WC7-FS displacement increase with increasing time/# cycles.....110
4.90 Gap between accent bands after fatigue testing.....111
4.91 Gap between accent bands after fatigue testing.....111
4.92 Axial force vs. time for TF-WC4, TF-WC5, TF-WC6, and TF-WC7.....112
4.93 Axial force vs. displacement for TF-WC4, TF-WC5, TF-WC6, and TF-WC7...112
4.94 Rotation of foil wrap on TF-WC5-FS sample.....114
4.95 Rotation of foil wrap on TF-WC6-FS sample.....114
4.96 Rotation of foil wrap on TF-WC7-FS sample.....114
4.97 Folding of foil wrap due to cable rotation.....115
4.98 Folding of foil wrap due to cable rotation.....115
4.99 Lack of foil wrap folding due to lack of cable rotation.....115
4.100 TF-WC4-FS seam weld fracture.....116
4.101 TF-WC4-FS seam weld fracture.....116
4.102 TF-WC6-FS seam weld fracture.....116
4.103 TF-WC6-FS seam weld fracture.....116
4.104 TF-WC7-FS seam weld fracture.....117
4.105 TF-WC7-FS seam weld fracture.....117
4.106 Comparison of stick slip experienced by TF-WC4, TF-WC5, TF-WC6, and TF- WC7.....119
4.107 Seam weld fracture showing 45° angle of fracture face.....121

Chapter 1
Introduction

1.1. Energy Crisis

Since the beginning of time, humans have learned to convert energy from forms that are less desirable to those that are better suited to meet their current needs (i.e. from wood to heat and from fossil fuels to electricity). As the world continues to become more technologically advanced, energy consumption continues to increase, and we are beginning to run out of ways to convert the forms of energy we possess to keep up with the demand. In 2008, worldwide energy consumption reached an all time high, with 85% derived from the combustion of fossil fuels [1]. While this reliance on fossil fuels has proven to be beneficial in years past due to its abundance, ease of conversion, and relatively low cost, today's massive demand for energy is causing a variety of other problems that are making fossil fuels less attractive. As a nonrenewable resource, fossil fuels require millions of years to develop under extreme conditions. Since we are using them at a faster rate than they can be replenished, we will quickly run out at the given rate of consumption, and once they are gone, they can no longer be part of our energy mix. Additionally, fossil fuels have a major environmental impact. The combustion of fossil fuels can be blamed for more than 80% of the greenhouse gas emissions, and when used in such large quantities, has led to other problems such as global warming [2]. While the use of fossil fuels has historically been very beneficial, the fact that they are non-renewable and have many adverse environmental affects has forced us to turn elsewhere as we look towards the future of energy. For the next few decades, there are only a few realistic solutions to the current energy crisis. These include:

- Increasing efficiency in power generation and use
- Expanding the use of renewable energy sources such as wind, solar, biomass, and geothermal
- Increasing the use of nuclear power

For the purposes of this thesis, we will be focusing on the latter; increasing the use of nuclear power.

1.2. Nuclear Power

Presently, the most viable solution for an abundant, low-emission, and efficient source of energy comes in the form of nuclear power. In addition to being a more environmentally benign source of energy, nuclear power promises long term energy production using less fuel due to its large energy density as compared to that of conventional fossil fuels. This nuclear reaction can take on two forms (fission and fusion), which differ based on the products of the reaction.

The process that is currently being used by nuclear power plants is called fission. Nuclear Fission refers to the splitting of a large atom into two or more smaller fragments by striking it with a neutron. During this process, neutrons are released at high speed, and large amounts of heat and radiation are generated. The benefit of fission over the combustion of fossil fuels is that the energy released by fission is a million times greater than that released in chemical reactions [8]. Compared to the electricity generated by burning fossil fuels, nuclear energy is also clean. No air pollution or carbon dioxide is created by nuclear power plants, but there are many sources of radioactive waste in the fission cycle, and the problem of waste disposal is yet to be solved. Fission reactors also carry the danger of a nuclear accident, where run-away reactors and meltdowns are a reality.

The alternative to fission is nuclear fusion. Nuclear fusion refers to the combining, or fusing of two or more light atomic nuclei into a heavier nucleus with a resultant loss in the combined mass and a massive release of energy. The use of nuclear fusion offers many advantages over both fission and the combustion of fossil fuels; the main one being its energy density. The energy released by fusion is three to four times greater than the energy released by fission, and about four million times more energetic than a chemical reaction such as the burning of coal, oil or gas [8]. Another key feature of fusion that makes it an attractive option as part of a future energy mix is that fusion fuels are abundantly available and inherently safe. Only tiny amounts of Deuterium and Tritium are necessary to fuel the fusion reaction, and both are readily available on Earth. Deuterium is found in water and Tritium can be bred on site using a Lithium reaction. Additionally, fusion emits no pollution or greenhouse gases. Its major by-product is Helium: an inert, non-toxic gas. Finally, there is no possibility of a run-away reaction

because the conditions for fusion are precise; any deviation from these conditions and the plasma cools within seconds and the reaction stops [5].

Despite its many advantages, fusion technology must overcome several obstacles before it can become a viable energy source; the main one being the confinement of the plasma. Plasma generation in a fusion reaction requires temperatures in excess of 100 million °C and no current construction material can withstand this heat. Naturally occurring fusion in the heart of stars is contained by the gravity of their enormous mass, but the gravitational forces of our universe can not be recreated here on Earth. Without the mass required to obtain a high gravitational field, fusion on earth must be controlled by some means other than gravity [4]. Therefore, the success of fusion energy on Earth depends on the development of an effective plasma containment device.

1.2.1. ITER

Headquartered in Cadarache, France, the ITER program is an international joint venture between seven nations (China, Europe, India, Japan, the Republic of Korea, the Russian Federation, and the USA) that aims to demonstrate the feasibility of fusion power for commercial energy purposes. The ITER program is based on the tokomak concept for magnetic confinement in which plasma is contained in a doughnut shaped vacuum vessel. The fuel, a mixture of Deuterium and Tritium, is heated to temperatures in excess of 150 million °C (ten times the temperature at the core of the sun), forming a hot plasma. Strong magnetic fields produced by superconducting coils surrounding the vessel and an electrical current driven through the plasma itself are used to keep the plasma away from the walls [7].

Though other attempts have been made to harness fusion energy in the past, no one has successfully met or exceeded the critical breakeven point with plasma. The plasma energy breakeven point describes the condition when plasma in a fusion device releases at least as much energy as is required to produce it. Fusion performance is measured by Plasma Power Amplification (Q), which is the ratio of fusion power output to power input. Plasma energy breakeven or Q = 1, has never been achieved: the current record for energy release is held by the Joint European Torus (JET), which succeeded in

generating 70% of its input power [6]. The goal of the ITER fusion program is to be the first of all fusion experiments to produce a net gain of energy, and set the stage for the demonstration fusion power plant (DEMO) to come. Scientists have designed the ITER device to produce 500 MW of output power from 50 MW of input power, or ten times the amount of energy put in (Q = 10). A conceptual cutaway view of the ITER tokomak design can be seen in Figure 1.1.

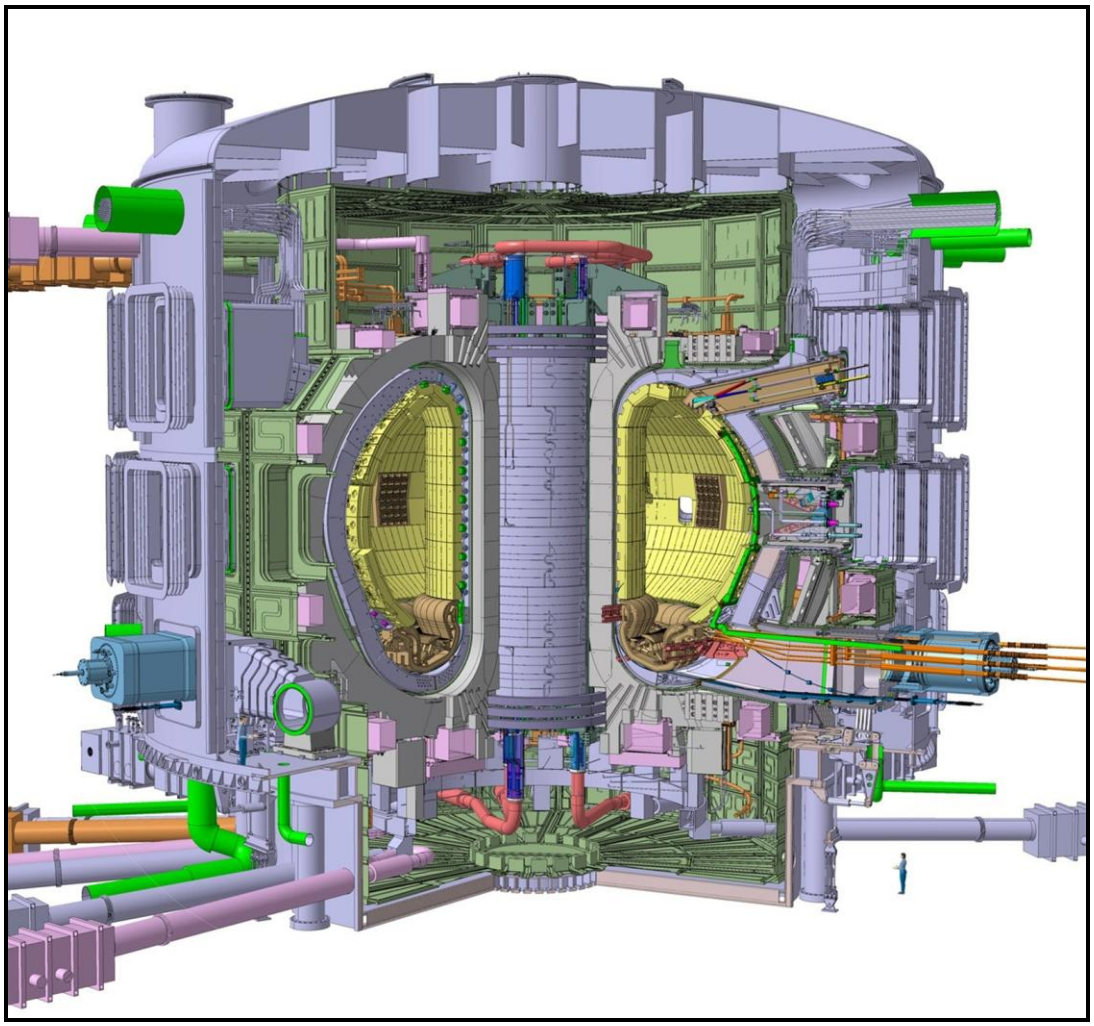

Figure 1.1: Conceptual cutaway view of the ITER tokomak [9]

1.3. Magnetic Confinement of Plasma

As was described earlier, the fuel in the ITER machine will be a mixture of Deuterium and Tritium that will be heated to temperatures in excess of 150 million °C.

At these extreme temperatures, electrons are separated from their nuclei and a gas becomes plasma. Plasma consists of charged particles (positive nuclei and negative electrons) that experience electromagnetic interactions and, therefore, can be shaped and confined by magnetic forces. Like iron filings in the presence of a magnet, particles in the plasma will follow magnetic field lines [3].

By exploiting the magnetic properties of plasma, ITER hopes to solve the problem of plasma confinement through the use of a tokomak. A tokomak is a device that uses a combination of magnetic fields in specific orientations to shape the plasma into the form of a torus (or ring). The most crucial of these magnetic fields being in the Toroidal and Poloidal directions; Toroidal direction referring to the long way around the circumference or axis of the torus, and the Poloidal direction running orthogonal to the toroidal direction, or the short way around the torus [10]. The interaction of these fields produces a resultant magnetic field that travels in a helical orientation about the center of the torus that causes the plasma particles to spin in a helical pattern. This spinning effectively confines the plasma by keeping the particles in a constant motion toward the center of the toroidal field and away from the vessel walls. A representation of this process can be seen in Figure 1.2.

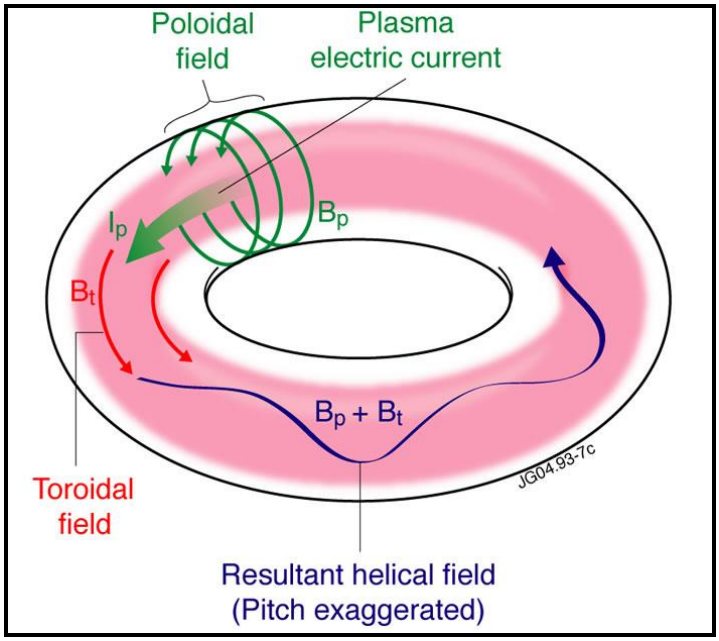

Figure 1.2: Schematic of the current and magnetic fields within a tokomak [11]

In the design of the ITER magnet system, such a field will be generated with 18 superconducting Toroidal Field coils, 6 Poloidal Field coils, and a Central Solenoid that magnetically confine, shape and control the plasma inside the Vacuum Vessel [12]. Weighing in at over ten thousand tons, these elements will generate a magnetic field some 200,000 times higher than that of our Earth. In order to minimize energy consumption and make the reactor as efficient as possible when generating such an extreme amount of power, ITER uses superconducting magnets that lose their resistance when cooled down to very low temperatures. A schematic of the ITER tokomak design can be seen below in Figure 1.3.

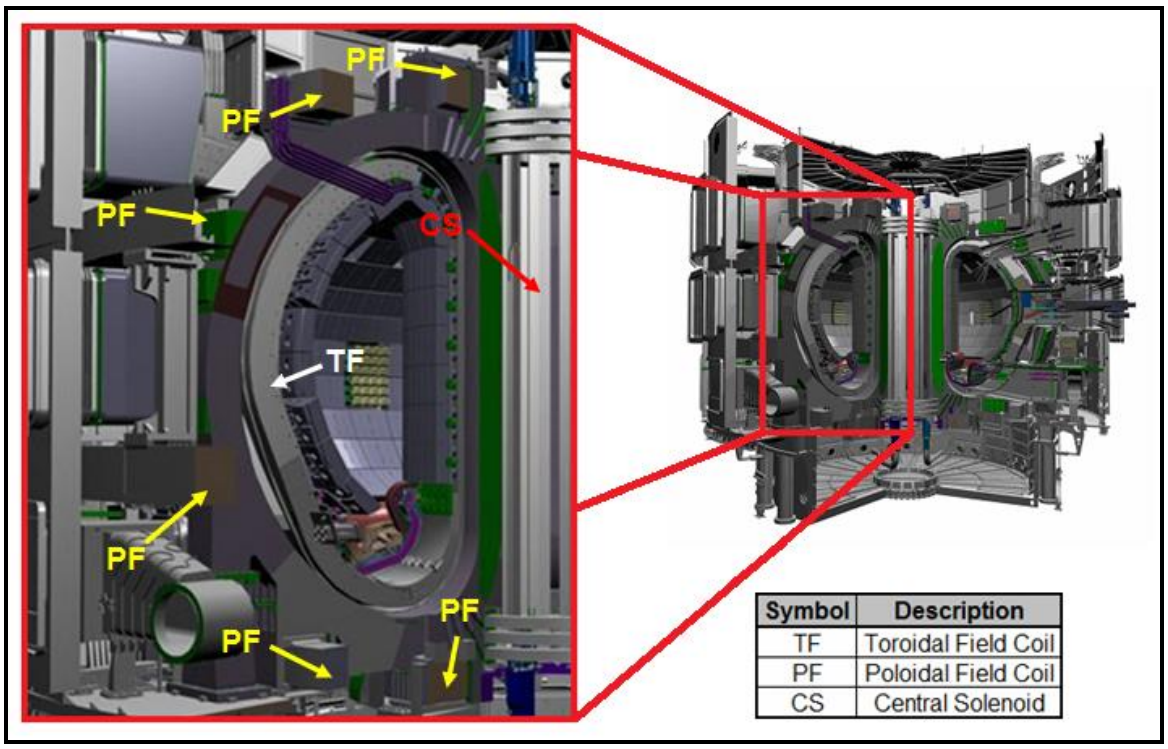

Figure 1.3: Rendering of the ITER tokomak highlighting the key components of the magnet system

1.4. Construction of Toroidal Field Magnetic Coils

The toroidal field that will assist in stabilizing the plasma in the ITER machine will be generated with a series of 18 individual D-shaped vertical Toroidal Field (TF) coils which will be positioned radially around the torus shaped vacuum vessel. Standing

close to 43 m tall and weighing in at a total of 6,540 tons, they are the biggest components of the ITER machine besides the Vacuum Vessel [14]. A rendering of one of the TF coils can be seen in Figure 1.4 below.

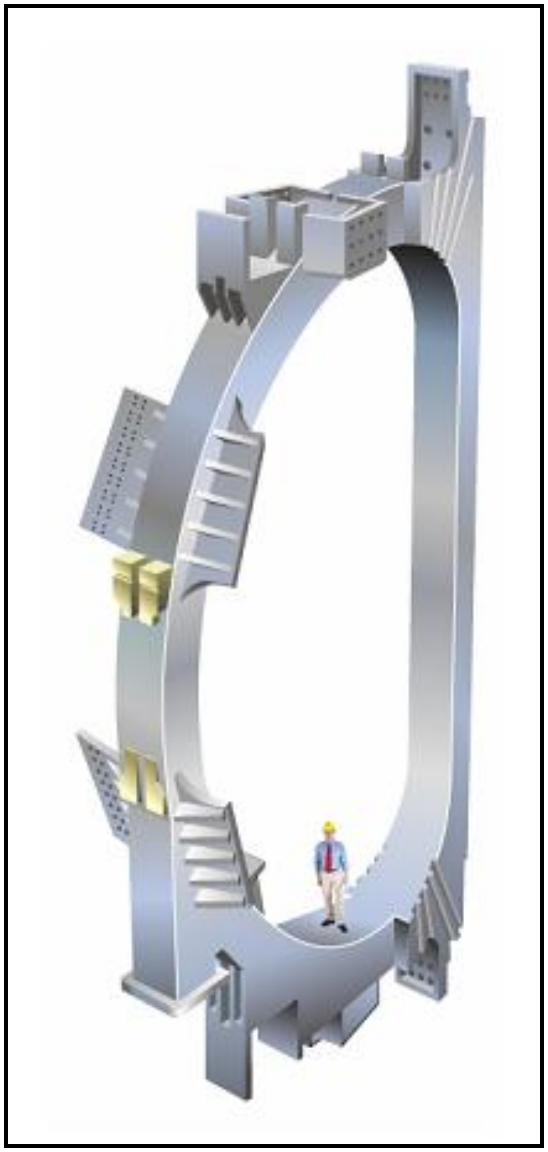

Figure 1.4: Rendering of Toroidal Field Coil design [13]

The heart of the TF coil is the Cable-In-Conduit superconductor which consists of a bundle of superconducting strands that are cabled together and contained in a cylindrical structural jacket (see Figure 1.5).

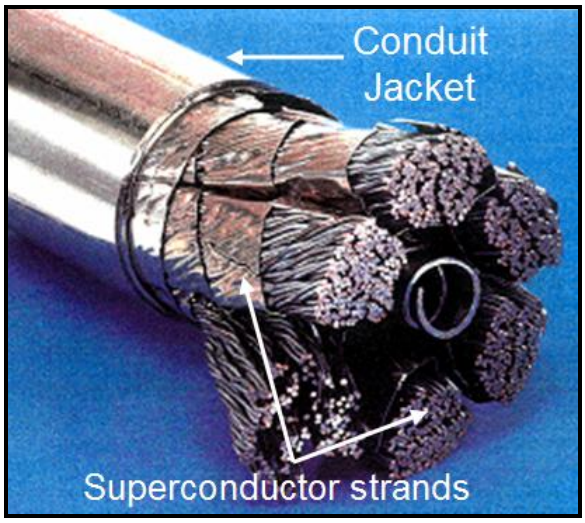

Figure 1.5: Assembled cable-in-conduit conductor

The ITER TF coils are designed to have a total magnetic energy of 41 gigajoules and a maximum magnetic field of 11.8 tesla. In order to generate a magnetic field of this magnitude, each TF coil will contain multiple layers of these cable-in-conduit assemblies wound on top of one another. This layering of cable windings can be seen in Figure 1.6 below which shows the cross section of the TF coil.

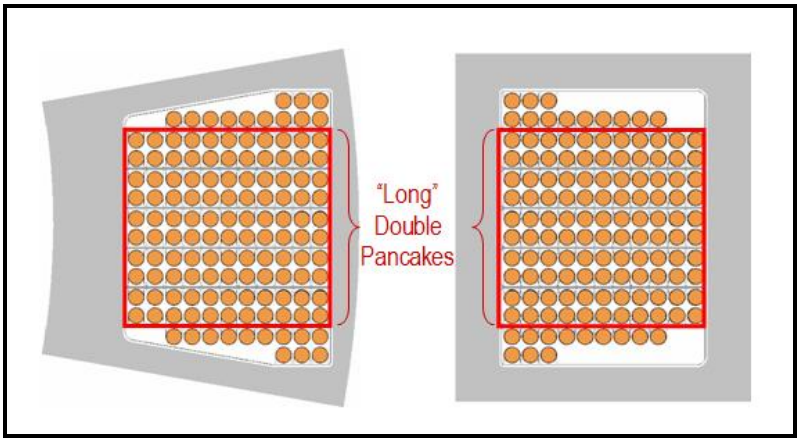

Figure 1.6: Cross section of TF coil to show the layering strategy of the cable windings

The term "long double pancake" refers to 1 conductor length of 800 m. Each of the 18 TF coils that will be used in the ITER machine consists of 5 of these double pancake configurations [15]. Therefore, 90 of the 800 m lengths of cable-in-conduit are required to make the TF coils in the machine.

1.4.1. Why an 800 meter Cable Pull?

As was previously discussed, the TF coils in the ITER fusion reactor will be made of Cable-In-Conduit superconductors in which a bundle of superconducting strands are wound into a cable and encased in a structural conduit jacket. This superconducting cable and conduit are initially two separate pieces that must be joined together before they can be wound into the coil. To minimize the movement of the cable when it is energized, the conductor and conduit are designed with very minimal ID and OD clearance. Additionally, the conductor is manufactured in 800 m sections. Because of these complications, integration (joining) of the cable and conduit is a process that could not be performed by hand. Therefore, the proposed method for joining these two components requires a force assisted cable pull.

When presented with this task, it was known that 800 m lengths of superconducting cable had to be pulled through 800 m lengths of conduit using some sort of winch device. However, the question of how to attach the winch line to the superconducting cable needed to be answered (see Figure 1.7). Therefore, this thesis will focus on the development of a gripping mechanism that is capable of pulling superconducting cable through conduit for Cable-In-Conduit Conductor Integration.

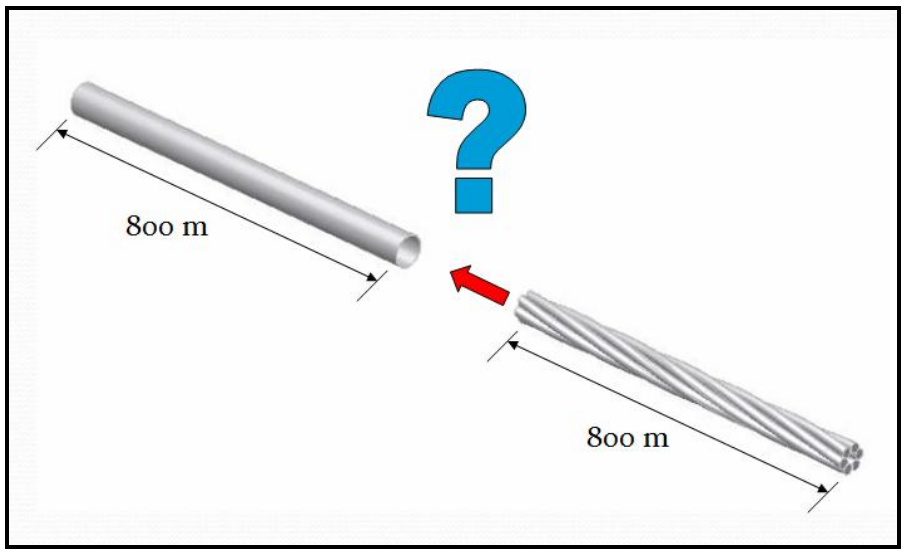

Figure 1.7: Illustration of problem statement

After a method for joining the cable and conduit is developed, the problem with finding a suitable location to perform the task must be addressed. At first glance this might not seem like much of a challenge, but when you consider the specific details of the cable pull, it becomes a lot more difficult. First of all, the assembled length of the cable-in-conduit will span 800 m. More importantly, the land must be as flat as possible, because any significant changes in elevation will introduce bends into the conduit which will make it more difficult to pull the cable through. Another major consideration is that the cable pull must take place in a secure area, meaning it can not simply be done on a back road in some remote area. After weighing all of the possible options, the most suitable location turned out to be a vacant airport runway in Florida. A Google Earth rendering of the proposed cable pull site can be seen in Figure 1.8.

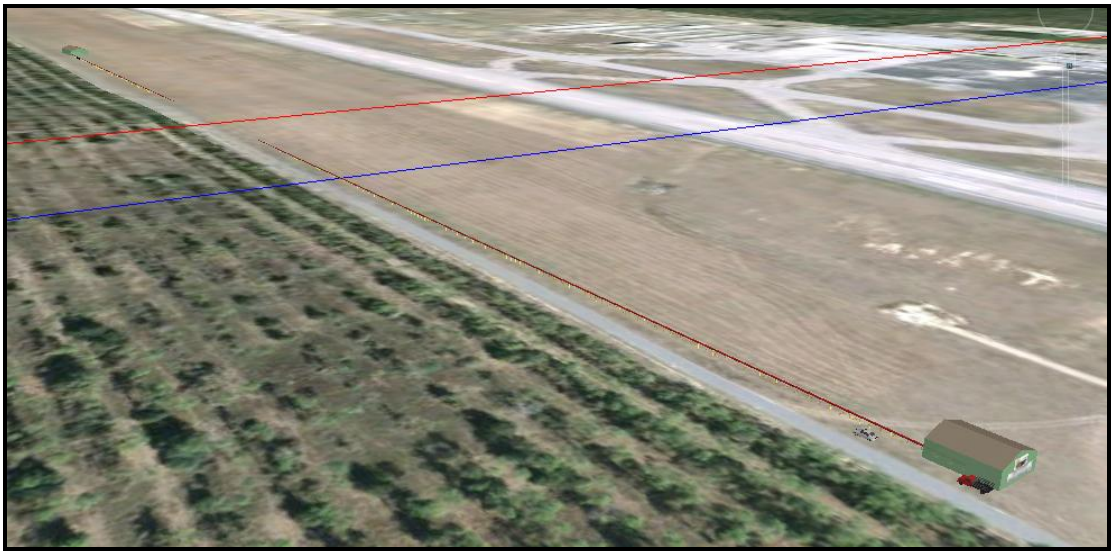

Figure 1.8: Proposed TF cable-in-conduit integration site at airport in Florida

1.5. Modeling Superconducting Cable as Wire Rope

When searching for a suitable gripping mechanism to perform the cable and conduit integration, the first step was to research how others in the industry were performing similar tasks. Surprisingly, there was no published documentation pertaining to cable pulls with superconducting cable. However, there was a great deal of information regarding the use of wire tope to apply tension over great distances. When you ignore its

electrical properties and focus on its mechanical aspects, superconducting cable is essentially wire rope. This basis of comparison is very valid when you consider the construction of both.

As the name implies, wire rope is a type of rope which consists of several strands of metal wire laid (or twisted) into a helix (see Figure 1.9).

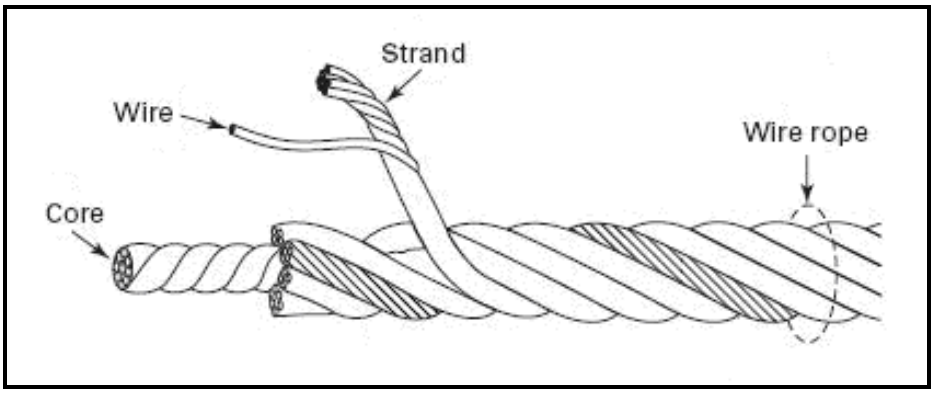

Figure 1.9: Schematic illustrating wire rope construction [16]

Despite the fact that it is designed for an entirely different purpose, the construction of the superconducting cable is exactly like that of a wire rope (see Figure 1.10).

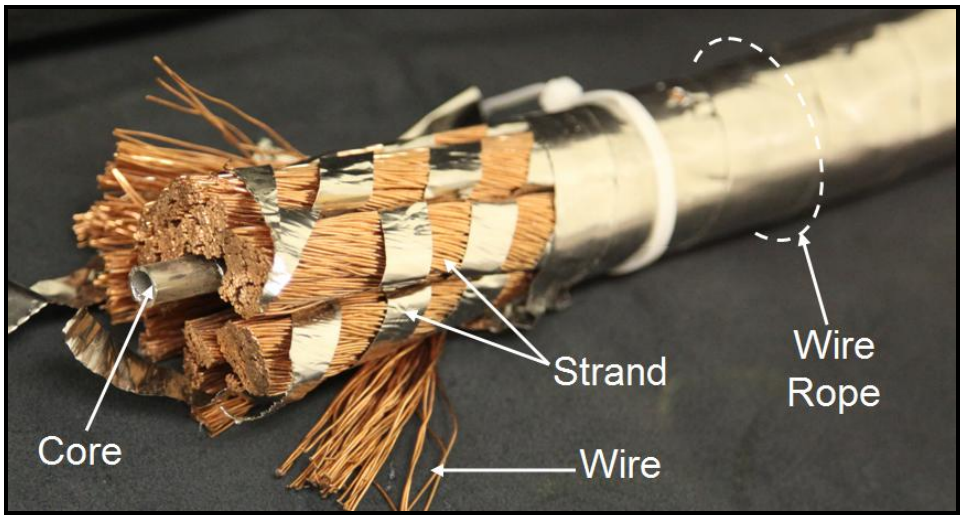

Figure 1.10: Schematic illustrating superconducting cable construction

As a result of this type of construction, wire rope exhibits many mechanical properties that make it ideal for situations involving tensile loading. Because it is used

almost exclusively in tensile loading applications, the mechanical properties of wire rope are also well documented. Even though it would not ultimately be used in this manner, construction of the toroidal field coils requires that the superconducting cable be subjected to tensile loading. Because of these similarities in construction and usage, superconducting cable can accurately be modeled as wire rope.

1.6. Methods of Cable Termination

The flexible nature and tensile strength of wire rope lends itself to be used in a wide variety of applications that require physical tension to be transmitted over long distances. A few of these applications include arresting gear on aircraft carriers, winch lines for utility trucks, elevator lift cables, structural members in suspension bridges, lift lines for cranes, and mooring lines for offshore oil production and drilling rigs, just to name a few. In all of these applications, at least one end of the wire rope features some sort of termination or gripping device that is used to attach the wire rope to the object that it is going to lift or secure. Due to the similarities between wire rope and superconducting cable, there was a good chance that some of the existing wire rope grips might fit our needs. Therefore, researching some of these off the shelf grips seemed like a good place to start the search. A few of the most commonly used terminations are as follows.

Loop termination with Ferrule

The most common type of end fitting for a wire rope is created by turning the loose end of the rope back against itself to form a loop. A ferrule is then swaged around both pieces of wire to hold them in place (see Figure 1.11).

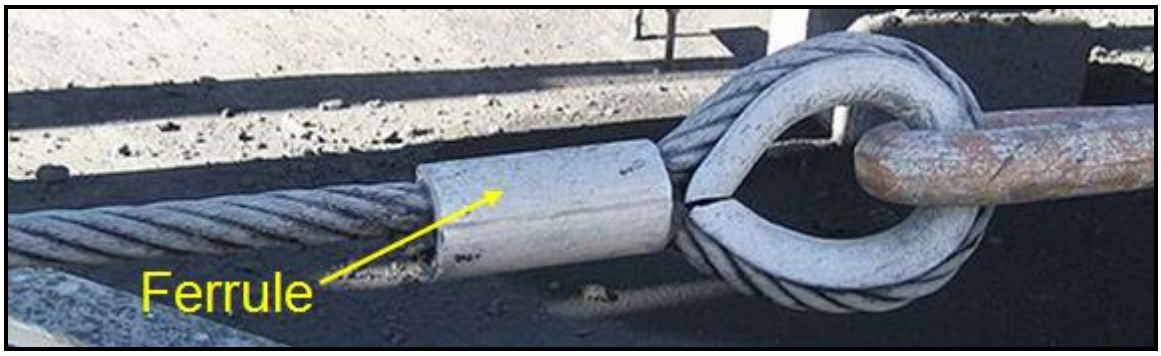

Figure 1.11: Loop termination with ferrule [17]

Another variation of this design is called an eye splice or Flemish eye. Rather than using a swaged ferrule to fix the ends together, the strands at the end of the rope are unwound a certain distance and spliced back into the rope to form the loop, or eye (see Figure 1.12). The benefit to this design over the use of the ferrule is that a swaging machine is not required.

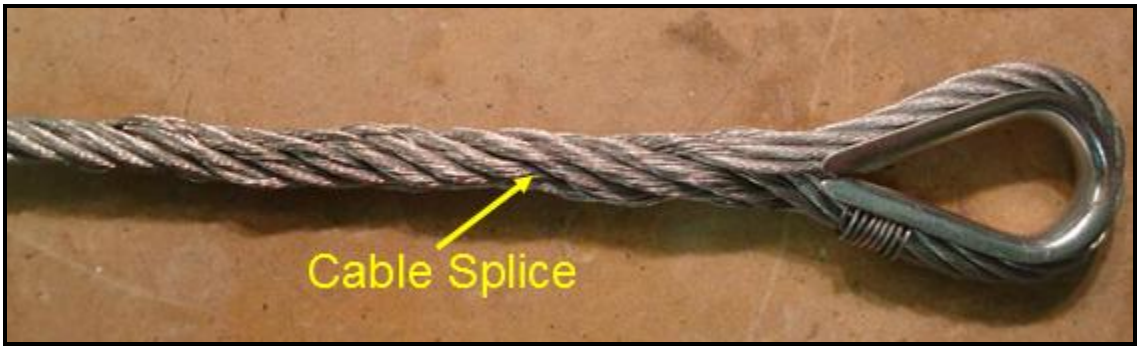

Figure 1.12: Eye splice rope termination [18]

One of the main benefits of these designs is that the looped end makes them a very universal termination because a wide variety of couplings for different applications can be attached. However, due to the fact that the end of the rope must be turned back against itself to form a loop, both of these designs are limited to ropes that possess good flexibility.

Loop termination with Wire rope clip

Another commonly used looped termination can be created with a wire rope clip. Similar to the loop with ferrule and the eye splice, the end of the rope is turned back on itself to form a loop, and then the ends of the rope are fixed together by bolting a series of wire rope clips around them (see Figure 1.13). The benefit of this design as compared to the use of the ferrule is that it can be assembled with the use of hand tools rather than a sophisticated swaging machine. However, as was the case with the other looped terminations, this design is also limited to use with flexible ropes.

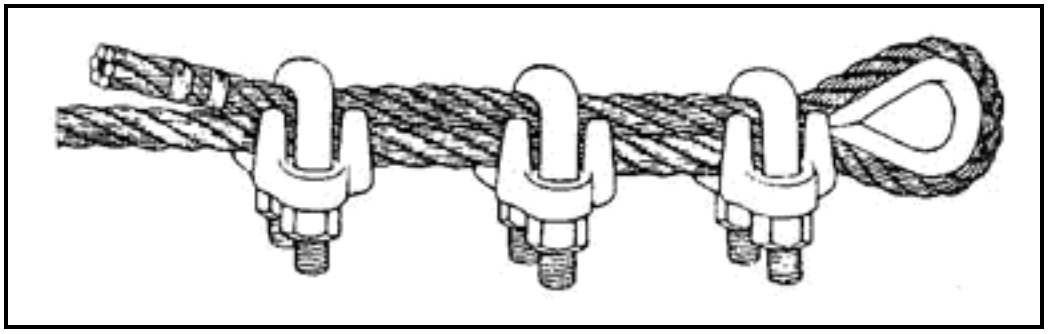

Figure 1.13: Loop termination with wire rope clips [19]

Wedge Socket Termination

With a wedge socket, the termination is created by feeding the wire rope into the end of the socket, looping it around the wedge, pulling the rope back through the end of the socket, and fixing it with a rope clip (see Figure 1.14). The result is a termination whose strength increases with load as the wedge is pulled tighter and tighter against the cable. In addition to being easy to install, another benefit to this design is that the grip does not create a permanent bond and can be easily removed when it is no longer needed. The major drawback to this design is that the rope must be fairly flexible because it has to be turned back against itself to loop through the socket.

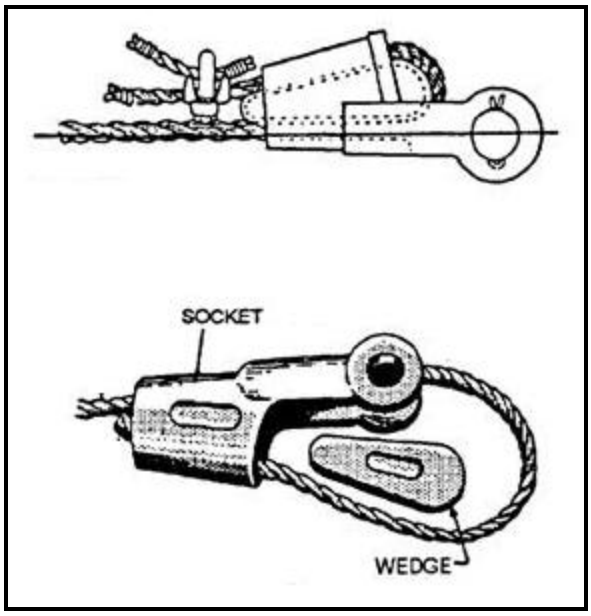

Figure 1.14: Schematic of wedge socket termination [20]

Lace-Up Grip Termination

Lace-up grips are a type of cable termination that does not utilize a loop to make a connection. Instead, the straight end of the cable is inserted into the cylindrical "lace" portion of the grip and then the grip is pulled taught. As tension is applied, a rigid connection is formed by the lace mesh constricting around the cable. Similar to the wedge grip, the strength of the lace grip increases as more load is applied because the lace continues to constrict. Due to their flat construction, lace-up grips offer a very low profile method of attachment (see Figure 1.15). Another benefit to this design is that they are easy to install and uninstall, and do not require the use of sophisticated tools. Additionally, this design is not limited to use with flexible ropes because they do not require the rope to be bent to form a loop.

Figure 1.15: Installation of Lace-up grip [21]

Spelter Sockets

Like the lace-up grip, spelter sockets are another non loop based termination that works by fastening a socket to the straight end of the cable. An example of this type of socket can be seen in Figure 1.16.

Figure 1.16: Rendering of various Spelter socket designs [22]

Attachment of the socket to the rope can be accomplished in one of two ways; a poured connection or a dry connection. In the poured method, the end of the cable is inserted into the central hole at the base of socket, the strands of the cable are flared out, and molten zinc is poured into the hole. Once the molten material solidifies, the cable is rigidly bonded to the socket. Despite the fact that this design produces a very strong

bond, the use of molten metal has many drawbacks; the main one being that the handling of molten material is an inherently dangerous operation. Additionally, working with molten metal requires access to a furnace to heat the zinc, which makes it difficult to use in remote areas. Finally, the bond between the cable and socket is permanent.

In the dry method, the end of the cable is slid into the central hole at the base of the socket, and the strands are unlaid a distance that is equal to twice the length of the socket. The wires are then wrapped with twine to form a knot. The unlaid wires are then bent over the knot and bound again by wrapping them with twine to create a knot that is too large to fit through the end of the socket. Finally, this knot is pulled into the basket of the socket to form a tight connection. This process is outlined in Figure 1.17.

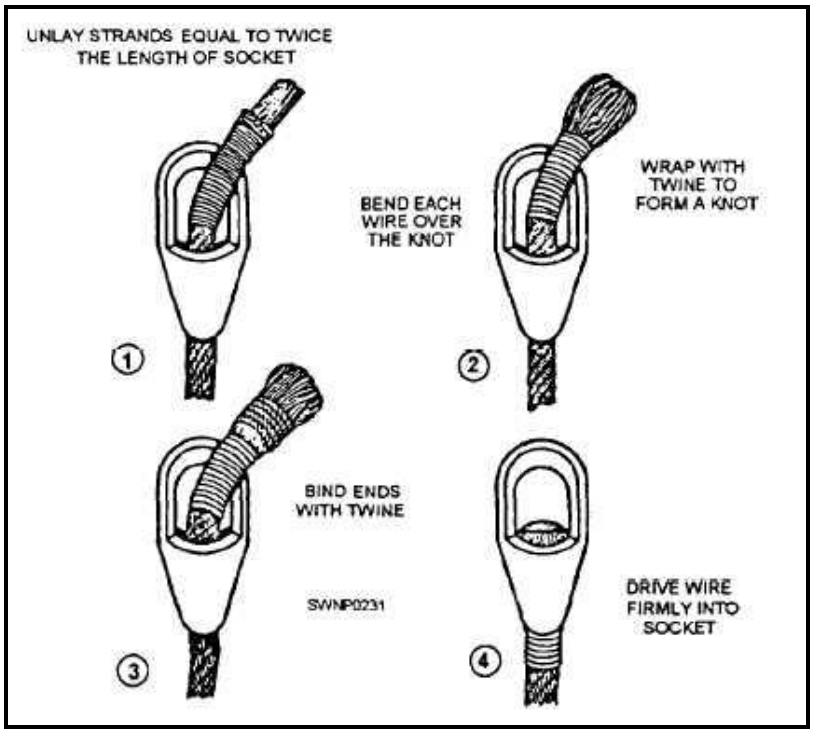

Figure 1.17: Stages of assembly of dry Spelter socket termination [23]

The benefit to this method as compared to the poured method is that it is much safer due to the absence of molten zinc, and it can be fabricated when facilities are not available to make a poured fitting. However, the strength of a socket made with the dry method is

reduced to approximately one sixth of that of a poured zinc connection. Furthermore, like the poured socket, this too is considered a permanent connection [23].

Despite their drawbacks, Spelter Sockets are installed on the straight end of the rope, making them ideal for ropes that are stiff or where bending in a short radius is difficult.

Non-Swage End Fittings

Non-swage wire rope fittings are similar to spelter sockets in that the connection is formed by attaching a socket to the end of the cable. An example of this type of socket can be seen in Figure 1.18.

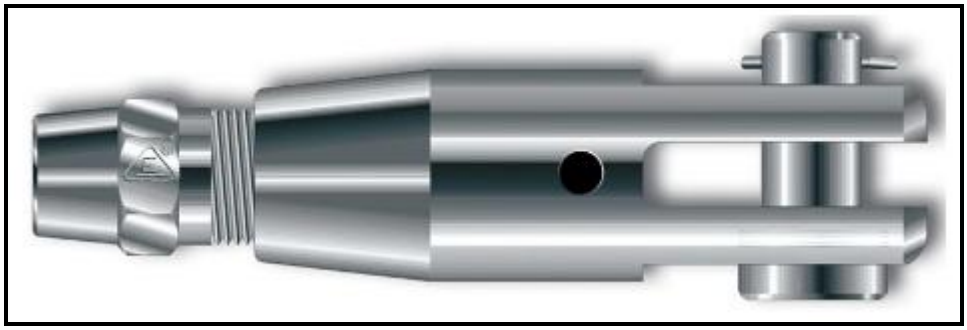

Figure 1.18: Rendering of non-swage fitting [25]

Rather than using molten metal or knots to secure the socket, the rope passes through a central hole at the base of a threaded sleeve, the strands are fanned out and a plug is inserted. As the plug is driven into the fanned end of the rope, the diameter of the rope end increases such that it can not dislodge itself by slipping through the end of the sleeve. Finally, the socket is slid over the sleeve and threaded on tight. This process is illustrated in Figure 1.19.

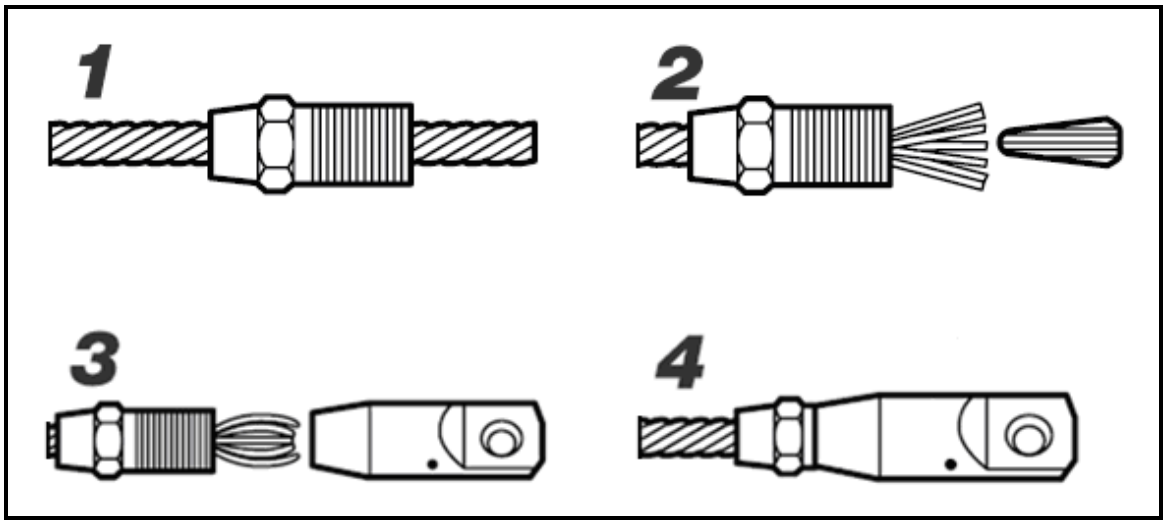

Figure 1.19: Stages of assembly of non-swage end fitting [24]

In addition to the ease of installation offered by this configuration, the biggest advantage is the fact that they do not require the expensive and bulky equipment that is inherent to swaging. Compared to other grips, these are also fairly low profile since they do not involve looping the rope back against itself. Additionally, this design is very effective for ropes that do not possess the greatest flexibility because they do not require the rope to bend.

Press-Fit Grip Sleeves

The press-fit grip sleeve design is another type of end fitting that creates a rope termination without the use of a loop. This type of connection is created by sliding a cylindrical tube (whose diameter is initially greater than that of the cable) over the end of the cable and swaging it down to a diameter that is less than or equal to the diameter of the cable. Doing so creates interference, and thus a contact pressure between the grip sleeve and cable strands, which creates a solid grip based on friction force alone. The assembly process for this type of grip can be seen in Figures 1.20 and 1.21.

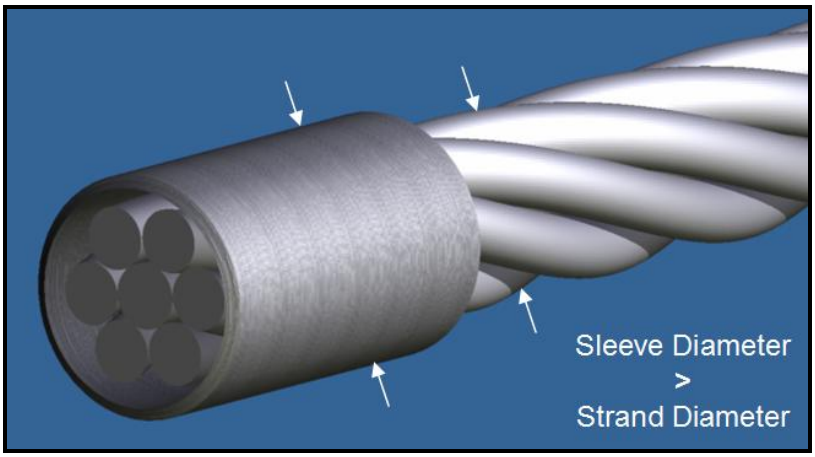

Figure 1.20: Grip sleeve and cable prior to swaging

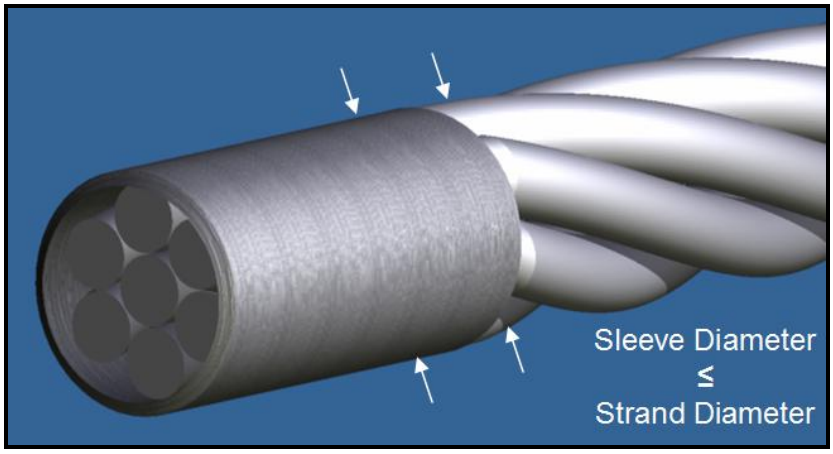

Figure 1.21: Grip sleeve and cable after swaging

As a result of swaging the grip sleeve to a diameter that is less than or equal to that of the cable, the press-fit grip is the most low profile termination out of all of the options that have been discussed. Despite the fact that it does require the use of a swaging machine for installation, this design is relatively easy to install and very inexpensive, consisting only of a single piece of cylindrical thin walled tubing. This design is also very effective for ropes that do not possess the greatest flexibility because they do not require the rope to be bent to form a loop. The only drawback to this design is that an additional coupling has to be connected to the grip sleeve since the grip sleeve itself does not possess an attachment point. This coupling can be in the form of a threaded lug, loop, hook, or other similar component which is welded to the end of the grip sleeve (see Figures 1.22 and 1.23).

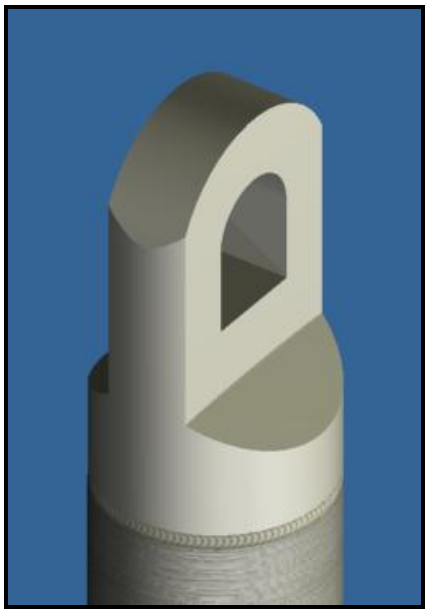

Figure 1.22: Rendering of loop socket auxiliary coupling

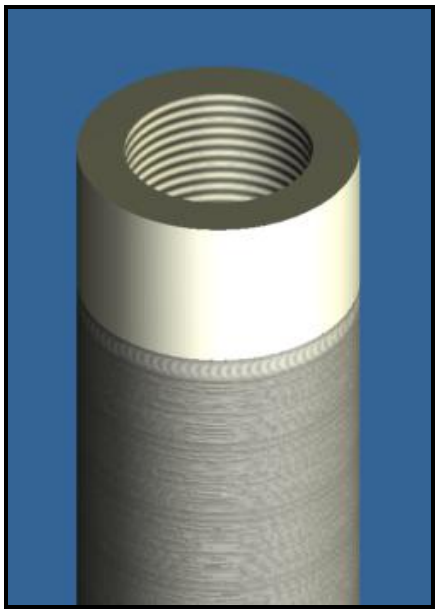

Figure 1.23: Rendering of tensile Lug auxiliary coupling

1.6.1. Cable Pull Requirements

When selecting the appropriate grip to use for the 800 m conductor cable pull, there were several factors that needed to be considered. These included the strength, overall size, and ease of manufacturing and installation of the gripping mechanism. Of the three criteria, the most important was the ability to withstand the required pulling load without failing. For the purposes of this application, failure refers to the grip detaching from the end of the cable by slipping or breaking such that the cable could not be pulled completely through the conduit. Should the grip sleeve fail during a cable pull, the conduit would have to be cut and the cable removed. Doing so would be a very costly mistake in terms of both time and labor; not to mention the possibility of damaging the irreplaceable toroidal field cable.

The second most important design criterion was the size of the gripping mechanism itself. In order to restrict the motion of the cable when it is energized, the 40.2 mm diameter conductor would be contained within a cylindrical conduit with an inner diameter of only 43.5 mm. These tight tolerances left a clearance between the conductor and conduit of roughly 3.25 mm. The last requirement was the ease of

manufacturing and installation of the gripping device. There are a total of 18 TF coils in the ITER magnet system, each of which is formed from 5 of these 800 m lengths of conductor. In addition to these 90 required pulls, 6 additional 800 m cable pulls are going to be performed to create dummy cables for test purposes. Therefore, this same cable pull would be performed at least 96 times, meaning 96 of these grips had to be fabricated, installed, and put to use. With a need for that many cable grips, the chosen device needed to be fairly simple to construct and relatively cost effective. Additionally, the grips would also be installed in the field at the time the pull test would take place, so installation needed to be prompt. Along these same lines, installation in the field meant that access to tools would be limited. Therefore, keeping the complexity of the installation procedure to a minimum was preferred.

As can be seen in the figures above, many of these off the shelf grip configurations were immediately eliminated based on the size requirement alone, as they would not come close to fitting through the conduit. All of the designs that required that a loop be formed at the end of the cable fell into this category as well since the size of the loop that would be created by turning the cable back on itself would exceed the inner diameter of the conduit; not to mention the fact that the superconducting cable is far too stiff to easily loop back on itself. The final requirement was the load bearing capacity of the grip. Even though it offers a very low profile design when compared to many of the other grips, the lace-up style grip would not support the kind of load that we would be subjecting it to.

Of all the designs discussed above, only two adhered to all of the specified criteria. These included the non-swage end fitting and the press-fit sleeve. Selecting the best design from the remaining two was done based on their simplicity. Among these, the press-fit grip sleeve turned out to be the least complicated and was the first to be tested. As will be described in Chapter 4, it turned out that the first and most basic design worked so well that other grips did not need to be tested. However, modifications were made to the original grip sleeve design to improve upon its effectiveness. Additional details regarding the construction and testing of this device are documented in Chapters 3 and 4.

Chapter 2
Review of Literature

2.1. Overview

Wire rope research and development has led to the creation of a wide variety of cabling devices that have found extensive use in hoisting and mooring applications where tension needs to be transmitted over great distances. Similarly, press-fit joints have proven themselves to be an effective means of creating a rigid connection between two objects. In both cases, there is a great deal of literature that documents the advancements and usage of both items. However, there is no current literature that documents the use of a press-fit grip as a termination method for a wire rope. Since there is a lack of literature that focuses on the exact type of work being done, this literature review will focus on the different characteristics that are inherent to the wire rope and press fit grips when used in a tensile loading application. The topics of interest will be explained and described as they pertain to this research. Since the overall performance of the grip sleeve will depend on how the grip sleeve and the wire rope behave individually, each component can be studied individually and experimental testing will be utilized to effectively predict how they interact with one another.

2.2. Mechanics of Wire Rope

Due to their helical construction, wire rope responds very differently to tensile loading than a straight or braided rope would. Unlike braided rope that will simply elongate when subjected to a tensile load, the wires and strands in a wire rope attempt to straighten themselves out or in other words, to "unlay". The degree to which the strands and wires untwist depends upon the magnitude of the force applied, the construction of the rope, and also upon the stiffness of the wires and strands. The lay of the wires, the lay of the strands, the way that each end of the rope is fixed, and even the number of layers that form the rope are all factors that can drastically influence the rope’s behavior.

2.2.1. Wire and Strand Lay Variations

As was briefly described above, the lay of the wires and strands in a rope have a major impact on its mechanical properties. The lay of a wire rope describes the manner in which the wires in a strand, or the strands in the rope, are twisted together to form the helix. Left hand lay and right hand lay refer to the orientation of the strands in the rope. To determine the lay of strands in the rope, a viewer looks at the rope as it points away from them. If the strands appear to turn in a clockwise direction, or like a right-hand thread as the strands progress away from the viewer, the rope has a right hand lay. If the strands appear to turn in a counter-clockwise direction, the rope has a left hand lay [27]. Both of these lay configurations can be seen in Figures 2.1 and 2.1.

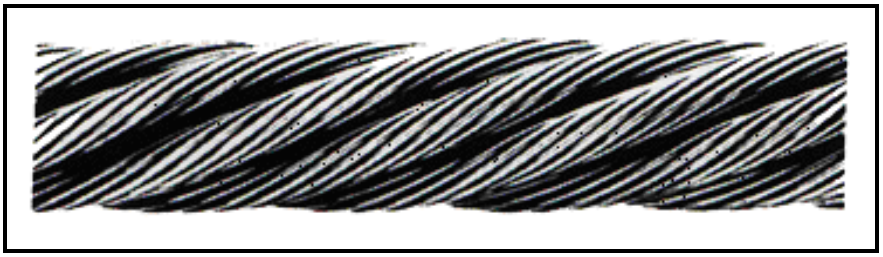

Figure 2.1: Wire rope featuring Left hand Lay strand orientation [26]

Figure 2.2: Wire rope featuring Right hand lay strand orientation [26]

Once the lay of the strands has been identified, a wire rope can be further distinguished by the manner in which the individual wires are laid to form these strands. The most common types of wire lay are Regular or Ordinary Lay and Lang's lay. To determine the lay of the wires, a viewer looks at the rope as it points away from them. With regular or ordinary lay, the outer wires follow the alignment of the rope, whereas with Lang's lay they are cross at an angle of about 45° [27]. In other words, regular lay

wires appear to follow in the same direction as the rope, while Lang's lay wires appear to follow the direction of the strands. A comparison of regular and Lang's lay for both strand lay directions are shown below in Figure 2.3.

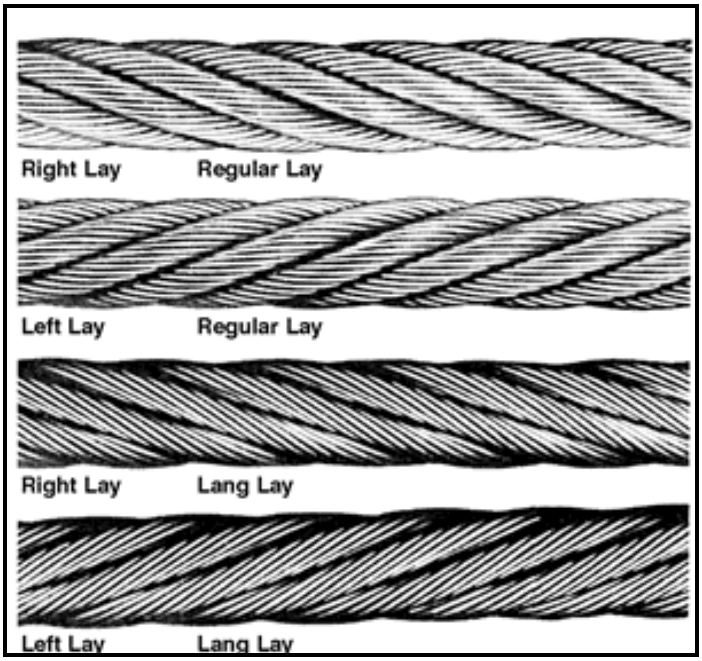

Figure 2.3: Comparison of the most common wire and strand lay combinations [28]

Finally, wire ropes may be classified even further based on their lay length. The length of a rope lay is the distance measured parallel to the center line of a wire rope in which a strand makes one complete spiral or turn around the rope. Similarly, the length of a strand lay is the distance measured parallel to the center line of the strand in which one wire makes one complete spiral or turn around the strand. Generally, strand lay length is the more important of the two parameters. An illustration that shows the measurement of the strand lay can be seen in Figure 2.4.

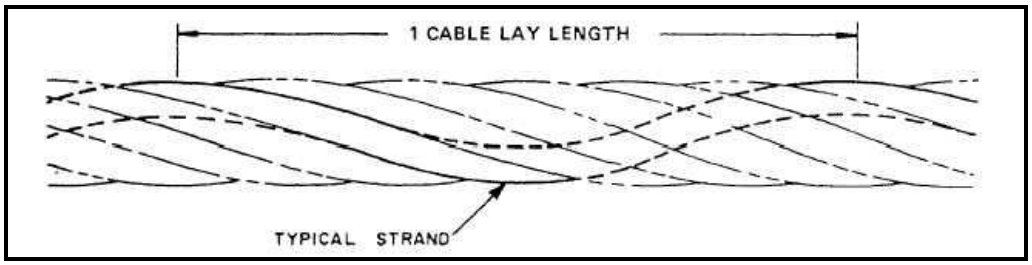

Figure 2.4: Illustration of strand length measurement of a wire rope [29]

Lay length has a major influence on the tendency of the rope to untwist under load. This is due to the components of force acting on the wires and strands. As can be seen below in Figures 2.5 and 2.6, the strands that comprise the straight lay rope have only a vertical force component, whereas the strands in the helically coiled rope (see Figures 2.7 and 2.8) have both horizontal and vertical components of force. When subjected to a force in the vertical direction, the straight cable strands will simply deform in a vertical direction, whereas the helical strands will deform both horizontally and vertically. The degree to which the helical strands deform in the horizontal direction depends on the angle of the strands with respect to the vertical axis. In general, the trend is that the greater this angle α (and the shorter the lay length), the greater the tendency of strands/wires to want to straighten out.

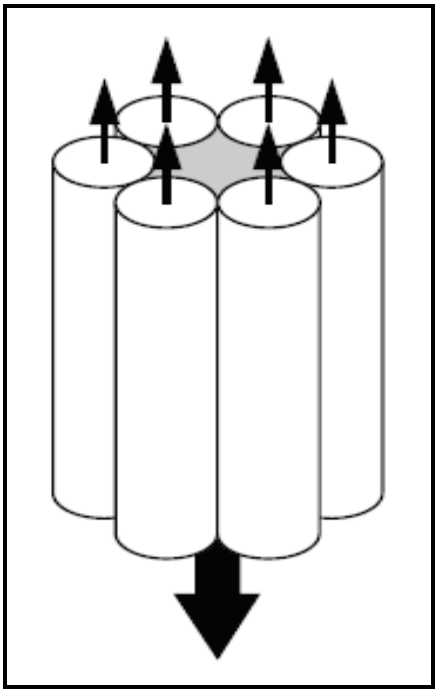

Figure 2.5: Forces acting on straight lay rope under tensile load [30]

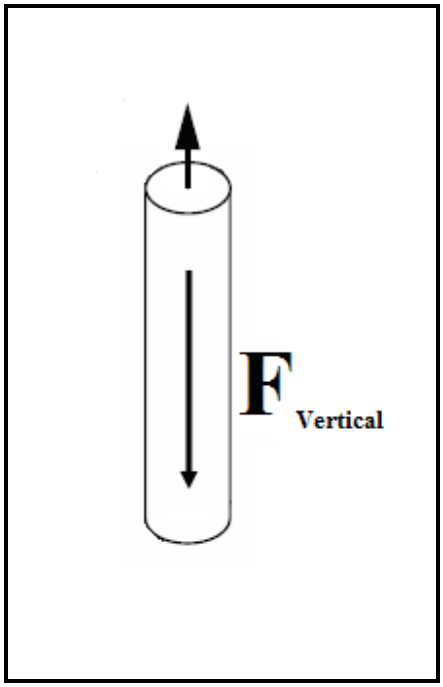

Figure 2.6: Force decomposition of straight laid wire rope

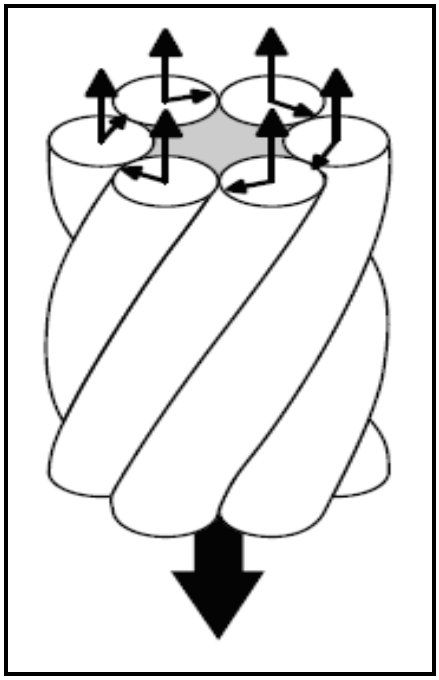

Figure 2.7: Forces acting on helically laid rope under tensile load [30]

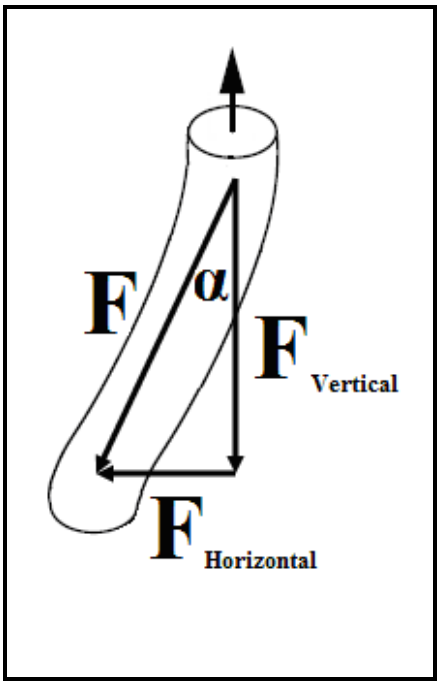

Figure 2.8: Force decomposition of helically laid wire rope

2.2.1. End Supports of Twisted Rope and Torque

As was previously discussed, when a rope is subjected to tensile loading, the wires and strands attempt to straighten themselves out. Depending on the type of end supports that the rope is utilizing (in other words the way that the ends of the rope are constrained); this tendency to untwist can result in two distinct actions [31]. If one end of the rope is free to rotate and the other fixed and a tensile load is applied, this straightening action of the strands and wires leads to a twisting motion at the free end of the rope. However, if both ends of the rope are fixed and the rope is subjected to a tensile load, this tendency to rotate produces a torque about the fixed ends of the rope. As was the case with the degree of untwisting, the torque or turn generated will depend upon the magnitude of the force applied and also the construction of the wire rope. Additionally, this tendency, if unrestrained, can transfer rotation into other parts of the system which are more sensitive to twisting.

2.2.2. Influence of Wire and Strand Lay on Torque

As was previously discussed, wire rope exists in a wide variety of configurations which differ based on their construction. Among these variations, one of the most important is the way in which the wires and strands are twisted together to form the rope. It turns out that these characteristics have a major impact on how the cable acts when subjected to tensile loading.

The most common types of strand construction are Right Lay and Left Lay. When subjected to tensile loading, the strands in a rope have a natural tendency to turn in the opposite direction to which they are laid in an attempt to straighten themselves out. This means a left lay rope will untwist to the right and a right lay rope to the left. This tendency is amplified based on the configuration of the wires that make up the strands in the rope. Strands are typically twisted together in a Regular or Ordinary Lay or a Lang's Lay pattern. Regular lay means that the wires are twisted together in the opposite direction of the strands, and Lang's Lay meaning that they are twisted together in the same direction as the strands. What this equates to is that regular lay strands reduce rope torque since the wires spin in the opposite direction of the strands, whereas Lang's lay strands increase rope torque since the wires spin in the same direction as the strands [32]. Single layer Lang's lay ropes have exceptionally bad rotational characteristics and must only be used in applications where both ends of the rope are securely fixed.

It has been observed that these torque characteristics have a major impact on the application of wire rope. In a situation where the cable is being used to hoist or pull, a coupling of some sort is required to attach the cable to the object it is pulling. A common type of cable termination is a threaded tensile lug that features standard right hand threads. As was discovered in the oil production industry, left lay rope has greatest usage in oil fields on rod and tubing lines because the rotation of right lay rope would loosen the couplings. The rotation of a left lay rope tightens a standard coupling [33].

2.2.3. Torque Balanced Cable

As was discussed above, twisted ropes have an inherent torque problem that makes then unsuitable for use in a wide variety of applications. This natural torque tendency, however, can actually be used against itself to combat this torque problem. As was mentioned above, a regular lay rope has somewhat of a rotation preventing characteristic due to its construction. Since the wires that make up the strands are twisted in the direction opposite to that of the strands, when the wires unwind, they partially counteract the untwisting of the strands. The result is a built in torque balance. Recognizing the potential in this configuration, multiple layer ropes were created.

In terms of their ability to resist rotation, wire ropes can be divided into several basic categories which are based on the number of layers they are constructed from. As can be seen in Figures 2.9 and 2.10, a few of these categories are single layer and two layer.

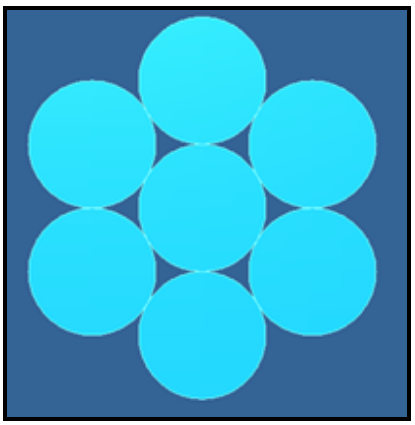

Figure 2.9: Cross-section of Single Layer Rope

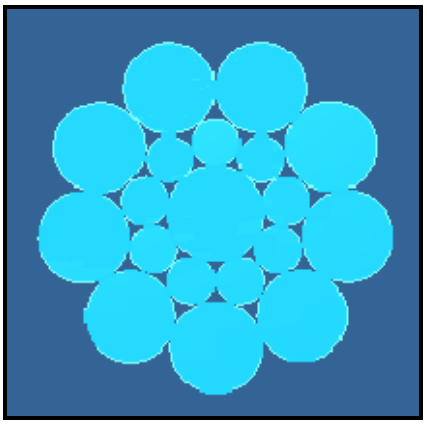

Figure 2.10: Cross-section of Two Layer Rope

Because they only contain strands in one lay direction, single layer ropes have a much greater tendency to rotate under load than the two layer ropes which, due to their multiple layers, can be constructed with strands oriented in opposing lay directions. Similarly, the three layer rope will have less of a tendency to rotate when compared with the two layer rope. The opposing strand orientations create a torsional balance between

the outer and inner layers which leads to rotational stability of the rope. Because of this torsional stability, two and three layer ropes are often referred to as being rotation resistant since they can be constructed to produce almost no rotation when loaded. A schematic illustrating this concept can be seen in Figure 2.11. Note the blue arrows represent the direction of rotation.

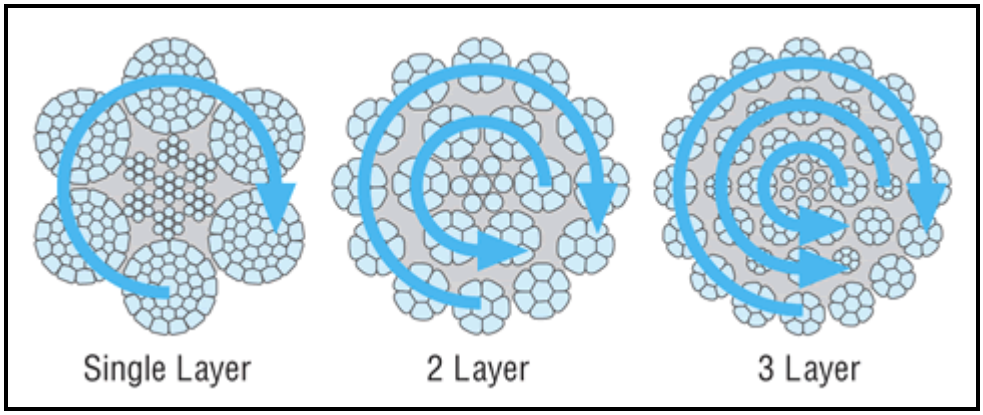

Figure 2.11: Schematic of rope layer cross sections to illustrate torque balancing [34]

2.3. Press Fit Analysis

In general, a press fit or interference fit refers to the process of inserting a shaft of larger diameter into a hub opening of smaller diameter. After the parts have been connected (pressed-on), the shaft diameter decreases and the hub opening increases until both parts settle on a common diameter [35]. Pressure in the contact area between the parts is then evenly distributed. Doing so creates interference (δ) between the rope and sleeve, and thus, a gripping force based on the friction between the two surfaces. Interference refers to the difference between assembly shaft diameter and hub opening diameter, as can be seen in Figure 2.12. The value of contact pressure, as well as loading capacity and strength of the fit, depends on the interference size.

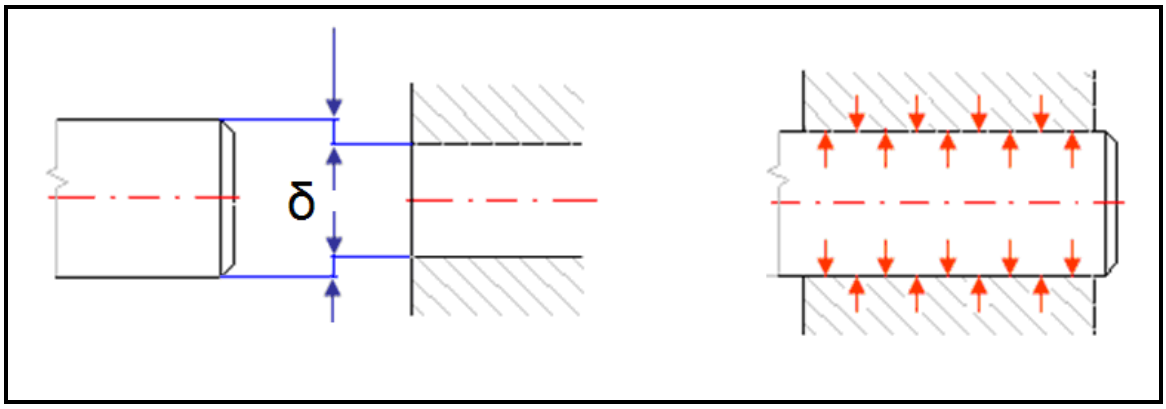

Figure 2.12: Schematic of a press fit grip illustrating interference and contact pressure

2.3.1. Stick Slip Condition

Stick-slip refers to the phenomenon of a spontaneous jerking motion that can occur while two objects are sliding over each other. Stick-slip is caused by the surfaces alternating between sticking to each other and sliding over each other, with a corresponding change in the force of friction. Typically, the static friction coefficient between two surfaces is larger than the kinetic friction coefficient. If an applied force is large enough to overcome the static friction, then the reduction of the friction to the kinetic friction can cause a sudden jump in the velocity of the movement.

Conditions with low sliding velocities lead to frictional vibrations (stick-slip effect). These vibrations appear as a saw-tooth shaped disturbance on the frictional force displacement curve. This behavior usually disappears as the velocity increases. The velocity where stick-slip behavior ends is termed the critical velocity [36].

2.4. Related Studies

As was previously stated, there is no documented research that pertains to the use of a press-fit grip sleeve as a termination for wire rope in a tensile loading application. However, there has been some published research regarding the torsional behavior of a wire rope. In a study performed by C.R. Chaplin, it was concluded that under conditions

of rotational restraint, conventional six strand ropes develop a torque which is approximately proportional to the tensile load, however this torsional response is modified by twisting or untwisting the rope [32]. In addition, it was shown that a reduction in the lay length of a rope increases the torque generated by applied tension.

In another study, Utting and Jones discovered significant differences in strand response between wire rope samples having fixed and free (zero torque) end conditions [37]. By referring to the free end condition as zero torque, it is clear that the significant differences the authors of this study are referring to are that a cable with fixed-free ends will rotate under load and produce no torque, while a cable with fixed-fixed ends will produce a torque under load.

Chaplin, Rebel, and Ridge discussed the usage of single layer Lang's Lay rope for mine hoists in South African gold mines in an article titled "Tension-torsion fatigue effects in wire ropes". They commented that this construction (Lang's Lay) has even greater tendency to untwist than the ordinary lay ropes that are used for traditional work wires in the offshore industry [31]. The authors of this article go on to discuss an experimental tensile-torsion fatigue test performed on cable samples with torsionally fixed ends compared to those with free ends. Identical tests were conducted on right hand ordinary lay and right hand Lang's lay ropes. The results of the testing showed that the torsionally restrained (fixed-fixed) samples displayed excellent fatigue endurance for both cable configurations (Lang's Lay and Ordinary Lay), whereas the torsionally unrestrained (fixed-free) samples displayed very poor fatigue endurance. In both cases, the Lang's Lay rope slightly outperformed the ordinary lay rope [31]. Since fatigue testing is performed at loads that are below the yield strength of the material and torque is proportional to the applied load, it is likely that the torque experienced by the fixed-fixed samples was not sufficient to cause the cable to fail or diminish its fatigue endurance.

Chapter 3
Methodology

3.1. Overview

The purpose of this research was to determine the feasibility of pulling TF cable with a press-fit sleeve grip design that utilizes friction to generate a gripping force. Such a design is being considered by ITER for integrating (joining) 800 meter lengths of superconducting TF cable and conduit. In order to see if friction alone had the potential to withstand the required pulling load, test samples were created and subjected to tensile and fatigue loading until failure occurred. Additionally, finite element analysis methods were used to obtain a better insight into the deformation behavior of the cables.

3.2. Experimental Testing

Unsure of the capabilities of the press-fit grip sleeve design, two trial samples of an arbitrary grip sleeve length were created. Both samples were subjected to monotonic tensile loading until failure (slippage of the sleeve) occurred. Using the results of these tests as a guide, a subsequent series of full scale grip sleeve samples were made using the same design and tested under identical conditions. In addition to its gripping strength (the load at which slippage between the sleeve and cable occurs) during tensile loading, it was also important that the grip would withstand the variable loading that will likely occur during the pulling process due to the friction between the cable and conduit. Therefore, a period of cyclic loading, prior to tensile loading, was also incorporated into the testing program. Based on the results of each experiment, additional modifications were integrated into the design to try and maximize its gripping strength. Once the grip sleeve design was optimized, additional samples were tested under identical conditions to establish repeatability. The testing setup and procedure as well as detailed descriptions of each test sample are outlined in the Chapter 4.

3.2.1. Test Sample Materials

The materials utilized in this experiment to construct the test samples consisted of three main components: superconducting cable, thin walled stainless steel tubing, and a perforated stainless steel tube. The superconducting cable from which the test samples were made consisted of 1,422 individual wires which were wound into 6 strands, and finally into the actual conductor. In terms of the wire rope classifications described in Chapter 2, this superconducting cable is a single layer Right Lay Lang's lay rope with a lay length of 500 mm as can be seen in Figures 3.1 and 3.2.

Figure 3.1: Cross-section of conductor showing its 6 strand single layer construction

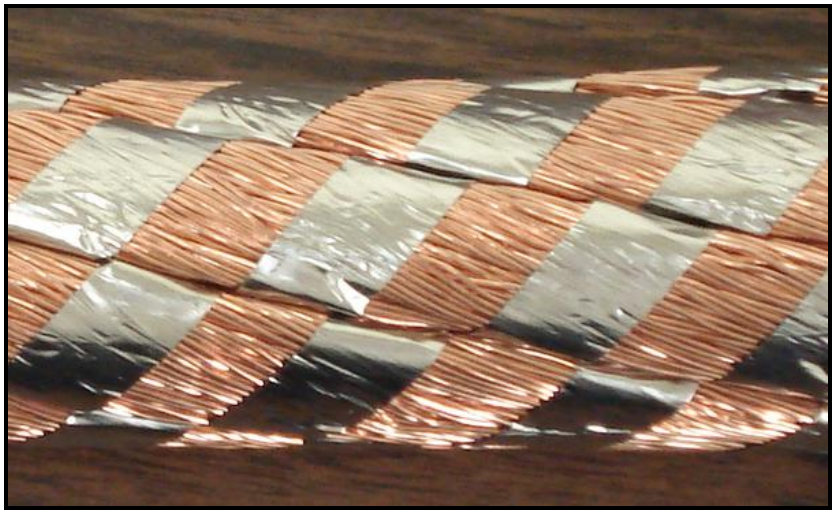

Figure 3.2: Side view of conductor showing its right laid Lang lay wire orientation

Each of the 1,422 wires that make up the cable strand has a diameter of 0.82 mm. The outer diameter of the conductor itself measures 40.2 mm with an estimated 8% void fraction amongst the packing of the strands and wires. Additionally, the conductor weighs approximately 0.41 lbs per inch, meaning each 800 m section will weigh over 13,000 lbs. The wires that will be used to create the actual conductor will be constructed from Copper with a core composed of a special alloy of Niobium and Tin (Nb_3Sn). Due to the expense of this material composition, the conductor used in these experiments consists only of Copper. Because of its non-superconducting properties, it is often referred to as "dummy" cable. The thin walled tube that was used in this experiment to construct the grip sleeves consisted of 47.6 mm dia. x 2.1mm wall thickness (1.875 in. x 0.083 in.) 316 Stainless Steel tube. The core tube that runs down the center of the conductor consisted of 9.52 mm dia. 1.25 mm wall thickness (0.375 in. x 0.05 in.) perforated stainless steel tube.

3.2.2. Types of Test Samples

All eight test samples that were utilized during this experimental process were of the press-fit configuration, meaning the only connection between the grip and the conductor were the forces due to friction. Unsure of the capabilities of this design, the testing process began by selecting an arbitrary grip sleeve length, constructing two samples, and tensile testing them until failure (sleeve slippage) occurred. Based on the results of these preliminary tests, a second set of grip sleeves were created, whose specific design parameters were based on the results of the previous experiment. This process was repeated until a total of 8 samples with 6 different grip sleeve configurations had been tested. Once the strength of the design exceed the physical limitations of the attachment coupling that was used to mate the sample to the testing machine, no additional changes were made and several identical samples were tested to establish repeatability. Details regarding the construction of each specimen and their test results are discussed in the results section found in Chapter 4.

3.2.3. Sample Construction and Preparation

All of the samples that were tested utilized the same press-fit design, but were built to a wide variety of specifications due to the outcome of each series of tests. As a result, some aspects of the construction process deviate from the standard procedure to accommodate these modifications. These specific design changes are not covered in this description, but will be described in detail as they occurred in the results section located in Chapter 4. A general summary of the construction of the first full scale sample is outlined below.

The design for the full scale test samples as proposed by ITER included an overall length of 1.1 m, of which 300 mm were compacted within each grip sleeve, and a section of exposed cable between the grip sleeves of no less than 500 mm. The term full scale corresponds to the distance between the grip sleeves, which for the TF cable is a minimum of 500 mm to allow for one full rotation of the cable based on its lay length. A rendering of this design can be seen in Figure 3.3.

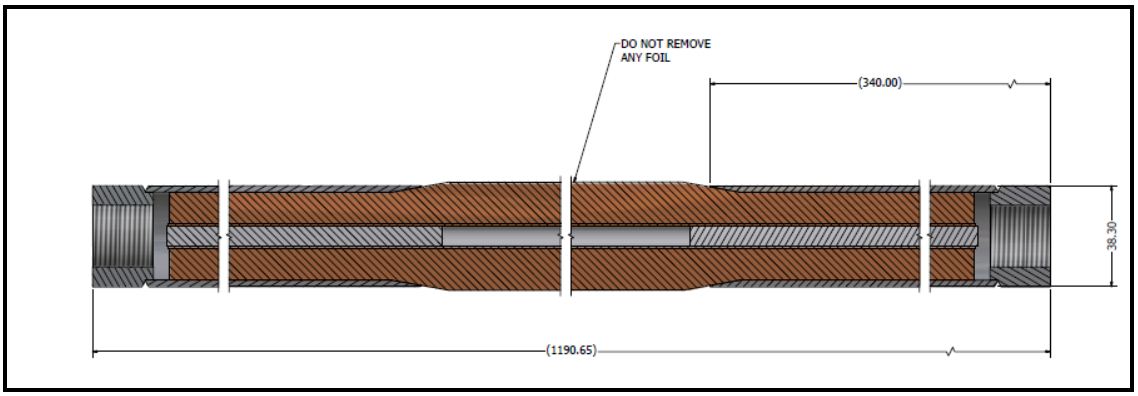

Figure 3.3: Rendering of full scale TF sample configuration [38]

Construction of a press-fit grip sleeve test sample began by creating 2 grip sleeves that would eventually be compacted around each end of the TF cable. This was done by cutting 2 pieces of the uncompacted TF conduit (47.57 mm diameter and 2.05 mm wall thickness stainless steel tube) to a length of 315 mm. The crimping machine was then used to swage one end of each piece down to a diameter of 38 mm so that a tensile lug

could be welded on before being "delivered to the field" for final crimping. Refer to Figures 3.4 and 3.5 for a schematic of the prepared sleeve.

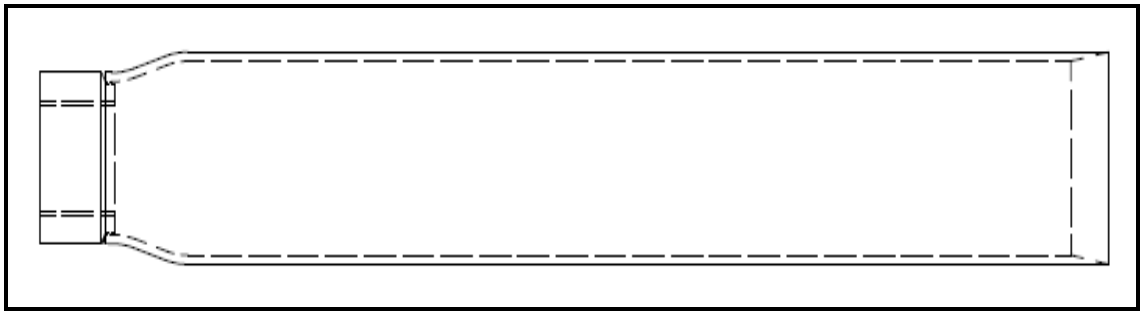

Figure 3.4: Proposed grip sleeve design with tensile lug [38]

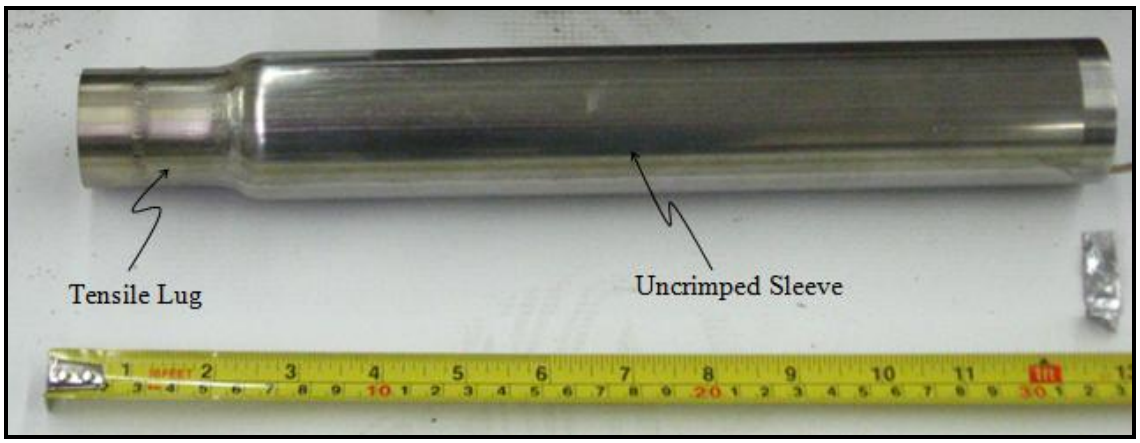

Figure 3.5: Actual pre-crimped grip sleeve with tensile lug

Next, the TF cable and assembled grip sleeves were laid out so that the appropriate length of cable could be determined. The drawing specified an overall cable length of 1132.68 mm, or roughly 300 mm inside each sleeve with 500 mm of exposed cable in between. This dimension had to be slightly modified due to the pre-crimping of the sleeves. As can be seen in Figure 3.6, the pre-crimping of the sleeve reduced its diameter to such a degree that the cable could only be inserted 270 of the proposed 300 mm.

Figure 3.6: Pre-crimped grip sleeve compared to nominal cable diameter

Therefore, the overall length of cable was reduced by 60 mm and cut to a length of 1069.975 mm to maintain the desired 500 mm of exposed cable between the sleeves. As can be seen in Figure 3.7, hose clamps were positioned at both ends of the cut to ensure that the cable and foil wrap would not unwind as it was separated.

Figure 3.7: Hose clamps positioned around cut to prevent unwinding

Next, a solid stainless steel rod (O-1 tool steel) of 7.5 mm diameter was cut into 292 mm lengths. One of these rods was then inserted into the core tube at each end of the sample (see Figure 3.8) by gently tapping the opposite end of the rod. Their purpose was to simulate the effect of a solid core within the region of compaction by providing additional rigidity and preventing the hollow core tube from being deformed during compaction.

Figure 3.8: Insertion of solid rod into core tube of TF cable

Then the ends of the cable were inserted into the grip sleeves in preparation for the compaction process as shown in Figure 3.9.

Figure 3.9: Grip sleeve positioned on TF cable prior to compaction

Finally, the sleeves were gradually swaged down with the crimping machine until an average outer diameter of 38 mm was reached. A summary of the swaging process is depicted in Figures 3.10 – 3.14.

Figure 3.10: Val Power material crimping machine used during test sample fabrication

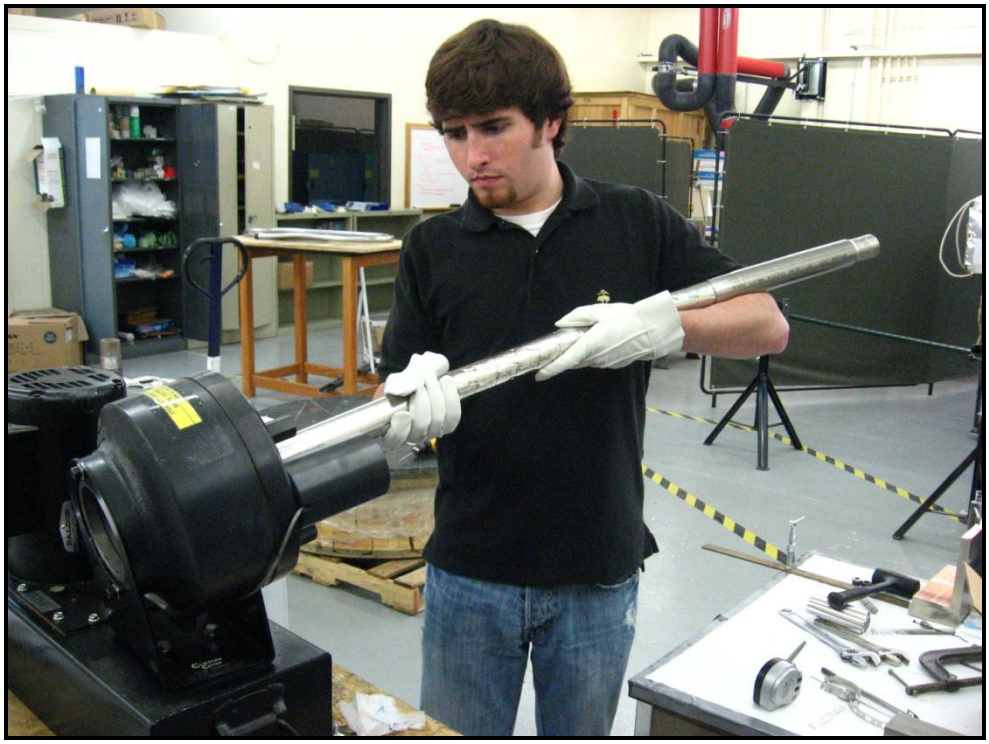

Figure 3.11: Initial stages of TF grip sleeve compaction

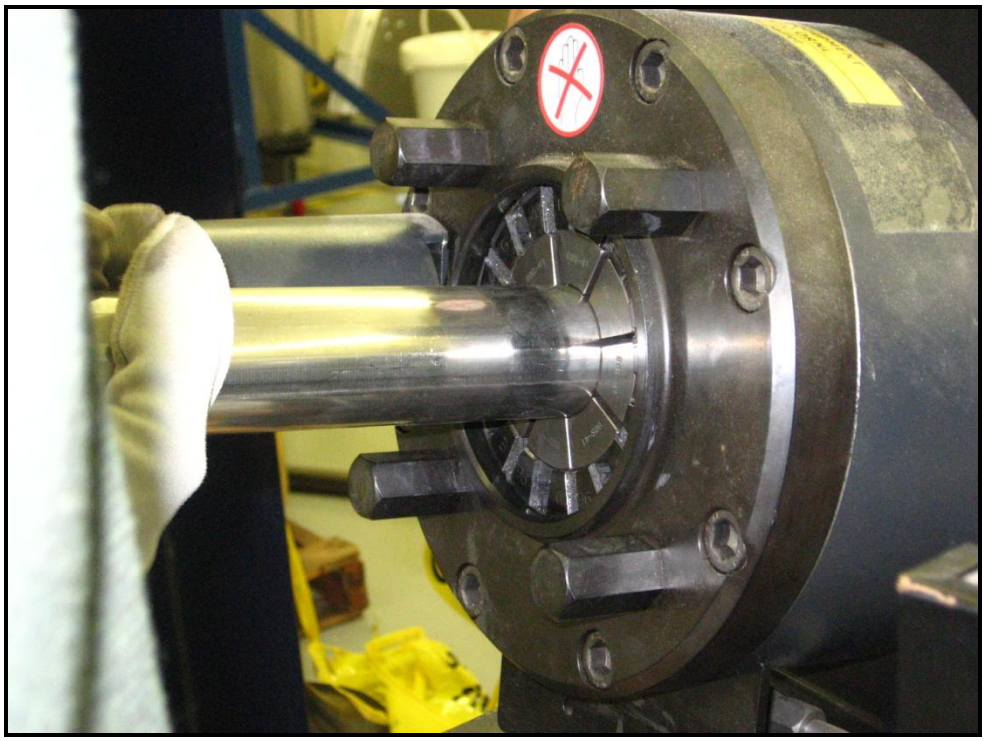

Figure 3.12: Jaws of crimping machine fully compressed around grip sleeve

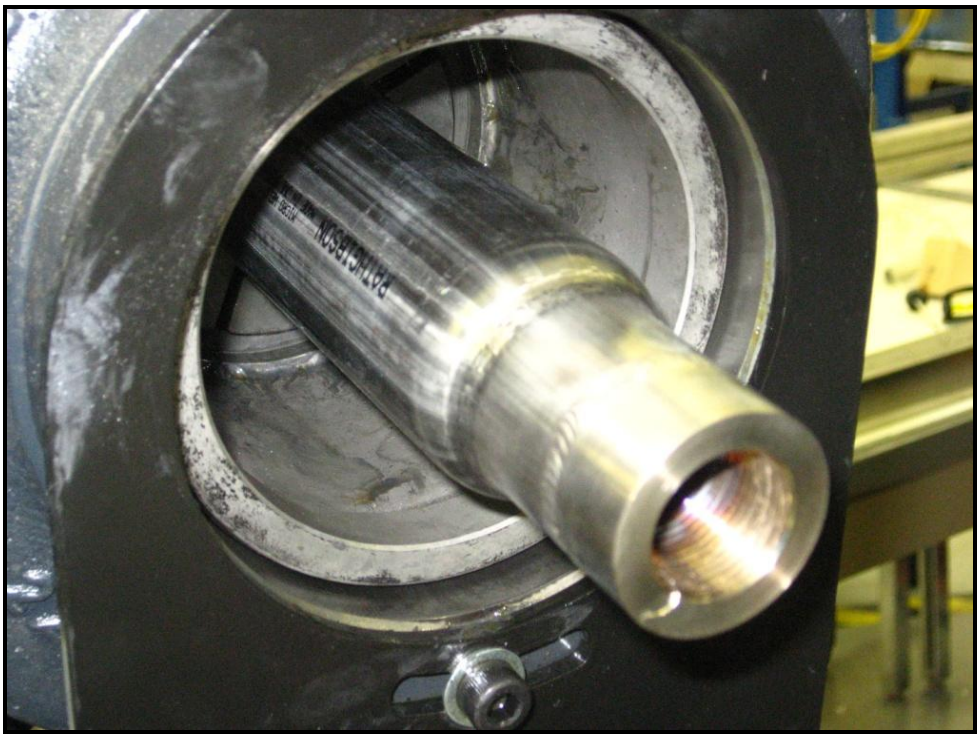

Figure 3.13: Grip sleeve exiting from crimping machine

Figure 3.14: Fully assembled full scale TF pull test sample

Throughout the fabrication process of the full scale sample, the average diameter of the grip sleeves as well as the overall length of the sample was measured. The results of this compaction process are displayed in Table 1. Note that the initial and final lengths and diameters of the sample are highlighted in red.

Table 1: Summary of TF Cable Compaction

After 0 mm of Compaction	
Length: 1.175 m	**Diameter:** 47.60 mm
After 1.5 mm of Compaction	
Length: 1.178 m	**Diameter:** 46.10 mm
After 3 mm of Compaction	
Length: 1.180 m	**Diameter:** 44.85 mm
After 4.5 mm of Compaction	
Length: 1.183 m	**Diameter:** 43.30 mm
After 6 mm of Compaction	
Length: 1.188 m	**Diameter:** 42.88 mm
After 7.5 mm of Compaction	
Length: 1.202 m	**Diameter:** 40.28 mm
After 9 mm of Compaction	
Length: 1.222 m	**Diameter:** 38.00 mm

Notes regarding compaction process:

- The first 6 mm of compaction were done in increments of 0.5 mm, while the final 3 mm in increments of 0.25 mm due to a noticeable overloading of the machine.

- Each stage of compaction was performed to both sides before moving on to a new setting.
- Multiple breaks were taken during the compaction process to allow the crimping machine to cool down. The machine used was not equipped with a cooling fan, nor was it designed to work on continuous duty, and would quickly overheat.
- Due to the slow rate of compaction as well as the need to allow the machine to rest, the entire process took around 12 hours to complete.
- The overall length of the sample increased by 0.047 m. during the compaction process.
- Due to the pre-crimping of the sleeves to weld on the tensile lugs, work hardening over a small area (see Figure 3.15) of the grip sleeve was observed.

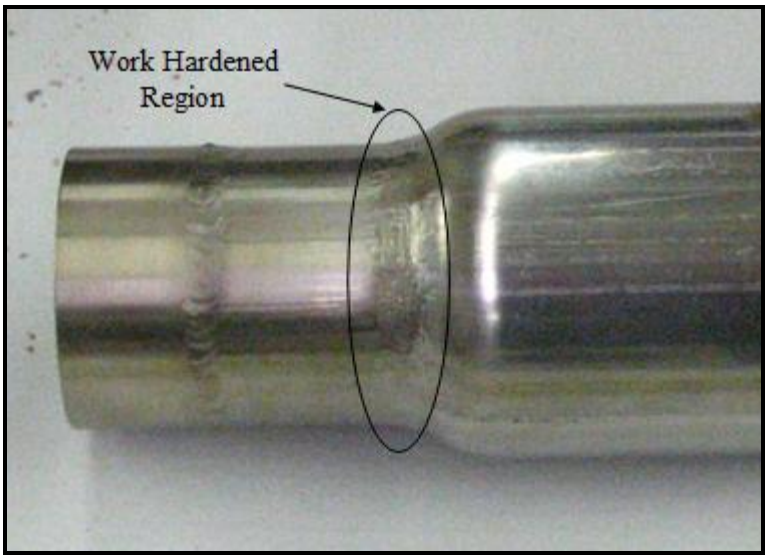

Figure 3.15: Work hardened region on pre-crimped sleeve

3.2.4. Method of Attachment to Test Fixture

Having settled on the press-fit sleeve design as the first configuration to test, the next step was to select a coupling to fasten the grip sleeve to the testing apparatus. This same coupling would also be used to join the conductor and the winch cable during the actual cable pull, so it had to be low profile enough to fit through the conduit. Of the

many potential designs, the best option was a threaded tensile lug. The tensile lug consisted of a cylindrical piece of steel of the same outer diameter as the grip sleeve that featured a female threaded axial hole (see Figures 3.16 and 3.17). The tensile lug would be connected to the grip sleeve with a circumferential seam weld. A threaded stud would then be used to connect the tensile lug and sample to the testing apparatus. This design was chosen for a variety of reasons, the main one being that it offered a very slim profile that would ensure it could easily be pulled through the conduit. Additionally, the ends of the grip sleeves could be pre-crimped and the tensile lugs welded on in advance, which would speed up the installation process and eliminate the need for a welder in the field. For the experimental tests, a tensile lug would be used to connect the sample at both ends.

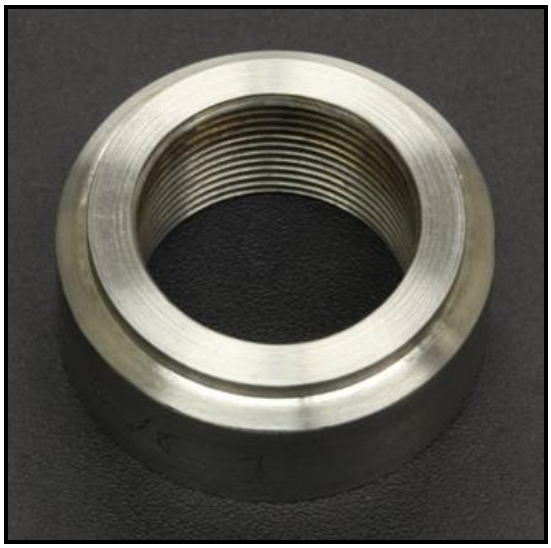

Figure 3.16: Bottom view of threaded tensile lug

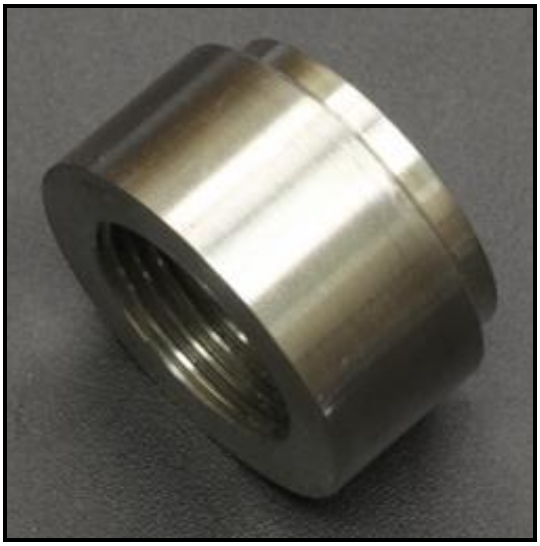

Figure 3.17: Side view of threaded tensile lug

3.2.5. Testing Descriptions

Tensile testing

Tensile testing of the samples was performed using 20kip MTS and 220kip Interlaken material testing systems, both or which were hydraulically actuated as opposed

to screw driven. As will be described in Chapter 4, two different machines had to be used because two sizes of samples were being tested, the longer of which was expected to withstand a much greater load. For tensile testing, the machines were operated in displacement control.

The requirements for the gripping device as provided by ITER did not specify any stress or strain limitations. Their only qualifications were that the grip could withstand the tensile load required to pull the 800 m length of cable through its conduit, which based on an experiment performed by the Russian, was 8000 lbs. Therefore, the only parameters which would be monitored during testing were force with respect to displacement and with respect to time. The performance of each sample would be evaluated based on a plot of each of these data sets. Increasing slope meant resistance to slippage, and similarly, decreasing slope meant slippage was occurring. In addition to observing failure with the graphical output, a visual inspection of each sample during testing would also be performed. Sleeve slippage, cable breaking, sleeve malfunction, and weld fracture would all be considered failure.

Fatigue testing

During this phase of testing, only one sample size was used, so the 220kip Interlaken machine was the only material testing system required. For fatigue testing, the machine was operated in load control mode rather than displacement control. As was the case with tensile testing, the only parameters of interest were force and displacement with respect to time. The performance of each sample would be evaluated based on a plot of each of these data sets. Additionally, the same failure criteria used for tensile testing would be applied to fatigue testing as well.

3.3. Finite Element Analysis

In order to validate the results of the experimental testing, finite element analysis was performed using the commercially available Comsol Multiphysics software. When performing a finite element analysis, the best approach is to use the simplest geometry

possible that still contains all of the features necessary to recreate the physical situation of interest. Often times, a three dimensional model can be accurately represented with a two dimensional model by utilizing axisymmetry. When a three dimensional model is mandatory and the geometry and stresses are symmetric, another common simplification is to "quarter" the work piece and only model a fraction of the actual geometry. However, due to the helical geometry of the work piece that was being modeled, neither of these simplifications was applicable. Furthermore, due to the complex geometry of the coil we were modeling, the drawing capabilities of Comsol could not accommodate all of the features. As a result, Autodesk Inventor CAD software was used to create the coiled feature of the cables and these parts were then imported into Comsol.

3.3.1. Geometric Modifications

Despite the fact that the traditional geometric modifications were not applicable, there were still several other ways to reduce the complexity of this model; the first being to modify the shape of the components. The actual superconducting cable consisted of a round sleeve with round strands and a round core, but in the FEA models, these same components were based on octagonal and dodecagonal cross sections. The purpose for this change came about due to the inability to obtain solutions to models with round strands in contact with a round grip sleeve. When you consider the contact surface between circular objects, the problem becomes clear. The contact area between a circular strand and sleeve is a straight line with no true surface area whereas the octagon and dodecagon sleeve have an actual surface area that can be calculated (see Figure 3.18 and 3.19). Note that the contact area is represented by the red lines between the surfaces.

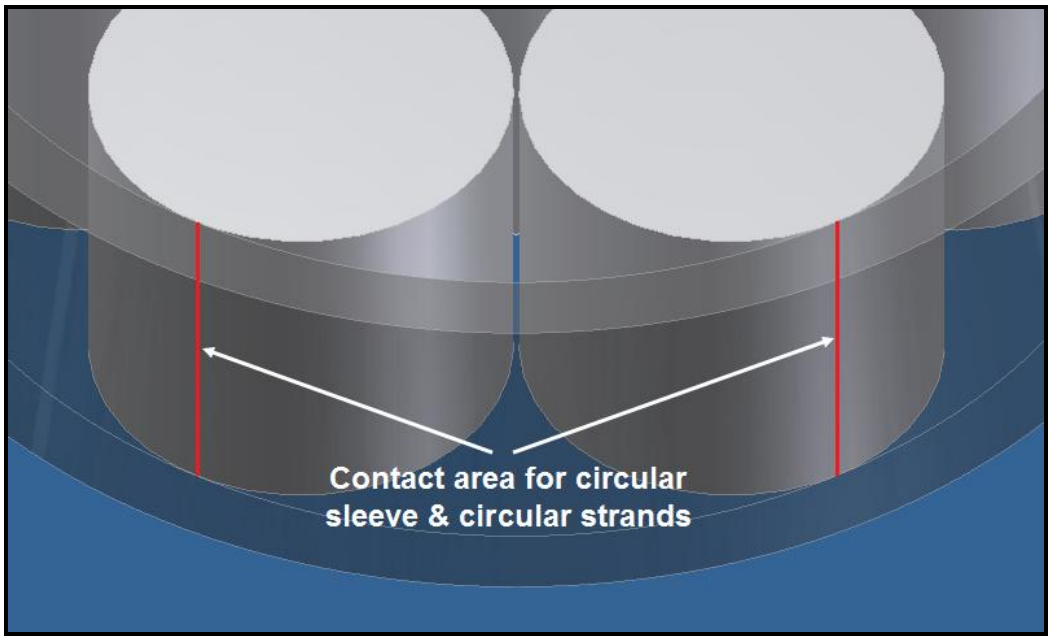

Figure 3.18: Contact area of circular strands with circular grip sleeve

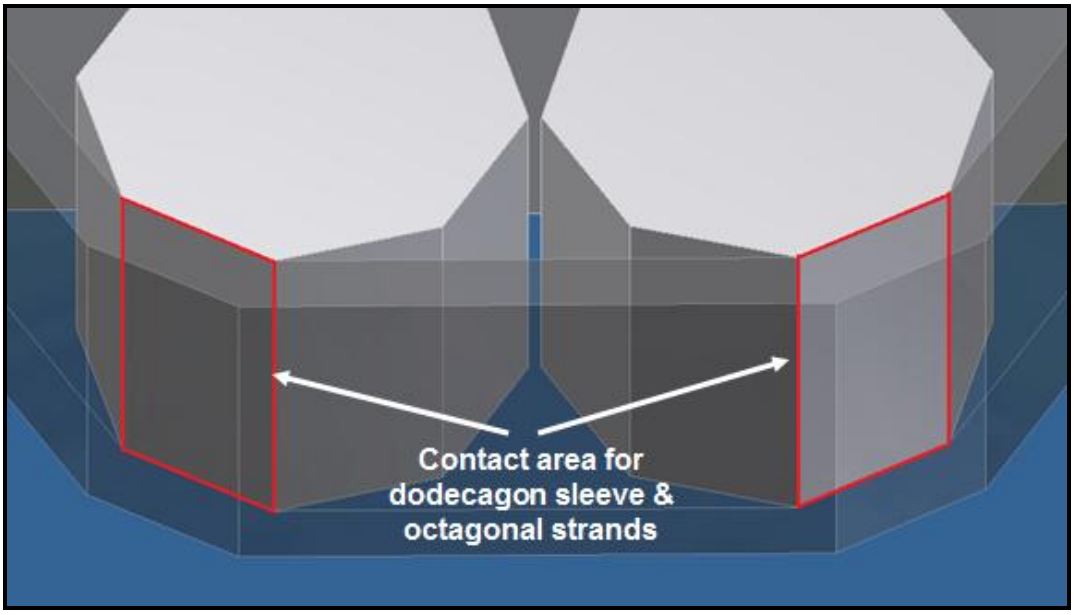

Figure 3.19: Contact area of octagonal strands with dodecagon grip sleeve

Based on this observation, several Comsol models of different geometries were created to test the effect of various contact schemes between the sleeve and strands. In each model, the bottom surface of the grip sleeve is fixed, a compressive face load is applied to all surfaces of the grip sleeve, the core is rigidly connected to the strands, friction holds the strands to the inner surface of the sleeve, and the top of each strand is

displaced vertically. As can be seen from Figures 3.20 and 3.21, the square strands with square sleeve and octagonal strands with octagonal sleeve showed a very similar pattern of displacement. Additionally, there were no problems with singularity due to the sufficient contact areas of both geometries, and solutions to both models were very easy to obtain. In order to develop a model which would eliminate the contact area problem while still providing an accurate cross section of the actual conductor, it was decided that all models would be based on an octagonal strands with a dodecagon sleeve.

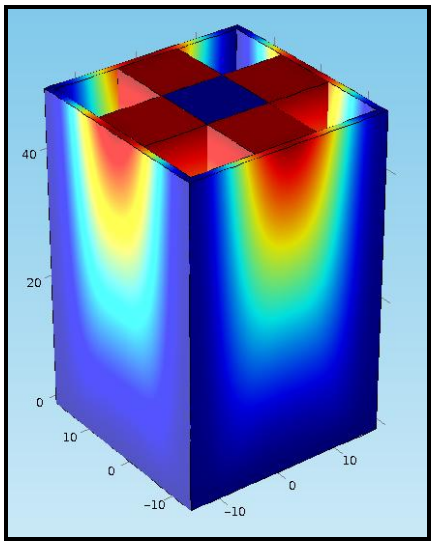

Figure 3.20: Displacement of square sleeve and strands subjected to tensile loading

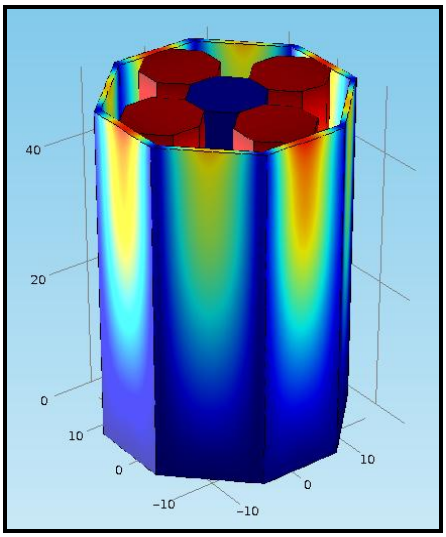

Figure 3.21: Displacement of octagonal sleeve and strands subjected to tensile loading

Another modification that was incorporated into the model was the reduction of the number of individual wires that make up the cable. The actual TF conductor consists of 1,422 wires that are wound together to form 6 strands or sub-cables, which are then wound together to form the conductor. Due to the complexity of modeling and meshing an object consisting of over 1000 parts, it was decided that the conductor could be accurately represented with a cross section of 6 solid strands with solid core in the middle. An example of this cross section can be seen in Figure 3.22. Note the octagonal strands and the dodecagonal core and grip sleeve.

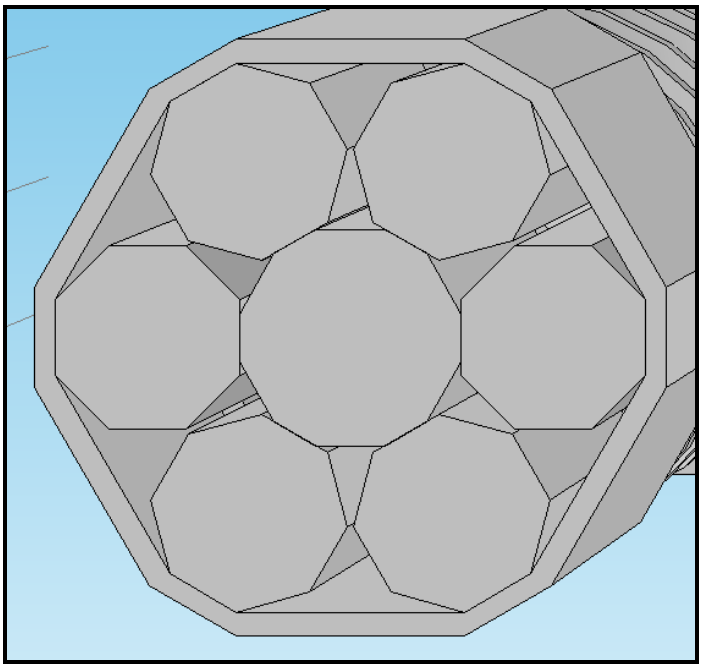

Figure 3.22: Cross-section of FEA model showing single layer 6 strand construction with octagonal strands and dodecagonal core and sleeve

Another modification was to make the portion of the strands that would be covered by the grip sleeve straight lay as opposed to helical lay on all of the models. Due to the long lay length of the conductor and the comparatively short length of the grip sleeve, the loss of cable length, and thus surface area between the grip sleeve and strands in an all vertical orientation as compared to a helical orientation would be insignificant. Furthermore, the sleeves compacted around this portion of the strands were preventing them from untwisting while under tensile load, so making them straight would not effect the results. Additionally, applying forces to straight strands proved to be much less complicated because it was easier to mesh and maintain continuity. It was very difficult to get the mesh elements to line up between the strands and sleeve when the cable and thus its elements are twisted but the sleeve and its elements are straight. This modification also made it easier to apply boundary conditions. Several of the loading conditions that were applied to the FEA models involved creating pairs between the surfaces that are in contact with one another. Due to the helical orientation of the cable, the same strand would actually come into contact with more than one surface, whereas

straight strands would only contact one surface. An example of this geometric modification can be seen in Figure 3.23 below. Note that the coiled portion of the cable is only 150 mm instead of the actual 500 mm in order to show more detail.

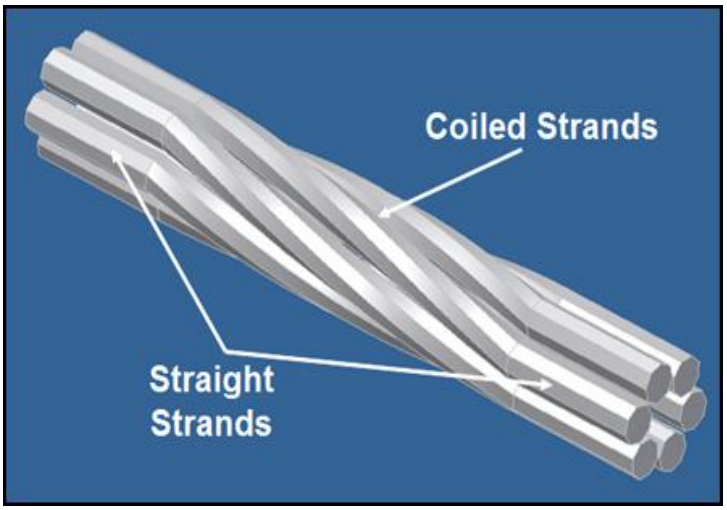

Figure 3.23: FEA model without grip sleeve to show combination of coiled and straight strand geometry

The final simplification was to model the samples without the tensile lugs attached to the ends. As was described above, the tensile lugs are only attached to the grip sleeve and do not interfere with the wires at all. Therefore, a load applied to the tensile lug would transfer that load to the grip sleeve in the same way that a load could be applied directly to the grip sleeve.

3.3.2. Solver Settings

In general, Comsol's default solvers are sufficient to obtain a solution to a standard type of model. However, when dealing with a model this complex, several specific features need to be incorporated into the solver settings to aid in convergence of a solution. These include a parametric solver and manual scaling of the variables. The parametric solver assists the standard direct solver in finding a solution by allowing it to vary the magnitude of the dependent variables over a specified range. For the purposes of the models used in this analysis, it was tied to the displacement of the grip sleeve. Rather

than trying to obtain a solution based on the entire displaced distance right away, the parametric feature allowed the solvers to begin with a fraction of that distance, then it would gradually increase that displacement value based on the prescribed range as the solutions began to converge.

The other crucial solver setting was the use of manual scaling. Manual scaling refers to the act of reducing the magnitude of the dependent variables in the model by scaling (or dividing) them by a number which is of the order of their calculated value. For example, assume that in a structural mechanics problem the displacements are of the order of 0.0001 m while the stresses are 1,000,000 Pa. The result is likely to be an ill-conditioned matrix. By scaling the displacement by 10^{-4} and the stresses by 10^{6}, the resulting variables are now of the order 1 [39]. Comsol is designed to take care of this procedure automatically, but depending on the complexity of the situation, solution times will become excessive and in many cases, the solver will reach its maximum number of iterations before a solution is able to converge. Therefore, if the order of magnitudes of the variables is known in advance, it is advantageous for the user to scale the variables themselves.

Chapter 4
Results and Discussion

4.1. Experimental Test Results

4.1.1. Preliminary Tests

A series of tensile tests were conducted on the proposed press-fit grip sleeve configuration to evaluate its feasibility for the 800m TF cable pull. Anticipating that each trial sample would fail at loads that were less than 20,000 lbs, the trial sample pull tests were performed using a 20kip MTS 810 Test System. A photograph of this equipment setup can be seen in Figure 4.1.

Figure 4.1: Equipment Setup for Preliminary Pull Tests

The grip sleeve design that was being tested during this experiment was of the press-fit configuration, meaning the only connection between the cable and grip sleeve was the friction force created when the sleeve is compacted around the cable. The grip sleeves consist of a length of thin wall stainless steel tube which was compacted around a piece of TF cable. Both samples were based on this same design, the only difference

being the perforated steel tube (outer diameter ~ 9.4 mm, wall thickness ~ 1 mm) that was placed at the core of one of the samples. In subsequent sections of this report, these samples will be referred to as TF – WC1 and TF – WOC1; TF indicating Toroidal Field conductor, WC and WOC indicating with and without core, respectively, and 1 being that these are the first samples in the series. Once both samples were compacted, a small groove was machined out of the center of the steel sleeve until the strands of the TF cable were visible around the entire perimeter. The purpose of this groove was to create two separate grip sleeves that could slip independently when placed in tension. A detailed schematic of each conductor sample and photographs of their cross-sections can be seen below in Figures 4.2 and 4.3.

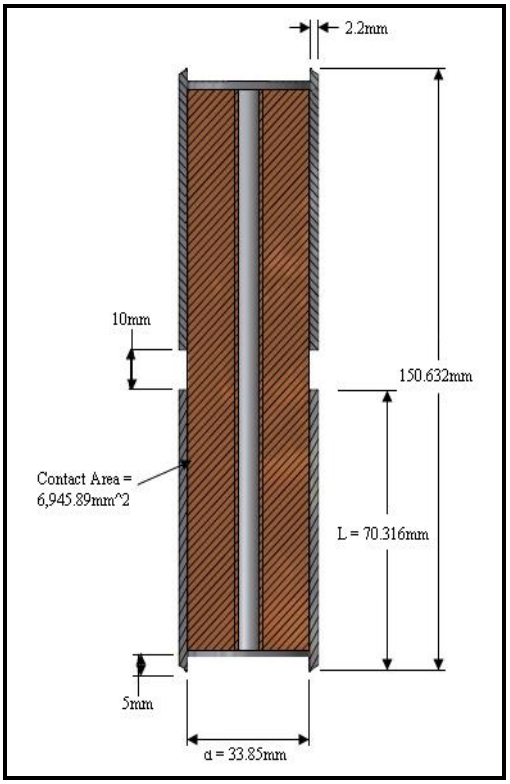

Figure 4.2a: TF – WC1 Schematic

Figure 4.2b: TF – WC1 cross-section

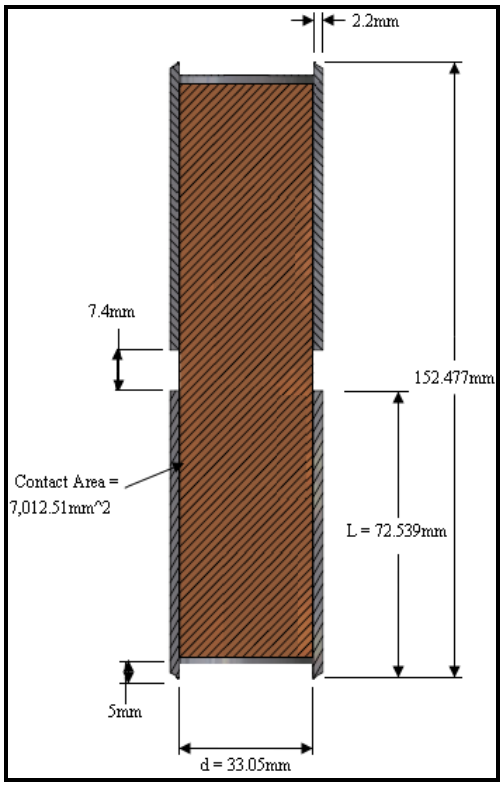

Figure 4.3a: TF-WOC1 Schematic

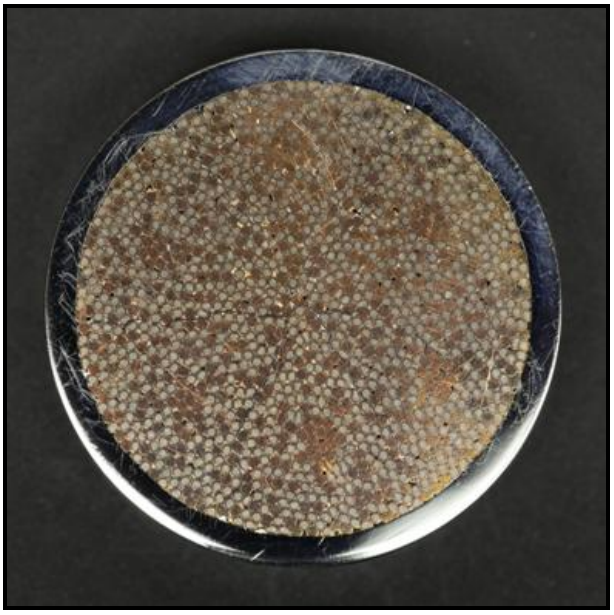

Figure 4.3b: TF-WOC1 Cross section

The first grip configuration to be tested was the TF – WC1 sample. Interested in the axial load required to cause the sleeve to slip from the conductor strands, the MTS machine was operated in displacement control mode rather than load control mode. Held in place only by friction forces, it was expected that the sleeve would slip fairly rapidly once tension was applied. Therefore, a conservative displacement rate of 0.1 mm per second was selected. Additionally, a sampling rate of 2 data points per second was chosen to ensure that a sufficient amount of data points were collected. The sample was then connected to the test fixture using 1 in. - 14 female thread stainless steel tensile lugs which were seam welded to both ends of the sample. Male threaded studs of a corresponding diameter were then used to attach the sample directly to the machine's load cells (See Figure 4.4).

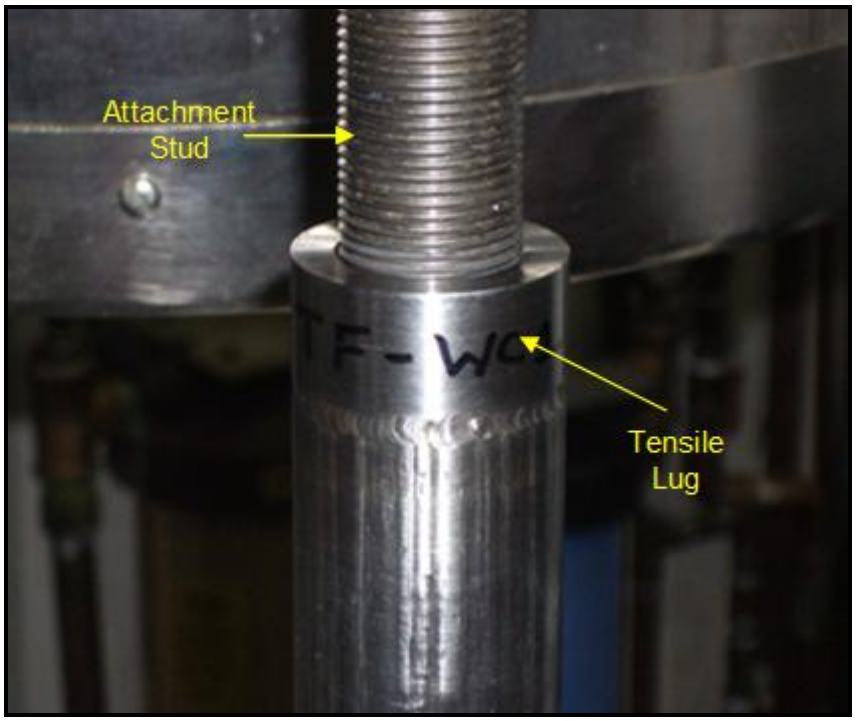

Figure 4.4: Threaded stud connected to tensile lug

In order to monitor slip between the grip and cable, an extensometer was positioned in the gap between the sleeves (See Figure 4.5).

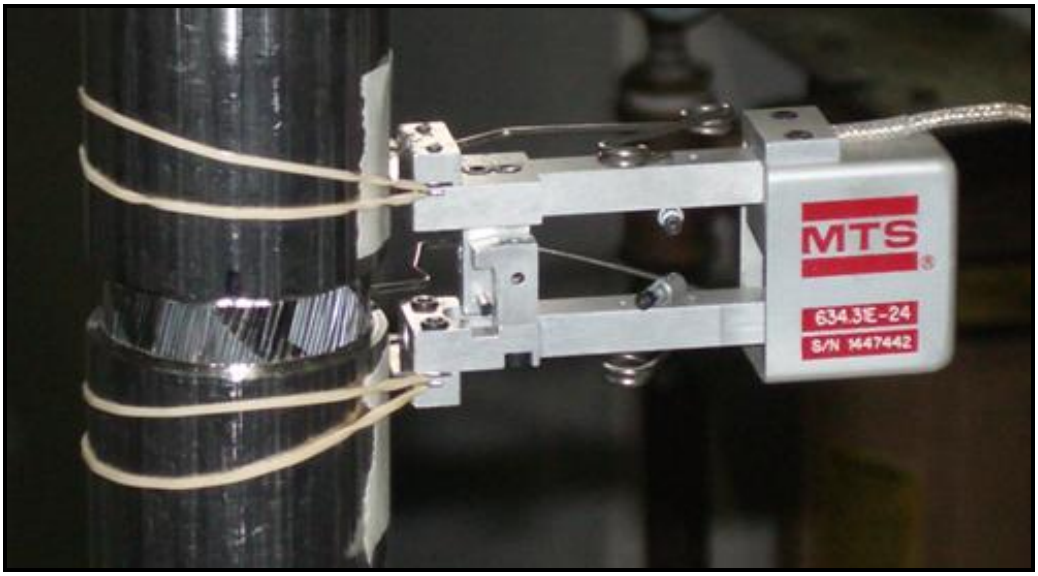

Figure 4.5: Extensometer set-up used in preliminary testing

Progress of the test procedure was monitored in real time by a graphical output of the axial force.

Before testing began on the TF-WOC1 sample, a slight change had to be made to the test procedure. Reaching its failure load after only 65 seconds, the displacement rate used for the TF-WC1 sample proved to be a bit too high and was reduced to 0.05 mm per second. Having obtained sufficient data during the first test, a data sampling rate of 2 data points per second was chosen for this test as well. Utilizing the same method of attachment as TF – WC1, this sample was then connected to the MTS machine and the same loading process was repeated.

Based on the force and displacement data collected during these tests, a series of plots were created to evaluate the performance of the TF-WC1 sample as compared to the TF-WOC1 sample. A comparison of the axial force versus time and axial force versus displacement for both configurations are displayed below in Figures 4.6 and 4.7. For clarification, a schematic of the samples being compared and a list of their key features are displayed next to each plot. Note: the number associated with each schematic is also displayed on the plot next to the data series that it represents.

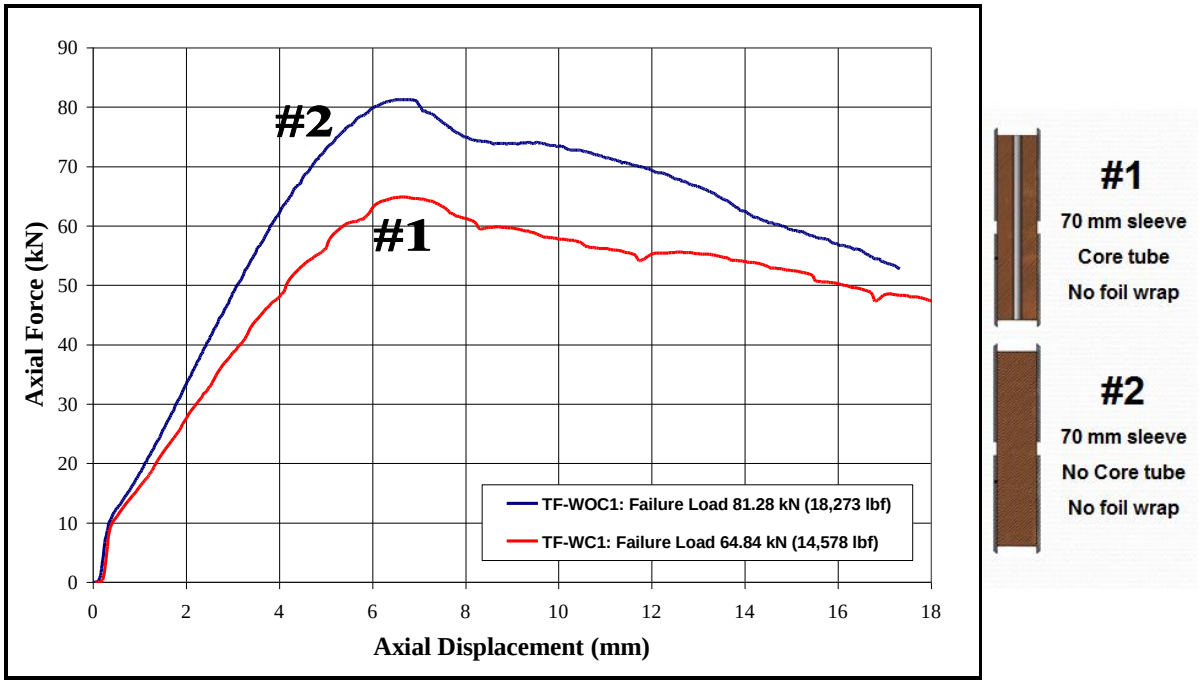

Figure 4.6: Axial Force vs. Displacement for TF-WOC1 and TF-WC1

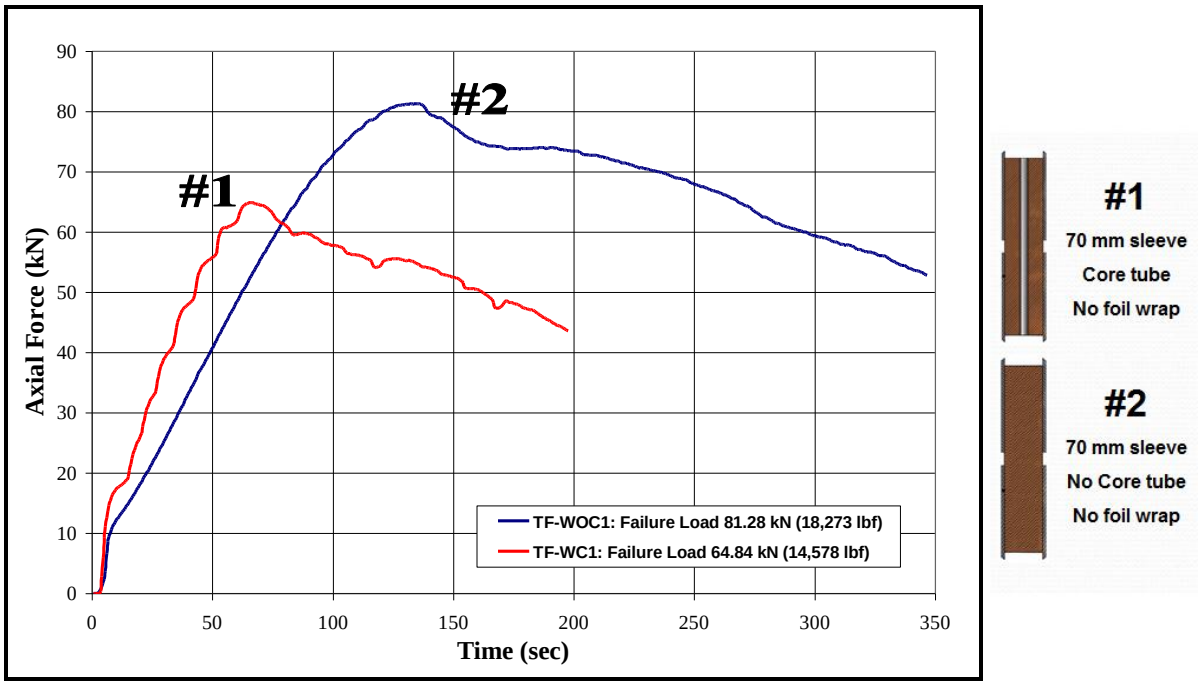

Figure 4.7: Axial Force vs. Time for TF-WOC1 and TF-WC1

As can be seen in Figures 4.6 and 4.7, TF-WC1 and TF-WOC1 reached maximum loads of 64.84 kN (14,578 lbf) and 81.28 kN (18,273 lbf), respectively. Based on these results, several observations can be made; the first being that both configurations of the trial grip sleeve withstood substantial loads before failing (slipping). A surprising observation is that TF-WOC1 failed at a load that was 16.44 kN (3,696 lbf) higher than TF-WC1. From Figure 4.2a and 4.3a we can calculate the cross-sectional area occupied by the strands in each sample. For the WOC1 and WC1 samples, this area is about 856 and 831 mm^2, respectively. Since both samples share the same number of strands and were compacted to within 0.8mm of the same outer diameter, one would expect that the sample with the core tube would experience a higher contact pressure because there is less area available for the strands. It was surprising to see that the WC1 sample failed at a lower load than the WOC1 sample. Additional tests need to be conducted to understand this unexpected behavior. There may be two possible explanations for this behavior: 1) the hollow perforated tube did not provide enough rigidity (as can be seen from the deformation of the core tube in Figure 4.2b, and 2) the strands in the WC1 specimen were deformed beyond their elastic limit (Yield Strength), thereby decreasing the reactive

force from the strands on the sleeve. With the help of photomicrographs of these samples, this issue is further discussed at the end of this section.

Another important observation to make from Figures 4.6 and 4.7 is the decrease in the load after the specimens reached their maximum value. The decrease in load was accompanied by the increase in space between the grip sleeves, as can be seen in Figures 4.8 - 4.11. This increase in space suggested that slippage of the grip sleeves with respect to the strands had occurred.

Figure 4.8: TF-WC1 grip sleeve position before testing

Figure 4.9: TF-WC1 grip sleeve position after testing

Figure 4.10: TF-WOC1 grip sleeve position before testing

Figure 4.11: TF-WOC1 grip sleeve position after testing

In addition to the axial force and displacement data collected by the test system, an extensometer was also utilized to measure the displacement of the grip sleeves, which it would then translate to an axial strain value. This particular extensometer was only capable of measuring up to a 5% extension of its 25.4 mm gauge length, meaning that it would quickly become ineffective when the sleeves slipped more than 1.27 mm. As can be seen in Figure 4.12, the recorded data proved to be insignificant as the extensometer exceeded its limit in a matter of seconds, as indicated by plateau of the load versus axial strain curves.

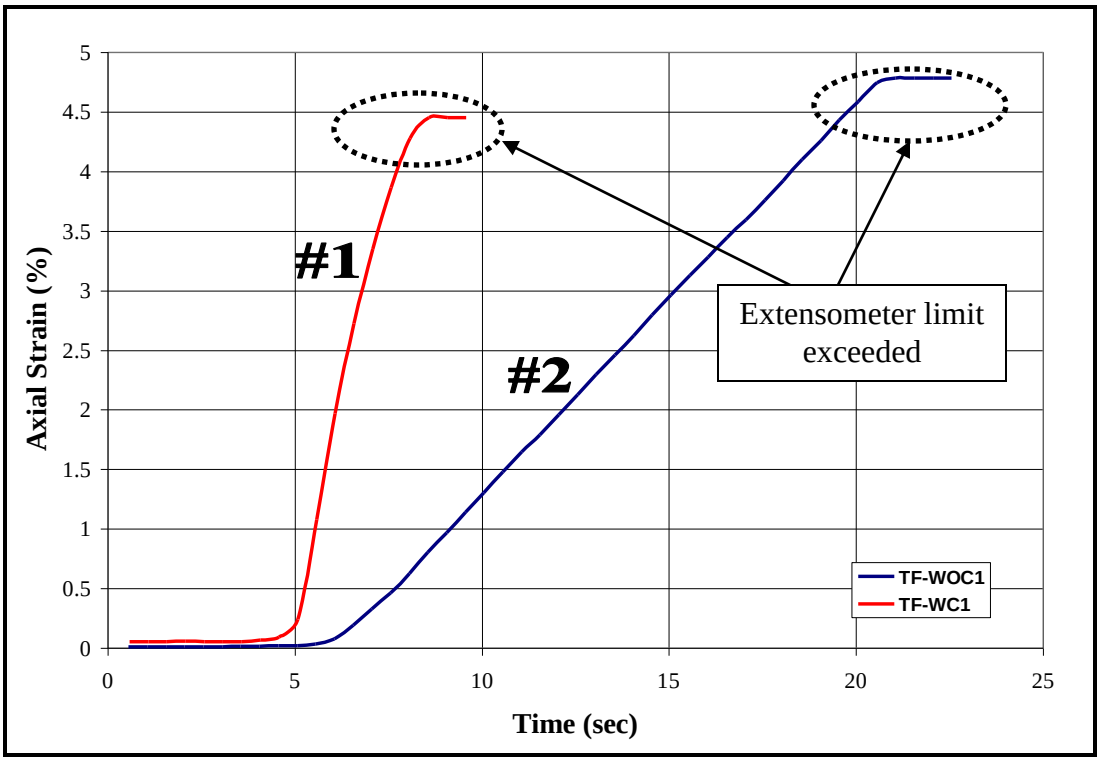

Figure 4.12: Axial Strain for TF-WC1 and TF-WOC1 measured by extensometer

In addition to the numerical results obtained with the MTS data acquisition software, a physical inspection of each specimen revealed a series of visual effects, one being the removal of the Chromium coating from the Copper conductor strands. When the TF cable is created, a thin layer of protective Chromium coating is applied that gives the cable a gray finish. After the pull test was performed, vertical lines of Copper appeared on the surface of the conductor strands from where the Chromium was scraped off as the grip sleeve slipped (See Figures 4.13 and 4.14). It is interesting to note that these sections of exposed copper took a completely vertical orientation, rather than following the pitch of the cable.

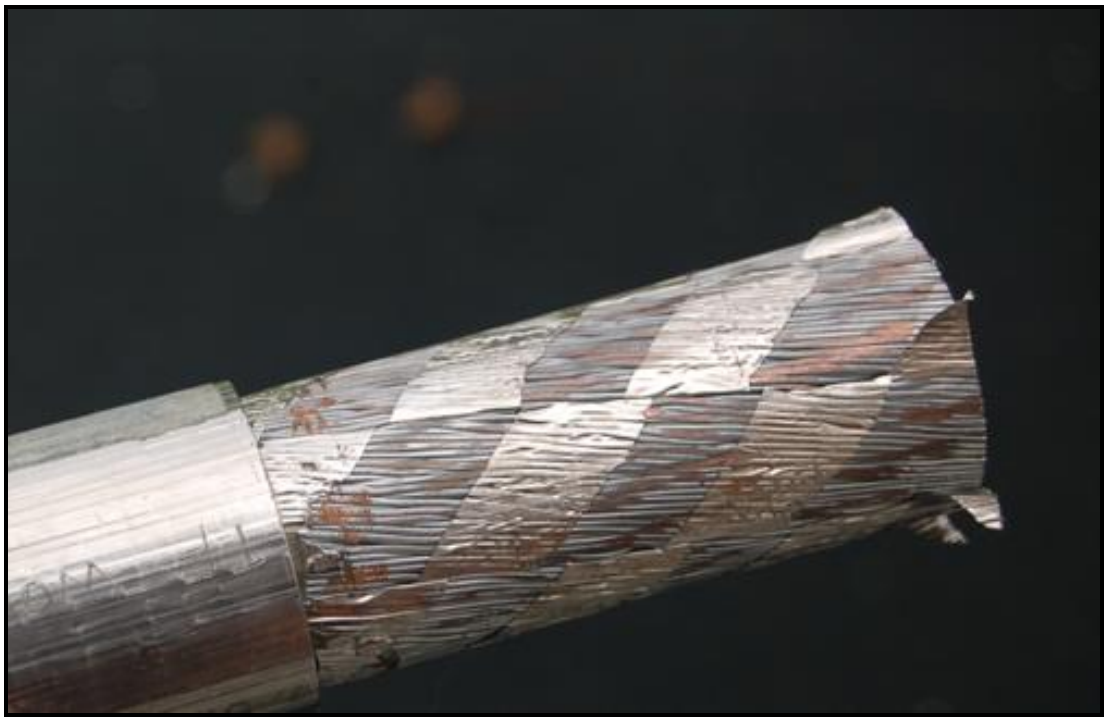

Figure 4.13: TF – WOC1 Copper Cable Exposure from grip sleeve slippage

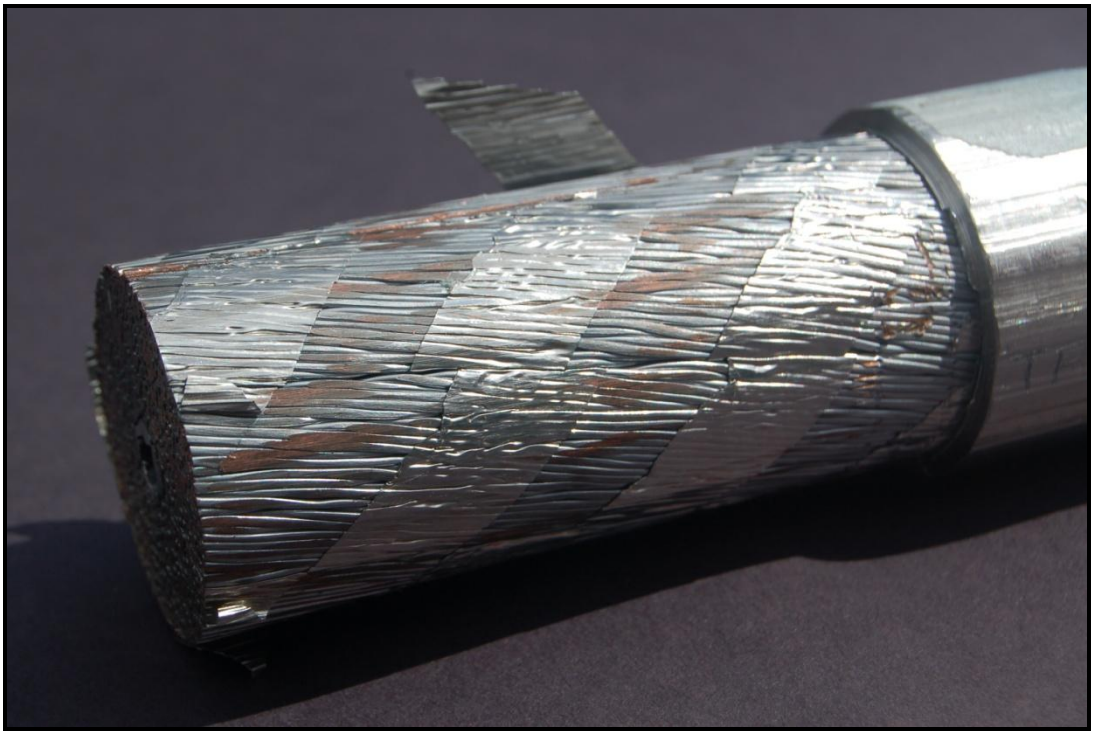

Figure 4.14: TF-WC1 Copper Cable Exposure from grip sleeve slippage

The final observation to be made from a visual inspection of each sample was that the strands of the cable embedded themselves into the inner surface of the stainless steel grip sleeve (See Figure 4.15). These sleeve indentations are believed to increase the frictional force between the sleeve and strands, and thus increase the gripping force of the press-fit sleeve design.

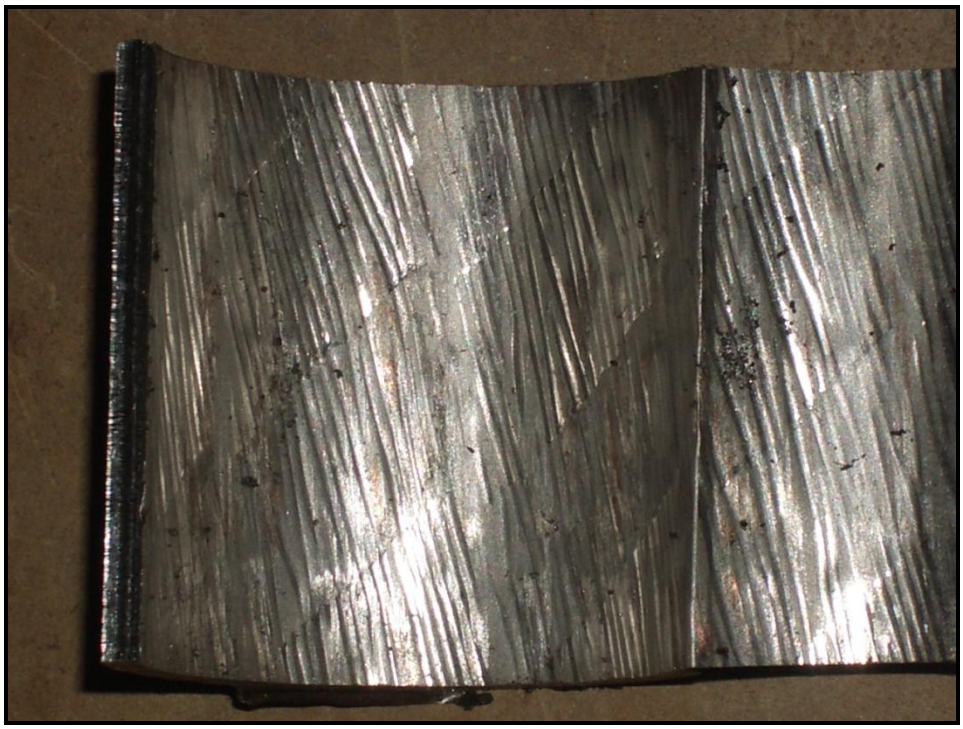

Figure 4.15: Indentions of cable strands on grip sleeve due to contact pressure

To examine the deformation of the strands due to the compaction of the sleeve on the strands, about 13 mm (½ in.) sections of each grip were cut out in the direction perpendicular the strands, polished and examined under an optical microscope. The intent was to look at the size and shape of the strands at different locations to evaluate the degree of deformation. These micrographs are shown in the appendix at the end of this section. More strand deformation was observed in the WC sample compared to that in the WOC sample. The sample with greater strand deformation is more likely to have plastically deformed, meaning that the strands are less resilient and would not be contributing as much to the contact pressure as strands that had only elastically deformed.

Based on these results, it can be concluded that the press-fit grip sleeve is an effective design that shows great potential for use in the 800 m TF cable pull. It can also be concluded that the TF-WOC1 sample was the more capable of the two variations, and all future designs should be based on this configuration. Despite the fact that the TF-WOC1 sample with its 75 mm grip sleeve was capable of a supporting a load greater than what is required, a second series of tests were performed with a larger grip sleeve. In addition to the larger grip sleeve, the length of exposed cable between the grip sleeves was increased to at least 500 mm to allow for one full rotation of the cable based on its pitch.

4.1.2. Full Scale Testing

Based on the results of the preliminary tests, the grip sleeve design was slightly modified and a tensile test was performed on the first of six full scale TF press-fit grip sleeves. Due to insufficient travel and load capacity, the 20 kip MTS testing system used for the TF-WC1 and TF-WOC1 samples could not be used to test these full size samples. Therefore, the pull test for the TF-WC2-FS sample was conducted using a 200 kip Interlaken Series 3300 universal testing machine. For more information regarding the specifications and construction of this sample, refer to 3.2.3 of this report. Because of the elevated loads that these specimens would be experiencing, the machine's standard hydraulic wedge grips would not suffice. Therefore, attaching the cable sample to the test fixture was accomplished using a combination of high strength threaded adapters. The main portion of the lower mount utilized a static connection, consisting of a 73 mm (2.875 in.) diameter externally threaded cylindrical coupling with an axial hole that would accept 25.4 mm (1 in.) diameter male threads. As can be seen in Figure 4.16, this coupling served as the lower anchor and was threaded directly into the test fixture's hydraulic actuator.

Figure 4.16: Base component of static coupling attached to hydraulic actuator

Adapting this lower anchor to the tensile lug on the test specimen was accomplished with a section of 25.4 mm (1 in.) diameter all-thread rod. This series of components and stages of their assembly are depicted in Figures 4.17 – 4.18.

Figure 4.17: All-thread rod to mate test sample and fixture

Figure 4.18: Fully assembled static coupling mounted to hydraulic actuator

The upper connection, though similar to the configuration of the lower coupling, required a more dynamic design. In the previous experiment, static connections were used at both ends, meaning both ends had to be screwed in simultaneously. Though this method proved to be effective, it only allowed for partial thread engagement of both tensile lugs and would need to be improved upon for the higher loadings expected of the full size samples. Like the lower unit, the upper mount also utilized a 73 mm (2.875 in.) diameter externally threaded cylindrical coupling to anchor the sample to the cross head of the testing machine. The difference between this component and the lower configuration was the way in which it joined the test sample and fixture. Unlike the all-thread rod used by the lower mount, this piece employed a 31.75 mm (1.25 in.) diameter unthreaded axial hole and a 25.4 mm (1 in.) unthreaded rod with hemispherical nut. This combination enabled the coupling to effectively support the test specimen and still permitted the attachment rod to rotate independently. Not only did this allow the attachment rod to fully engage the sample's upper tensile lug, but it also introduced a degree of freedom into the system by allowing the sample to rotate as it was subjected to

loading. The components that comprised the upper dynamic coupling and the stages of their assembly are depicted in Figures 4.19 – 4.24.

Figure 4.19: Main anchor component for upper dynamic coupling

Figure 4.20: Hemispherical nut for upper sample support

Figure 4.21: Unthreaded attachment rod to join sample and test fixture

Figure 4.22: Assembled upper sample attachment rod

Figure 4.23: Assembled dynamic coupling to illustrate attachment rod clearance

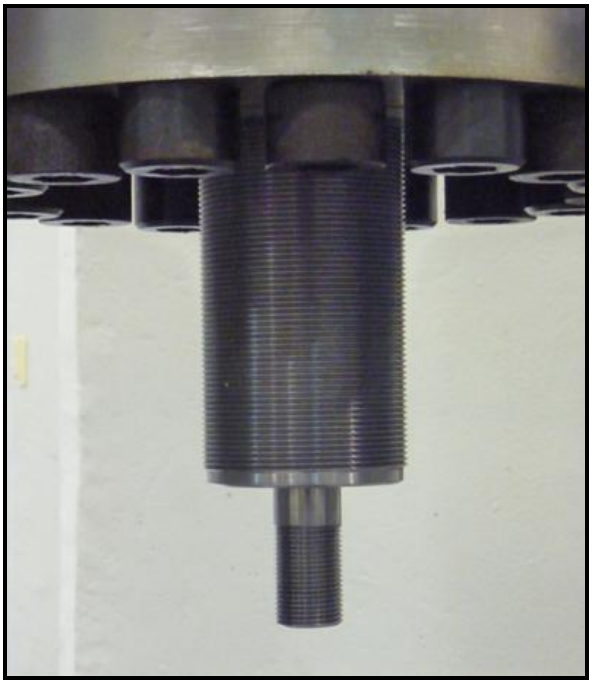

Figure 4.24: Fully assembled dynamic coupling installed on cross head

Interested in the amount of axial loading that would cause the grip sleeve to separate from the strands; solid black bands were painted with a permanent marker around the junctions between the strands and sleeve of the sample. Their purpose was to serve as a reference point of the initial positions of the grip sleeves, as well as provide a drastic contrast to the color of the specimen so that slippage could more easily be seen. An example of one of these colored bands is depicted in Figure 4.25.

Figure 4.25: Contrasting colored band to indicate sleeve slippage

Attachment of the sample to the test fixture began by screwing the hemispherical nut onto the appropriate end of the unthreaded attachment rod (see Figure 4.22). Next, the unthreaded attachment rod was inserted into the hole of the 73 mm (2.875 in.) threaded cylindrical steel coupling, such that the hemispherical nut would match up with the spherical recess (see Figure 4.23). The attachment rod was then screwed into the tensile lug of the test specimen as shown in Figure 4.26. It is important to note that the attachment rod was screwed in until it bottomed out within the grip sleeve. Doing so ensured that full engagement of the threads within the tensile lug had been obtained. Note the 31.75 mm (1.25 in.) gap between the top of the tensile lug and bottom of the cylindrical threaded coupling (see Figure 4.26). This slack was incorporated into the design of the coupling so that the lower mount could be threaded in without unscrewing the top.

Figure 4.26: Dynamic coupling connected to upper tensile lug

Next, the assembled dynamic coupling was screwed into the cross head as shown in Figure 4.27.

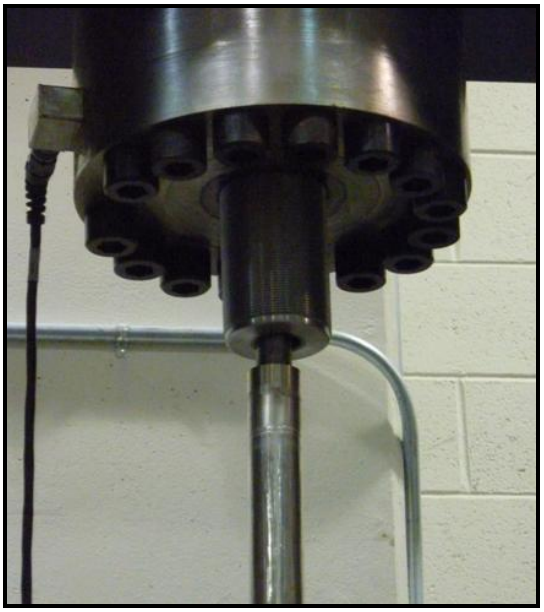

Figure 4.27: Test specimen mounted to fixture’s cross head

Then, the all-thread rod was screwed into the tensile lug on the bottom of the sample. As was the case with the upper coupling, the all-thread rod was also screwed into the tensile lug until it bottomed out (see Figure 4.28).

Figure 4.28: All-thread rod installed in lower tensile lug

The crosshead of the testing machine was then lowered until the all-thread rod made contact with the lower coupling on the hydraulic actuator. It was then lowered an additional 31.75 mm (1.25 in.) so that the sample could be screwed in. This was made possible by the slack between the upper tensile lug and coupling as well as the ability of the attachment rod of the upper coupling to rotate freely. These stages of assembly are depicted in Figures 4.29 and 4.30.

Figure 4.29: All-thread rod contacting lower coupling

Figure 4.30: Test specimen mounted to fixture's hydraulic actuator

Finally, the crosshead was raised back up until a load of about 200 lbs. was applied to the sample. Doing so ensured that any slack left in the system of couplings had been removed. Note that the sample was also pulled taught enough that it began to straighten out, as can be seen in Figure 4.31.

Figure 4.31: TF-WC2-FS mounted to Interlaken testing machine

Once the sample was affixed to the test frame, a piece of tape was wrapped around the all-thread rod that was used to mate the hydraulic actuator and bottom tensile lug. A vertical line was then drawn onto the tape and another onto the tensile lug directly above it (see Figure 4.32). The purpose of these lines was to provide a visual reference of the initial position of the sample so that any rotation that occurred during the loading process could be monitored.

Figure 4.32: Vertical markings to monitor displacement due to rotation

After all of the sample preparation steps were completed, the system's data acquisition software was configured. Interested in determining the load that would cause the grip sleeve to fail; the test machine was operated in displacement control mode. Based on the results of the trial samples, it was witnessed that slippage between the sleeve and conductor occurred fairly rapidly once a load was applied. Therefore, a relatively low displacement rate of 0.2 cm per minute was selected. Additionally, a sampling rate of 1 data point per second was chosen to ensure that a sufficient amount of data points were collected. Lastly, the equipment was activated and progress of the test procedure was monitored in real time by a graphical output of the axial force versus displacement. The test was concluded when the specimen was pulled until the stroke of the machine's hydraulic actuator reached its limit.

Based on the force and displacement data collected during the test, a series of plots were created to evaluate the performance of the TF-WC2-FS sample as compared to the TF-WOC1 sample. When analyzing this data, it is important to keep in mind that TF-

WOC1 and TF-WC2-FS are not identical samples. As can be seen in Figures 4.33 and 4.34, both the grip sleeve length and contact area of the TF-WOC1 sample are about one quarter of the size of the corresponding values for the TF-WC2-FS sample. A comparison of the axial force versus time and axial force versus displacement for both configurations are displayed below in Figures 4.35 and 4.36.

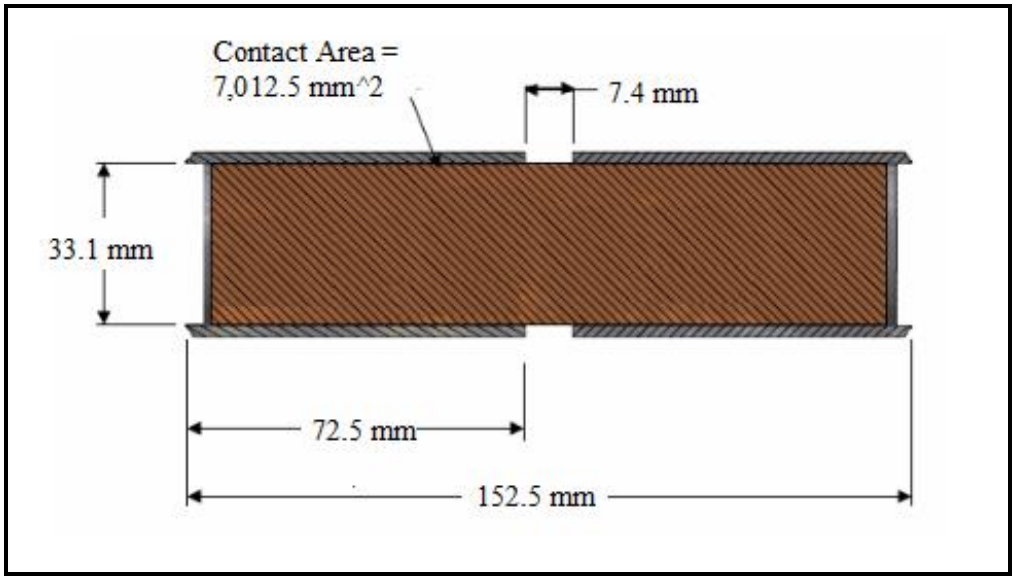

Figure 4.33: Schematic of TF-WOC1 specimen

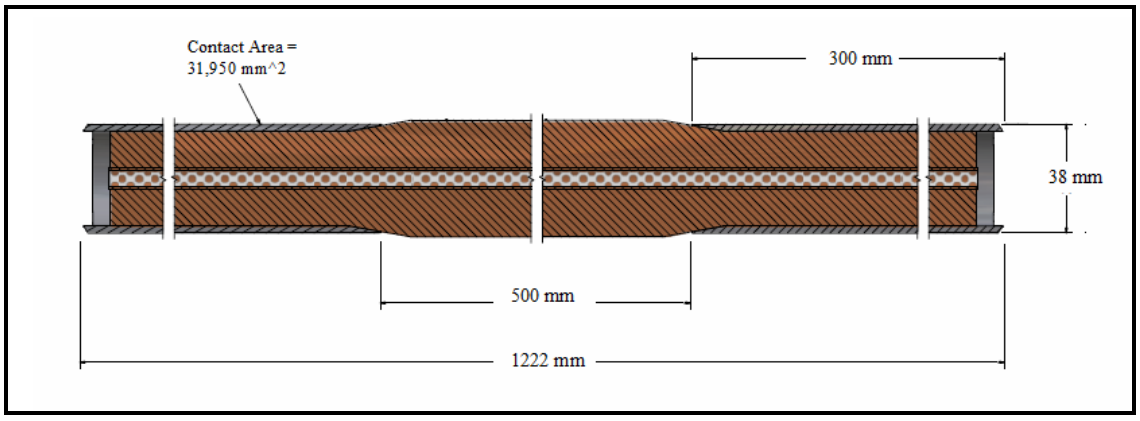

Figure 4.34: Schematic of TF-WC2-FS specimen

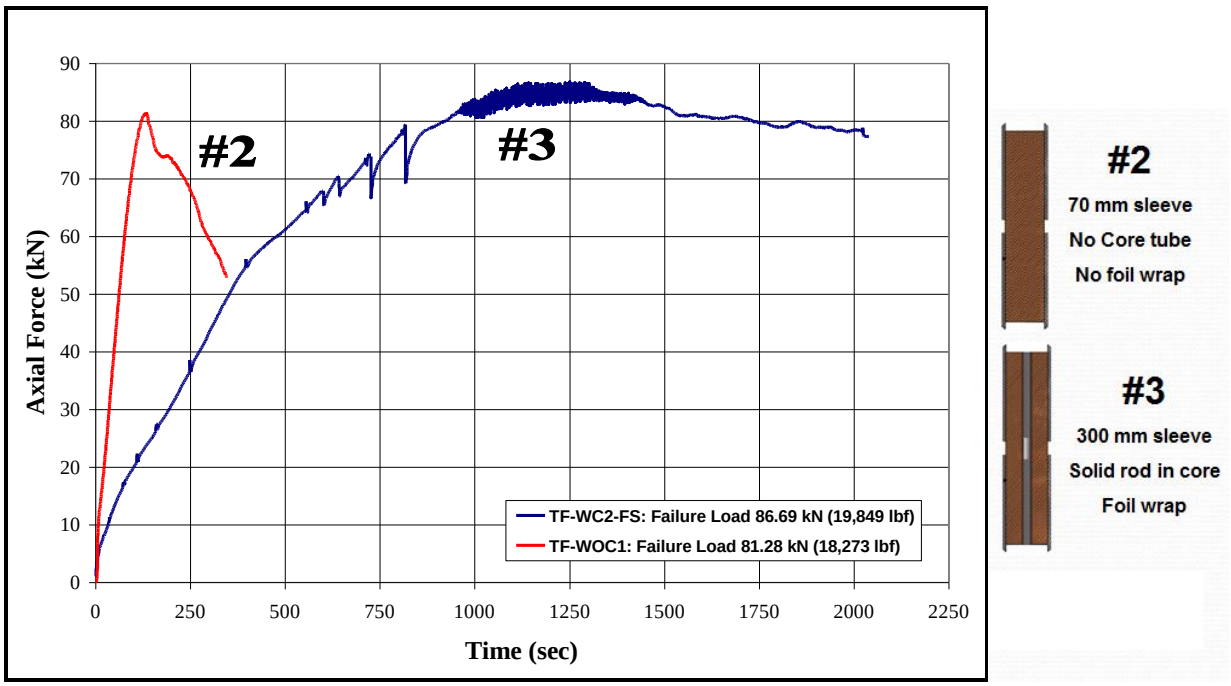

Figure 4.35: Comparison of axial force vs. time for TF-WOC1 and TF-WC2-FS

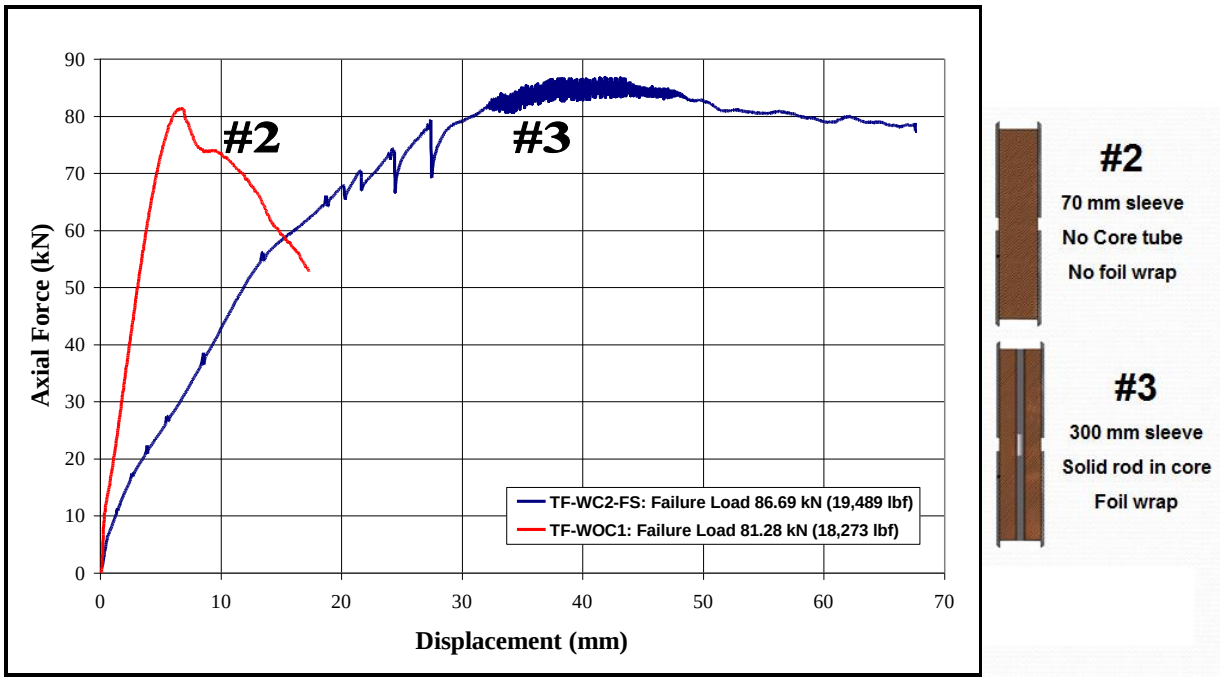

Figure 4.36: Comparison of axial force vs. displacement for TF-WOC1 and TF-WC2-FS

As can be seen in Figures 4.35 and 4.36, TF-WOC1 and TF-WC2-FS withstood axial loads of 81.28 kN (18,273.2 lbf) and 86.69 kN (19,489.62 lbf), respectively. It was believed that increasing the length of the grip sleeve would increase the load that it could support, but with an increase in grip length from 75 mm (for the TF-WOC1 sample) to 300 mm (for the TF-WC2-FS sample), the increase in maximum load turned out to be insignificant.

A variety of factors may be responsible for the insignificant increase in the maximum load for a specimen with the longer grip length.

- During the tensile loading, the strands will undergo a reduction in their cross-sectional area due to Poisson's effect [40]. Since the Poisson's ratio of copper is slightly larger than that of steel (0.33 versus 0.27 to 0.3), the strands will undergo a larger transverse deformation than the steel sleeve. Therefore, it is likely that the contact force between the strands and the sleeve that was initially present decreased with increasing tensile load, thus reducing the effect of the increased sleeve length.
- The design for the smaller sleeve length sample (TF-WOC1) had minimal exposed cable between the crimped sleeves. Although the couplings would allow for rotation in this setup, there was none due to the short cable exposure. However, the couplings for the longer sleeve length sample (TF-WC2-FS) were specifically redesigned to allow rotation. In fact, the TF-WC2-FS sample rotated by more than 270^{o} during the loading process due to the fact that the 500mm of exposed cable was allowed to rotate freely. This rotation under load may have produced a relative motion between the strands and the sleeve, and thus, further reduced the contact force.
- The final step in the construction of the TF cable involves wrapping the outer surface with a thin layer of protective foil. When the TF-WOC1 sample was created, this protective foil wrap was removed before the sleeve was compacted, whereas the protective foil was left intact on the TF-WC2-FS sample. As can be seen in Figure 4.37, compaction of the cable without the protective foil resulted in a very visible deformation of the inner surface of the TF-WOC1 grip sleeve. This

deformation was caused by the strands of wire and sub cable foil (see Figure 4.38) becoming embedded into the stainless steel sleeve. These sleeve indentations are believed to increase the frictional force between the sleeve and strands, and thus provide another mechanism to resist slip. In the TF-WC2-FS sample, we expect that the existence of the protective foil wrap effectively distributed the load from compaction and prevented the strands from becoming as deeply embedded into the sleeve as the strands in the TF-WOC1 sample. The shallower strand indentations and lack of deformation from the sub cable foil wrap on the TF-WC2-FS grip sleeve confirm this (See Figure 4.39).

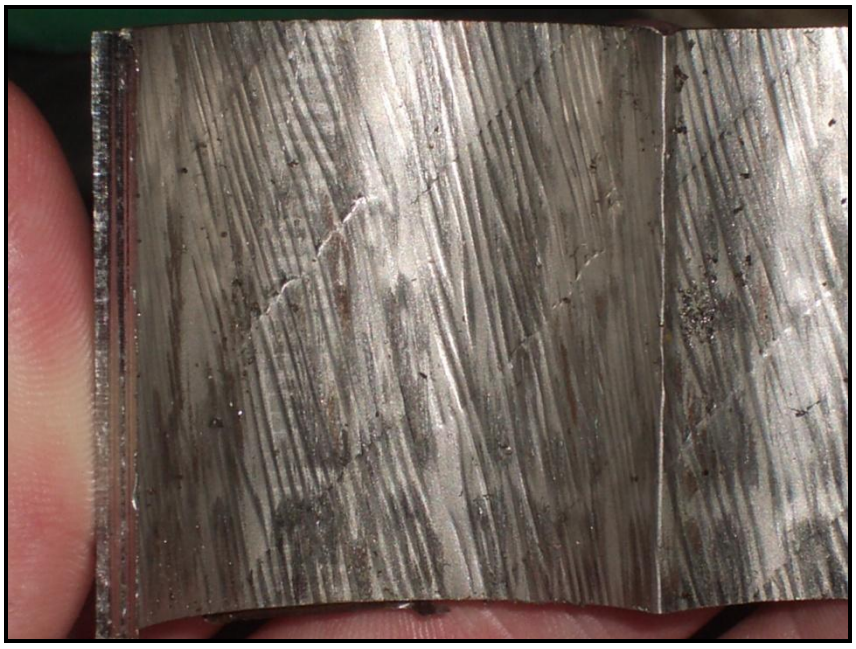

Figure 4.37: Indention of cable strands on inner surface of TF-WOC1 grip sleeve without the protective foil – This sample did have sub-cable foil on it

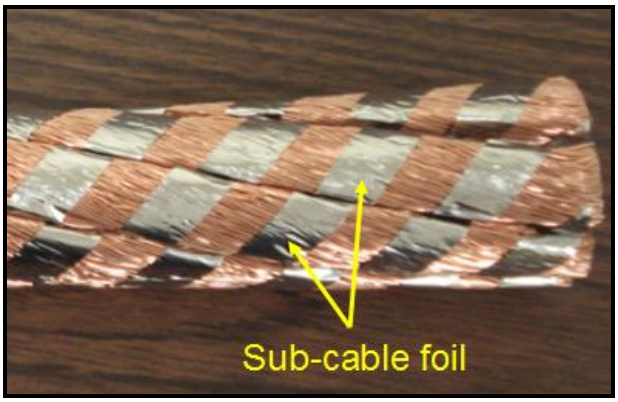

Figure 4.38: Conductor cable showing sub-cable foil wrap

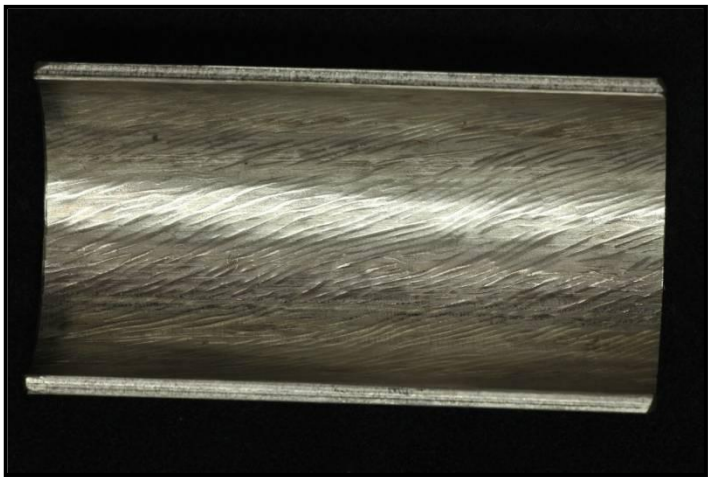

Figure 4.39: Indention of cable strands on inner surface of TF-WC2 grip sleeve with the protective foil – This sample also had sub-cable foil on it

- The diameters and lengths of the grip sleeves were measured before and after the tensile testing. Due to the lack of uniformity in the swaging process, the diameters of the samples were not equal at all locations (the values varying from 37.87 mm to 38.02 mm). Because of this level of inconsistency, the diameter of each sleeve was checked at three axial positions, which included both ends and the center. This lack of uniformity was also present in the radial direction. As a result, sleeve diameters were measured at two positions (from 12 to 6 o'clock and from 3 to 9 o'clock), and their average was taken. To ensure consistency, grip sleeve lengths were measured from the outside edge of the tensile lug to the end of the sleeve where the strands become exposed. Unlike the sleeve diameter, the sleeve lengths did not show any variations when checked from different positions. Schematics

showing the measured lengths, diameters, and their locations as well as the distance that each grip sleeve slipped are displayed in Figures 4.40 – 4.43. Comparison of the measured sleeve lengths and diameters before and after the pull test does not show any trend, i.e. the sleeve lengths and diameters appear to be unchanged. It is important to note that due to safety considerations, these final sleeve dimensions had to be taken after the sample was completely detached from the testing machine and was not under any load.

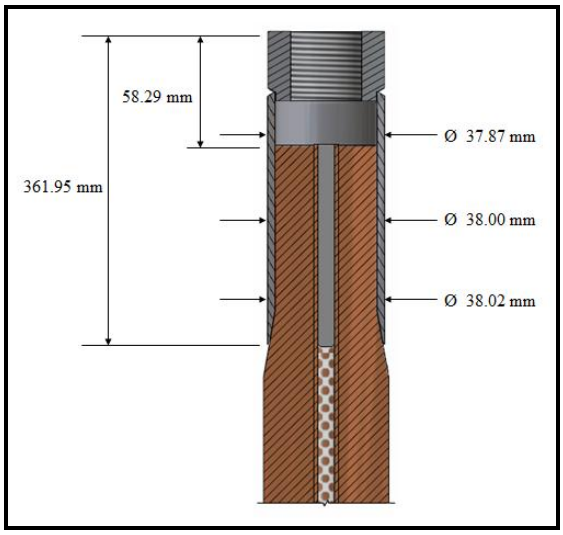

Figure 3.24: Dimensions of TF-WC2-FS upper grip sleeve before pull test

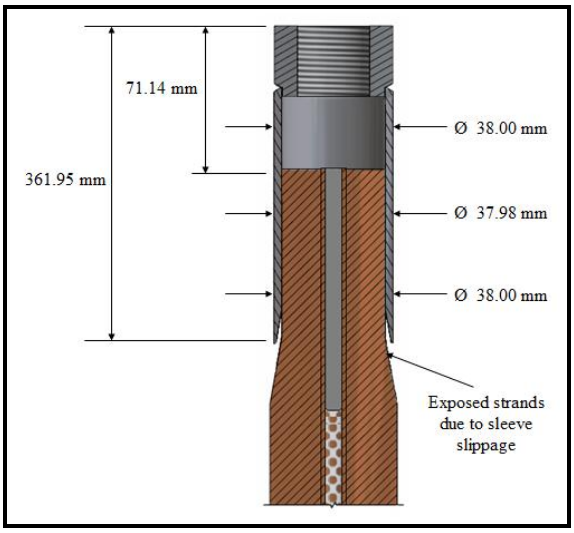

Figure 3.25: Dimensions of TF-WC2-FS upper grip sleeve after pull test

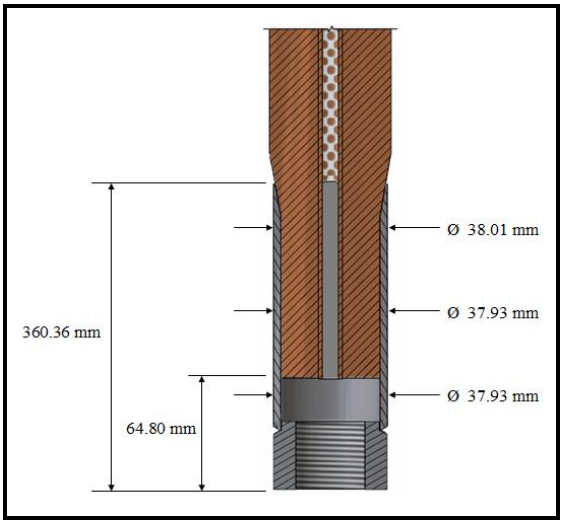

Figure 3.26: Dimensions of TF-WC2-FS lower grip sleeve before pull test

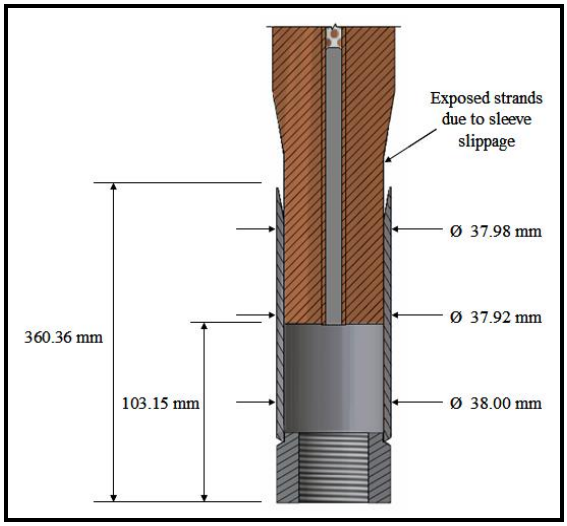

Figure 3.27: Dimensions of TF-WC2-FS lower grip sleeve after pull test

The final observation in the load-time and load-displacement curves of TF-WC2-FS samples (Figures 4.35 and 4.36) is the existence of a stick-slip mechanism. Stick-slip refers to the intermittent jerking motion that occurs between two objects that slide against one another when the coefficient of kinetic friction between the surfaces is less than the coefficient of static friction. The two contact surfaces will stick until the sliding force reaches the value of the static friction. The surfaces will then slip over one another with a small valued kinetic friction until the two surfaces stick again. We believe that this same phenomenon is occurring within the grip sleeves of the pull test samples because of shear stress created by the indentations of the strands into the sleeve. As the sample is loaded, the shear stress builds up between the strands and sleeves until either the sleeve or strands deform and slip occurs. Since the stick-slip type of deformation was not observed in the TF-WOC1 sample (see Figures 4.35 and 4.36), it is possible that the stick-slip deformation in the TF-WC2-FS sample may have been caused by the specimen rotating during loading.

Four distinct cases of this stick-slip mechanism were observed on the force versus displacement plot of the TF-WC2-FS sample, and a plot was created for every occurrence. These plots are illustrated in Figures 4.44 – 4.48.

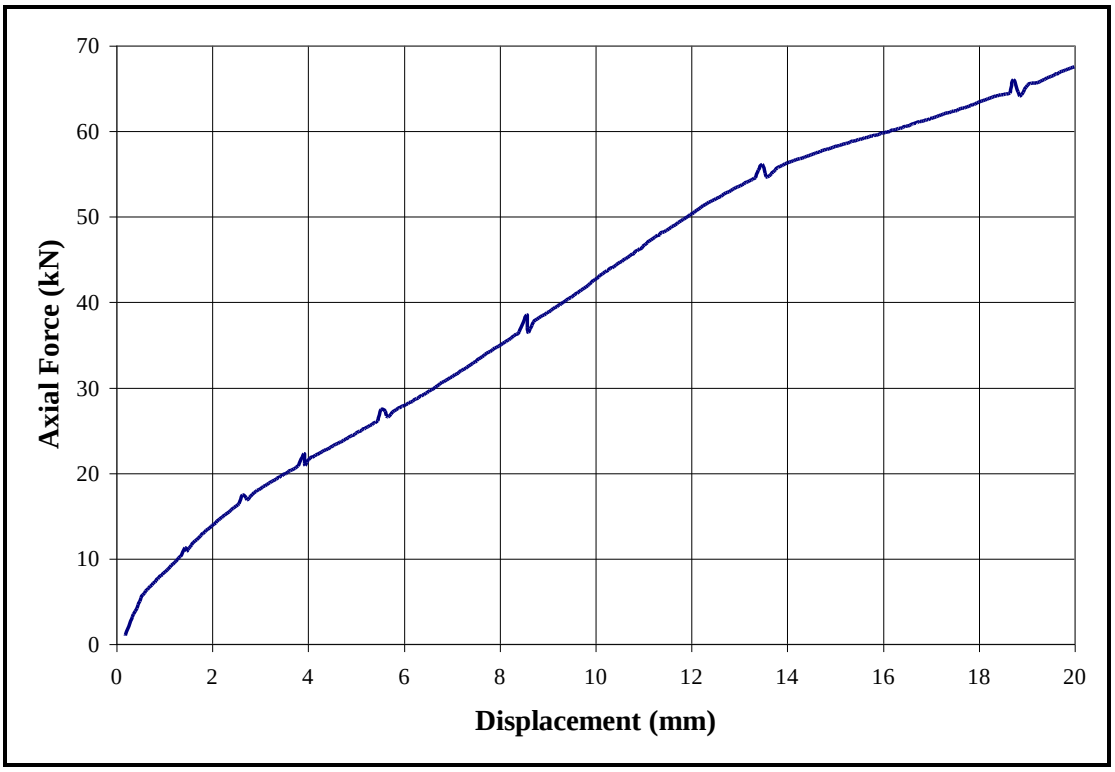

Figure 4.44: First occurrence of stick-slip mechanism for TF-WC2-FS

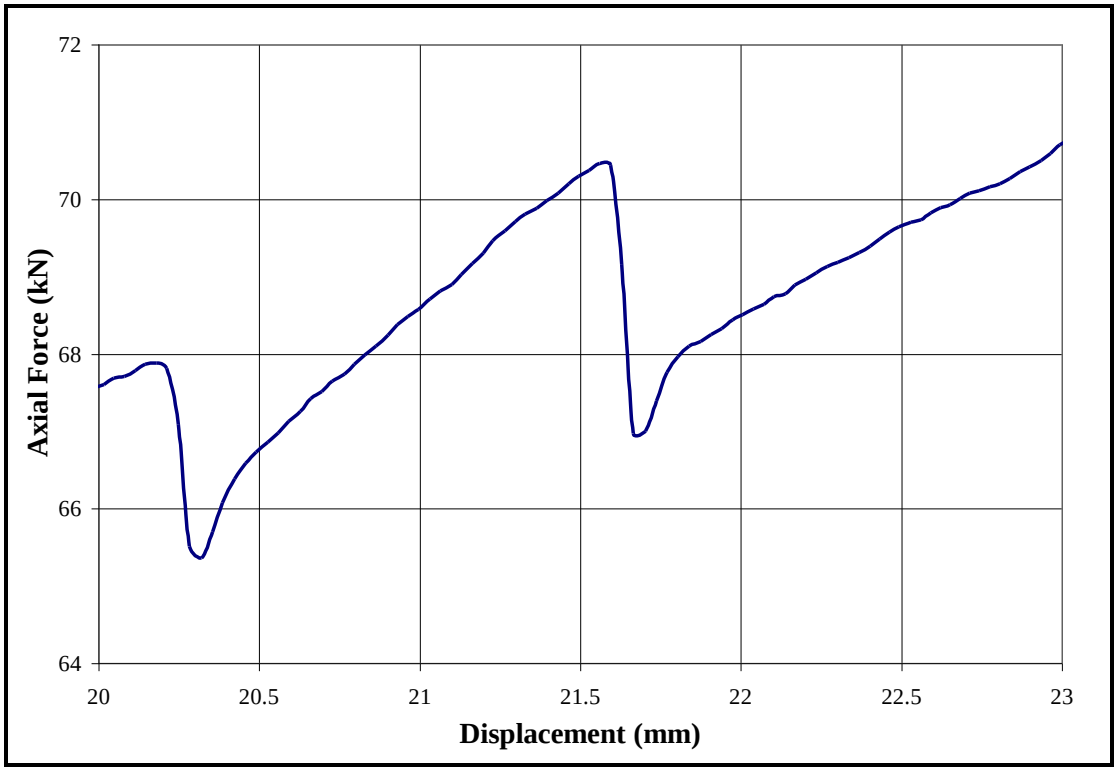

Figure 4.45: Second occurrence of stick-slip mechanism for TF-WC2-FS

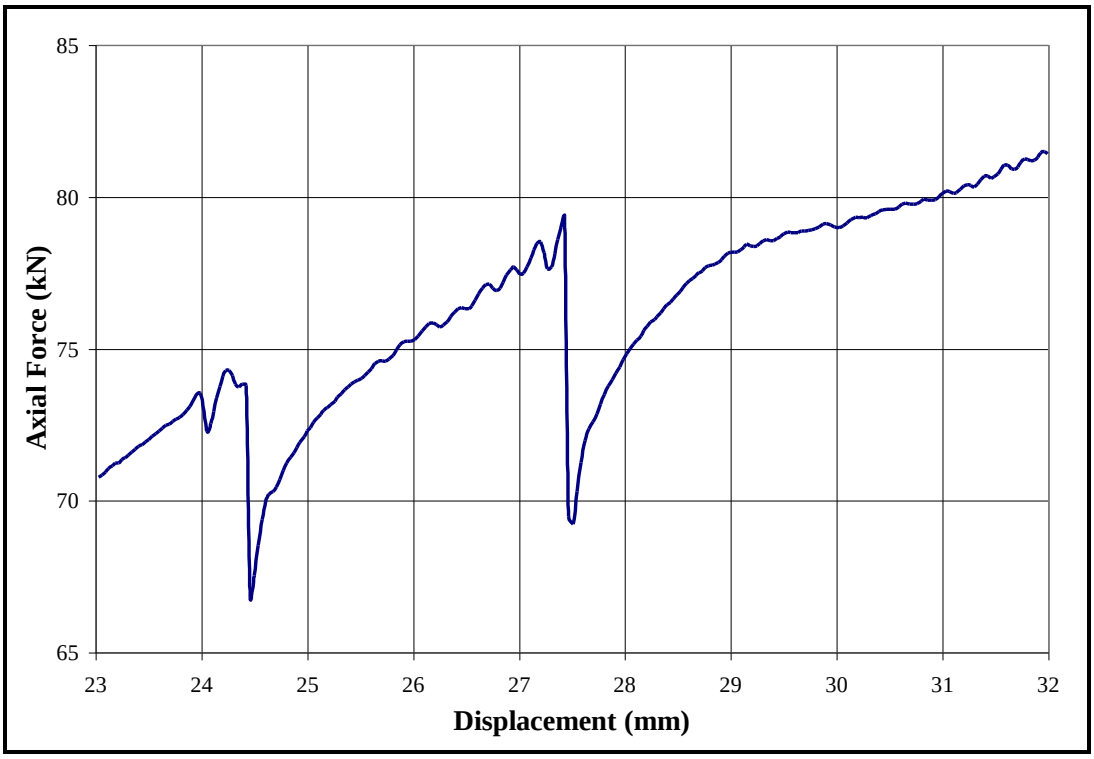

Figure 4.46: Third occurrence of stick-slip mechanism for TF-WC2-FS

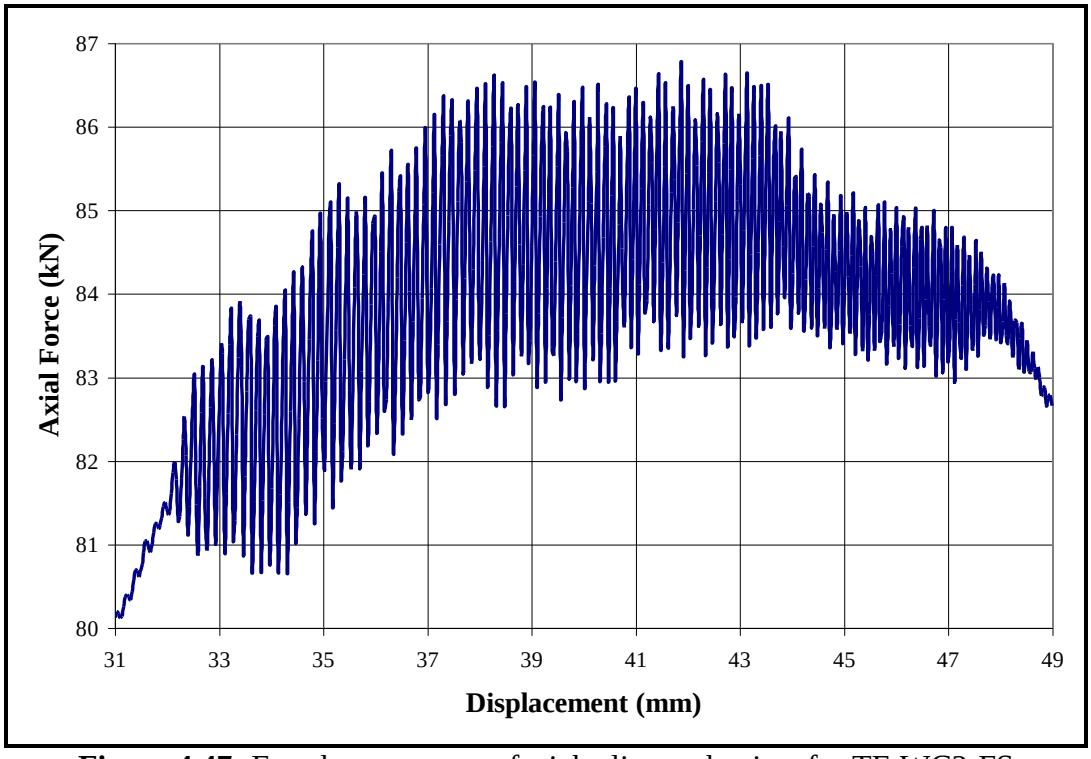

Figure 4.47: Fourth occurrence of stick-slip mechanism for TF-WC2-FS

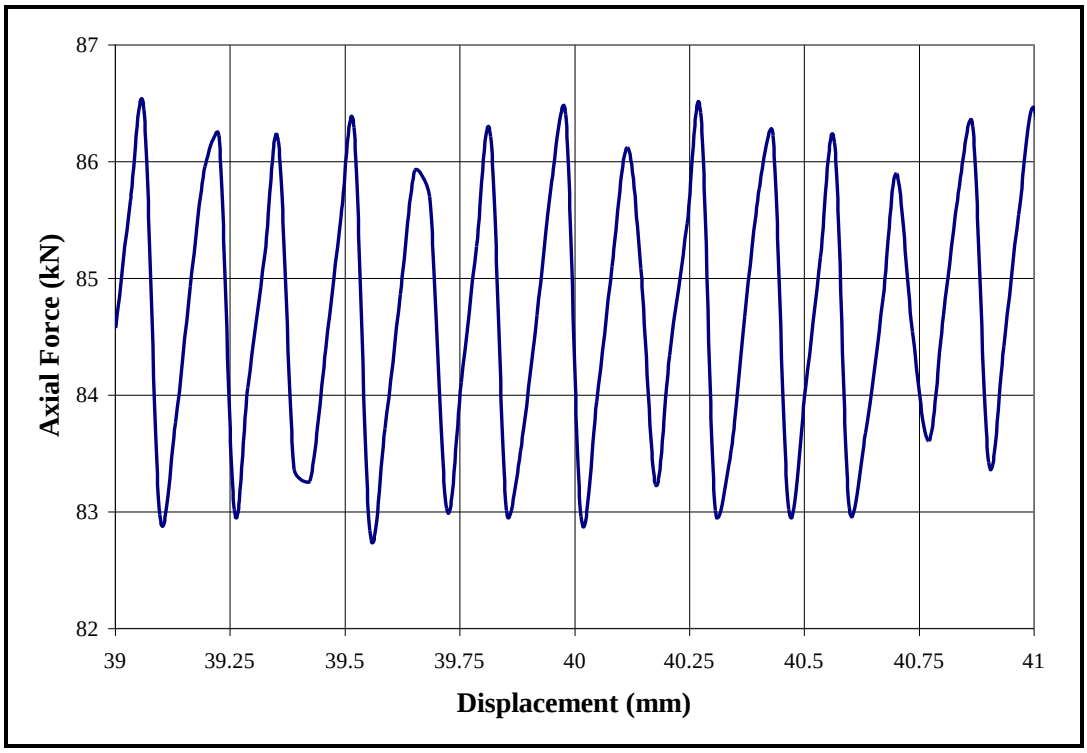

Figure 4.48: Close-up of fourth occurrence of stick-slip for TF-WC2-FS to show constant magnitude of oscillation

The four occurrences of stick-slip were identified based on the magnitude of the oscillations that were visible on the force versus displacement plots. As can be seen in Figures 4.44 – 4.48, the magnitude of the oscillations increased with increasing axial load, until a value of ~82 kN was reached. At this point, the slope of the force versus displacement curve leveled out and the magnitude of the oscillations remained constant for about 400 seconds. Eventually these oscillations began to die out as the failure mode transitioned from stick-slip to a strictly slip condition. This trend indicates that the critical load of the system had been reached. The force versus displacement plot for the TF-WOC1 sample clearly illustrates this trend because of its rapid decrease in slope as soon as 81 kN was reached. It is interesting to note that these same oscillations were not nearly as visible on the TF-WOC1 curve as they were on the TF-WC2-FS curve.

Several photographs (see Appendix B) of the regions painted with permanent marker were taken during the loading process. These photographs show the slippage

between the sleeve and strands as tensile load increased. The photographs are presented in chronological order, beginning with the lower painted strand/sleeve junction.

4.1.3. Modified Grip Design

Based on the results of the first full scale test, tensile tests were performed on the second and third of six full scale TF press-fit grip sleeves. Both of these samples shared the same basic dimensions as the previous specimen (TF-WC2-FS, refer to Section 4.1.2.). The pull tests for the TF-WC3-FS and TF-WC4-FS samples were also conducted with the same universal testing machine. Due to the similarities between the samples and the fact that one of the intents of these tests was to establish repeatability, all of the previous testing parameters remained unchanged. Among these included the method of attachment to the testing apparatus, equipment settings such as displacement rate and data sampling rate, and testing procedure.

In hopes of improving upon the performance of the TF-WC2-FS sample, the previous grip sleeve design received three distinct modifications.

1. The first of these modifications, which was incorporated into both TF-WC3-FS and TF-WC4-FS, was the removal of the protective foil wrap from the sections of cable that would be compacted within the grip sleeves. As was witnessed with the TF-WC1 and TF-WOC1 samples, removal of the protective foil allowed the strands of wire to become embedded into the inner surface of the grip sleeves. This interference between the grip sleeve and strands of wire is believed to increase the frictional force between these surfaces and provide another mechanism to resist slip.

   Removal of the protective foil wrap began by wrapping each end of the cable with tape so that the foil would not prematurely unwrap. Next, grip sleeves were slid over each end of the cable and reference lines were painted on the foil to indicate the length of cable that was covered by the grip sleeve. The grip sleeves were then

slid back by 12.7mm (0.5 in.) and a second reference line was painted on the foil to indicate the point at which the foil should be cut. Finally, the grip sleeves were taken completely off and the protective foil was removed. Cutting the foil 12.7mm (0.5 in.) too short meant that the grip sleeves would overlap the foil by 12.7mm (0.5 in.) and help hold it in place. When the actual 800 m cable pull takes place, a great deal of friction will be acting against this foil. If the foil is not secured, it could potentially unwrap and create more resistance against the pulling force. While this is not a concern during the testing phase, it is still important to incorporate this detail into the design. Figures 4.49 – 4.53 below outline the foil removal process.

Figure 4.49: Wrap end of cable with tape to prevent foil from unwrapping

Figure 4.50: Slide uncompacted sleeve over end of cable

Figure 4.51: Reference lines marked to indicate where to cut foil

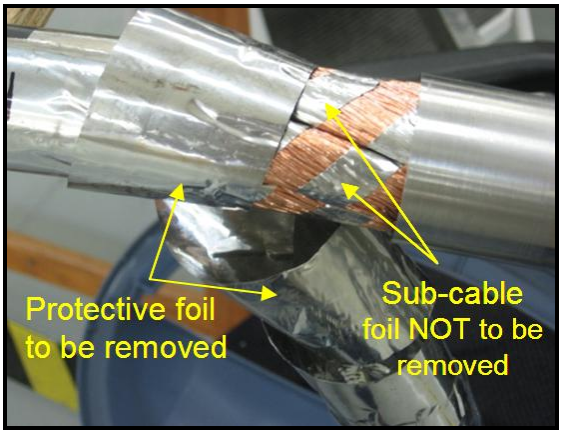

Figure 4.52: Protective foil being removed, revealing sub-cable foil

Figure 4.53: End of cable with foil removed showing 0.5” foil band for grip sleeve overlap

2. The second modification, which was only incorporated into the grip sleeve design of the TF-WC4-FS sample, was the addition of a reinforcement grip ring around the base of each grip sleeve (see Figures 4.54). The reason it was added only to TF-WC4-FS and not TF-WC3-FS was so that the affect of the protective foil removal could be evaluated separately. As was witnessed in the previous tests, the grip sleeves would fail by allowing the cable to slip when the applied tensile load exceeded the force due to friction between the sleeve and cable strands. It was suggested that constricting the end of the sleeve would prevent the cable strands from sliding out from within the grip sleeve. The presence of the solid rod within the core of the cable in the sleeve region would further restrict the relative motion between the sleeve and cable strands by preventing the hollow core tube from deforming, and thus maintaining the contact pressure between the strands and sleeve.

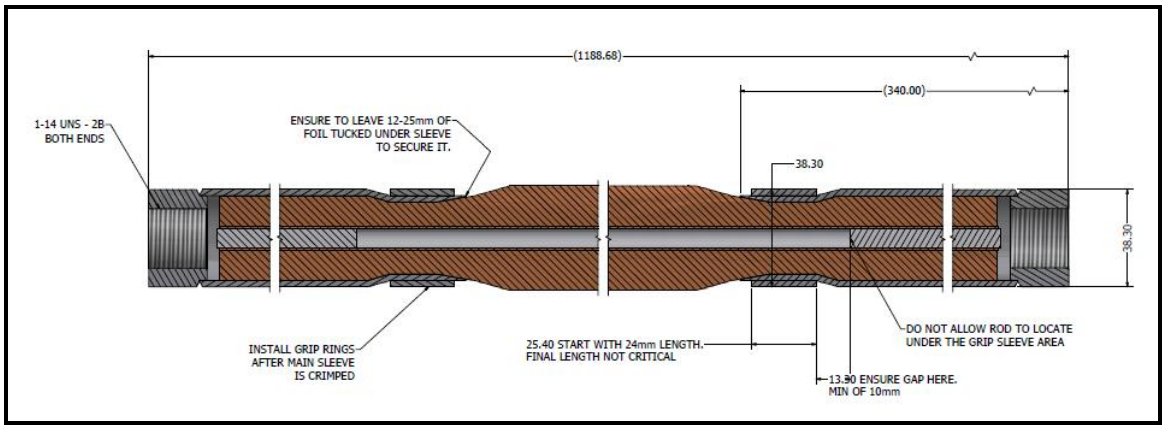

Figure 4.54: Schematic of modified TF grip sleeve design [38]

The reinforcement grip consisted of a 25.4 mm wide section of 2.05 mm thick by 47.5 mm diameter stainless steel tube. The uncompacted TF conduit stock that was used to create the grip sleeves was used. It was positioned flush with the base of the grip sleeve (opposite the tensile lug), and compacted to a diameter of 38.75 mm. To accommodate for this grip ring, the TF-WC4-FS sample required an additional modification to the solid rod that is placed in the core tube of all of the samples. To allow for sufficient compaction of the reinforcement grip ring, the 292 mm rod that has been used with the previous samples was shortened to 241 mm. Shortening the rod ensured that the reinforcement grip ring would not be compacted over the solid rod, but just the hollow core tube and cable.

Once the grip sleeve was compacted to the appropriate diameter, the un-compacted grip ring was slipped over the grip sleeve on one side of the sample and positioned flush with the sleeve/strand interface. To hold the ring in place while it was fed into the crimping machine, a piece of tape was used (see Figure 4.58). The ring was then compacted around the sleeve to an outer diameter of roughly 38.75 mm. This same process was repeated to install a second grip ring on the other end of the sample. A series of photographs illustrating this process can be seen in Figures 4.55 – 4.59.

Figure 4.55: Reinforcement grip rings prior to install

Figure 4.56: Uncompacted grip ring compared to partially compacted sleeve

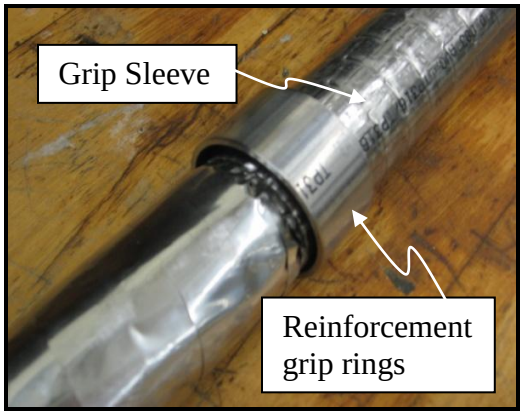

Figure 4.57: Grip ring positioned on compacted grip sleeve

Figure 4.58: Grip ring taped in place in preparation for swaging

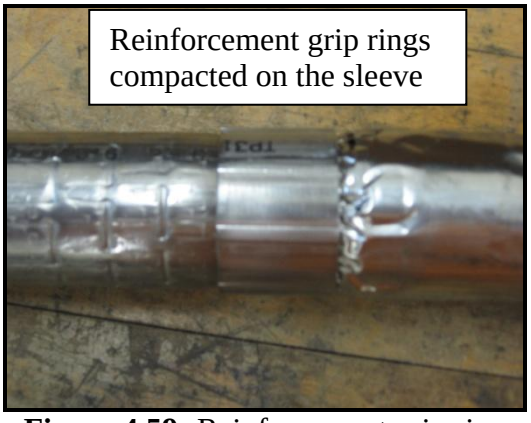

Figure 4.59: Reinforcement grip ring after compaction around grip sleeve

3. The final modification that was made to both TF-WC3-FS and TF-WC4-FS was the procedure for compaction of the grip sleeve around the cable. For each of the previous specimens, the grip sleeves were compacted in increments of 0.5 mm to ensure straightness and uniformity. As a result, fabrication of the first full scale sample proved to be a very time consuming process. More importantly, the gradual compaction was actually making the grip sleeve progressively more difficult to compact due to work hardening; so much so that the capabilities of the crimping machine were exceeded and the micrometer failed. To speed up the process and avoid the affects of work hardening, it was determined that the samples should be compacted from their nominal diameter of 47.5 mm down to 38 mm in one step. This proved to be a very successful technique in terms of speed, ease of compaction, and quality of results. The only visible affect due to this more rapid swaging technique was the pattern of indentations on the grip sleeve. As can be seen in Figures 4.60 and 4.61, gradual compaction resulted in a relatively smooth surface due to the evenly distributed deformation of the dies, whereas full compaction in one step left a series of rings on the sleeve due to more concentrated deformation. Another noticeable effect of compaction in one step was that the samples had a smaller overall length than samples that were compacted gradually (1201.7 mm and 1209.7 mm for TF-WC3-FS and TF-WC4-FS, versus 1222.4 mm for TF-WC2-FS).

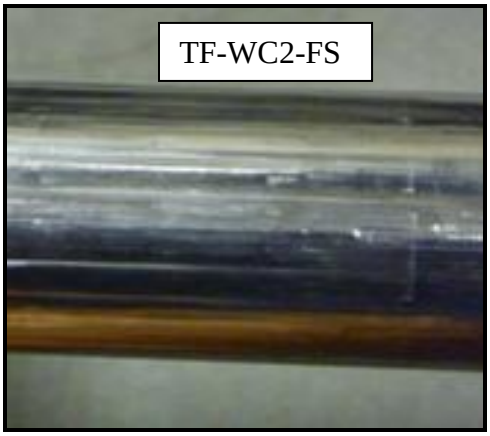

Figure 4.60: Smooth grip sleeve surface due to incremental compaction

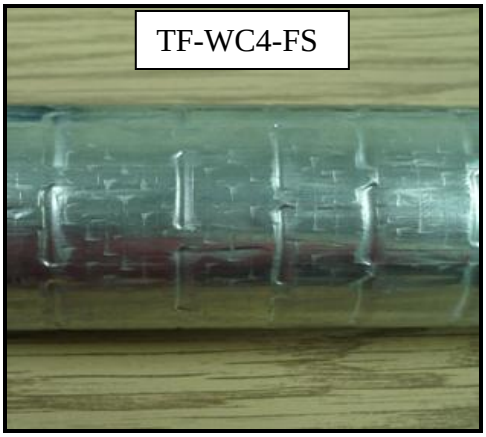

Figure 4.61: Deformed grip sleeve surface due to compaction in one step

The accent bands that were painted around the junction between the strands and sleeve on the TF-WC2-FS sample proved to be a very effective reference point of the initial positions of the grip sleeves, as well as a drastic contrast that made grip sleeve slippage more visible. Therefore, this technique was utilized with the TF-WC3-FS and TF-WC4-FS samples as well. However, due to the addition of the reinforcement grip ring, TF-WC4-FS was marked slightly different than TF-WC2-FS and TF-WC3-FS. In addition to the typical accent band around the sleeve/strand interface, a similar band was painted around the sleeve/reinforcement grip ring interface as well. An example of these colored bands is depicted in Figures 4.62 and 4.63.

Figure 4.62: Single accent band for samples without reinforcement grip ring

Figure 4.63: Double accent band for samples with reinforcement grip ring

As was the case with the previous tests, we were interested in monitoring the movement of the sample during the loading process. Because of the pitch orientation of the sub cables, it was observed in the previous test that the cable had a tendency to straighten itself out by rotating in a counter clockwise direction (the direction opposite to the helical direction of the wires). Additionally, the tensile lugs that were used to attach the sample to the test fixture utilized standard right hand threads at both ends. Due to their opposing orientations, this meant that tightening one end would loosen the other, and vice versa. In terms of the actual specimen behavior during testing, this counter

clockwise rotation caused the upper tensile lug to rotate counter clockwise, while the lower tensile lug remained fairly stationary. What this translated to was a partial unwinding of the exposed cable between the grip sleeves, rather than a uniform rotation of the entire specimen. Therefore, the TF-WC3-FS and TF-WC4-FS samples were screwed all the way down against the lower coupling (see Figure 4.64) so that their motion was completely restricted. The configuration of the upper coupling, however, still allowed for rotation. Therefore, a vertical black line was painted on the tensile lug and a corresponding horizontal line on the bottom of the main body of the upper threaded coupling (see Figure 4.65) so that the behavior of the upper end of the specimen could be monitored.

Figure 4.64: Tensile lug flush with lower coupling to prevent rotation

Figure 4.65: Reference lines to monitor specimen rotation

Based on the force and displacement data collected during these tests, a series of plots were created to evaluate the performance of the TF-WC3-FS and TF-WC4-FS samples as compared to the TF-WC2-FS. When analyzing this data, it is important to keep in mind that each of the three samples was slightly different. Because TF-WC2-FS was the only unmodified sample, it can be thought of as a baseline configuration, to which the effectiveness of the modifications made to the subsequent samples can be evaluated. A comparison of the axial force versus time and axial force versus displacement for all three configurations are displayed below in Figures 4.66 and 4.67.

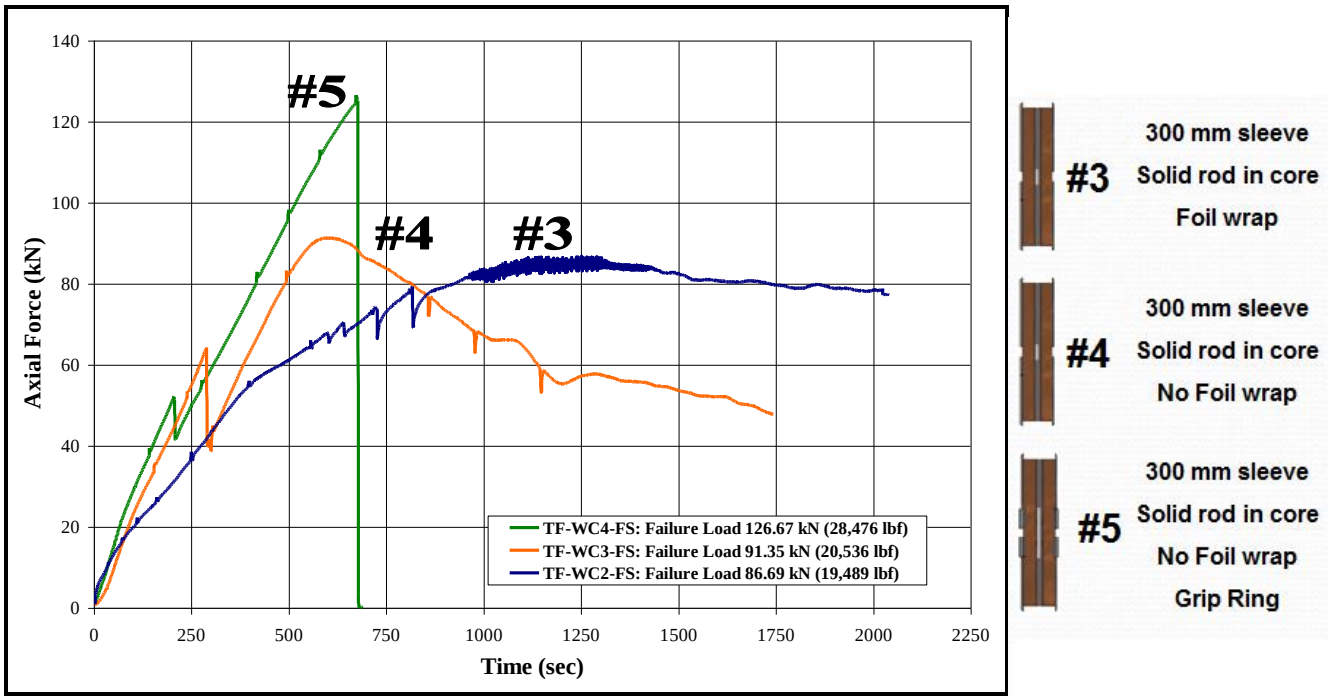

Figure 4.66: Comparison of axial force vs. time for TF-WC2-FS, TF-WC3-FS, and TF-WC4-FS

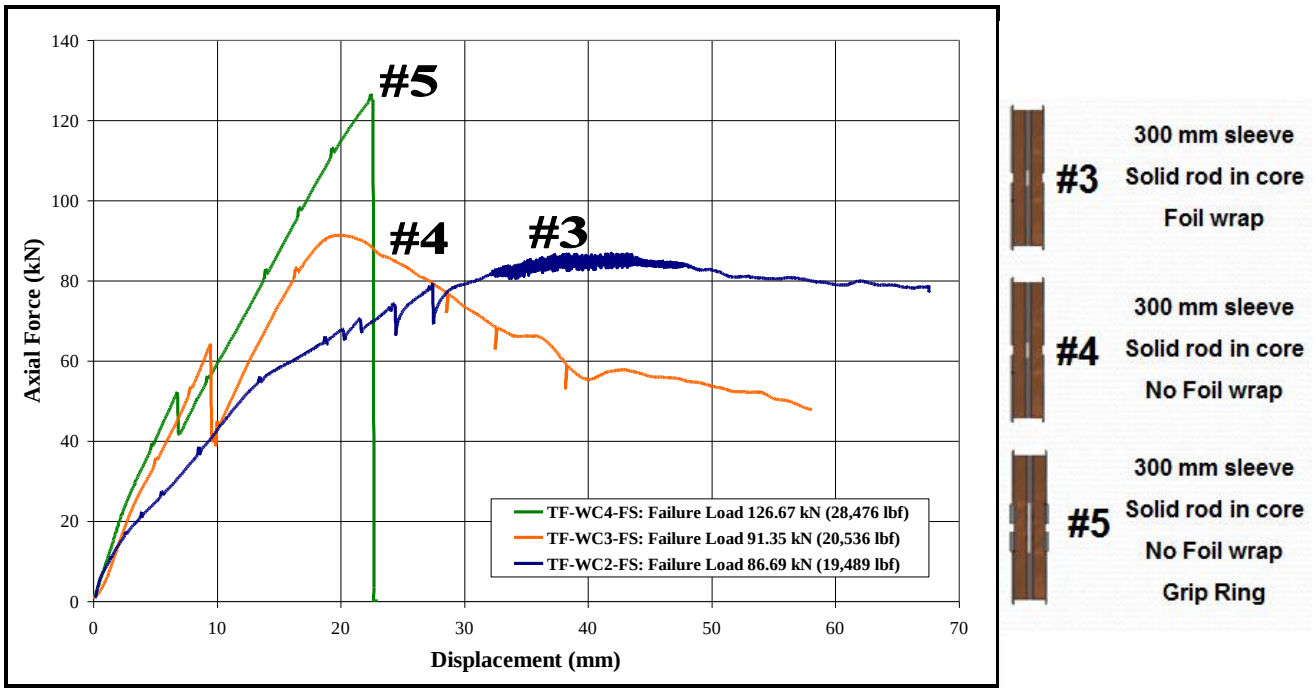

Figure 4.67: Comparison of axial force vs. displacement for TF-WC2-FS, TF-WC3-FS, and TF-WC4-FS

As can be seen in Figures 4.66 and 4.67, TF-WC2-FS, TF-WC3-FS, and TF-WC4-FS reached maximum loads of 86.69 kN (19,489.62 lbf), 91.35 kN (20,536.41 lbf), and 126.67 kN (28,475.77 lbf), respectively. Based on these results, several conclusions can be drawn about each of the modifications to the grip sleeve configurations.

It was believed that removal of the protective foil wrap would increase the load that the grip could support, but with an increase in axial load of only 4.66 kN (1,046.79 lbf), this modification turned out to be insignificant. Two opposing mechanisms are believed to be responsible for the negligible difference in the maximum loads for the two types of specimens (with the protective foil and without the foil):

- The samples that still have the protective foil wrapped around the strands will have a greater volume within the grip sleeve than the samples without the foil due to the additional thickness of the foil. Because all of the samples (with or without the foil wrap) are compacted to the same outer diameter, the samples with the larger volume will have a greater pressure within the grip sleeve. This increased residual pressure will translate to a greater resistance to slippage than the lower volume sample.

- The presence of the protective foil may prevent the copper wires from deforming the inside of the sleeve during the compaction process. This would imply that the surface roughness inside the steel sleeve would be less due to the presence of the foil. The decrease in the surface roughness will increase the likelihood of slippage.

The addition of the reinforcement grip ring, however, turned out to be a very significant improvement in the grip sleeve design, increasing the failure load by 35.32 kN (7,939.36 lbf). The effectiveness of this ring can be attributed to a variety of factors.

- The compacted reinforcement grip ring further reduced the cross sectional area of the hole through which the cable must slip in order to fail.

- Since the diameter of the cable is prevented from reducing because of the solid rod that is installed at its core, a greater contact pressure and thus a greater amount of friction remains between the strands and sleeve. This will translate to greater resistance to slip.

A great deal of additional information about the behavior of these samples can be obtained by looking at the slope of the force vs. displacement curves. As can be seen in Figure 4.67, the slopes of TF-WC3-FS and TF-WC4-FS were not only steeper than TF-WC2-FS, but they also remained essentially linear until failure occurred. Since the slope of these points was a ratio of the change in axial load to the change in displacement, we see that not only do TF-WC3-FS and TF-WC4-FS support more load than does TF-WC2-FS, but the linear nature of their slopes is an indication that both specimens did not slip until they reached their failure loads. However, the nonlinear behavior of TF-WC2-FS indicates that the sample was essentially slipping the entire time until it finally failed.

Another important observation to make from Figures 4.67 is the slope of the force vs. displacement curves at the time that the failure loads are reached. These slopes provide some insight into the way in which each sample failed. As can be seen in Figure 4.67, samples TF-WC2-FS and TF-WC3-FS had fairly moderately decreasing slopes after reaching their failure loads, which indicated that the grip sleeves were slipping. This type of grip failure can be seen by comparing Figure 4.62 with Figure 4.68.

Figure 4.68: Grip sleeve failure due to sleeve slippage

As can be seen in Figure 4.66, TF-WC4-FS failed catastrophically without any warning. This drastic failure was actually caused by a seam weld fracture between the tensile lug and grip sleeve body (see Figure 4.69 and 4.70).

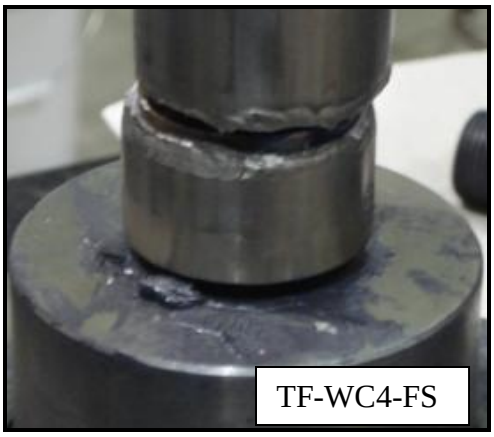

Figure 4.69: Grip sleeve failure due to seam weld fracture

Figure 4.70: Grip sleeve failure due to seam weld fracture

Another factor to consider when evaluating these results is the existence of a stick-slip mechanism (refer to Section 4.1.2.) during the loading. One distinct case of this stick-slip mechanism was observed at two different locations on the force versus displacement plot for the TF-WC3-FS and TF-WC4-FS samples. These plots are illustrated in Figures 4.71 and 4.72.

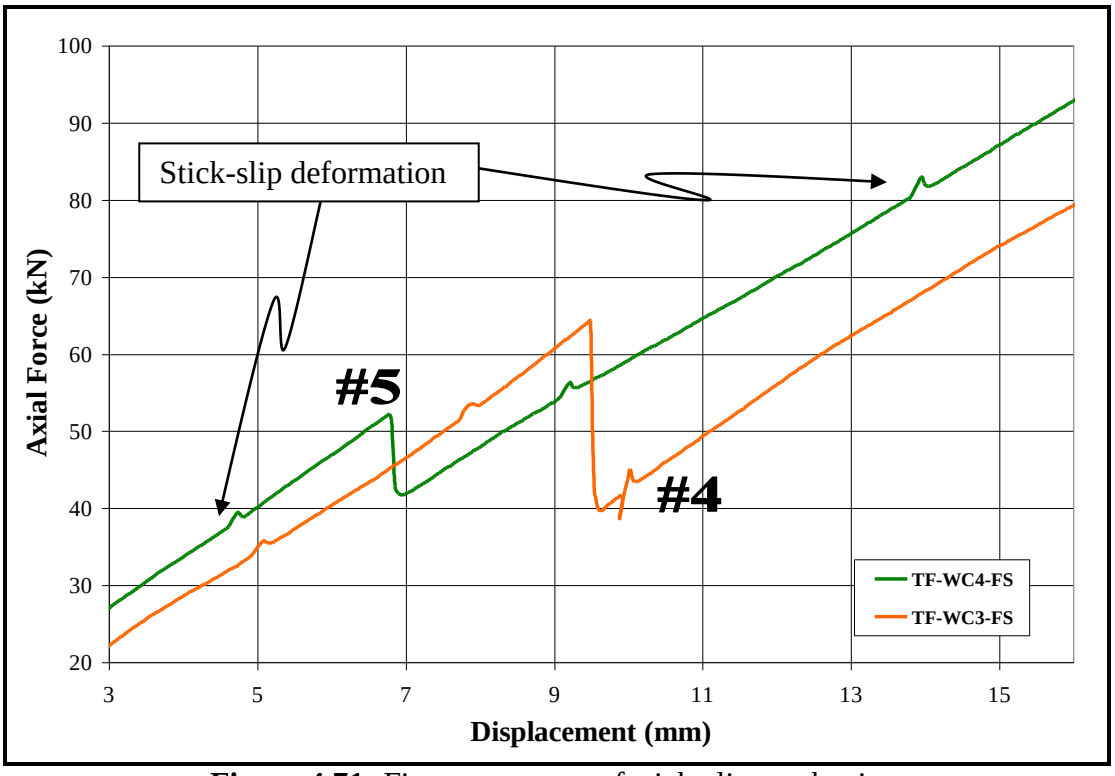

Figure 4.71: First occurrence of stick-slip mechanism

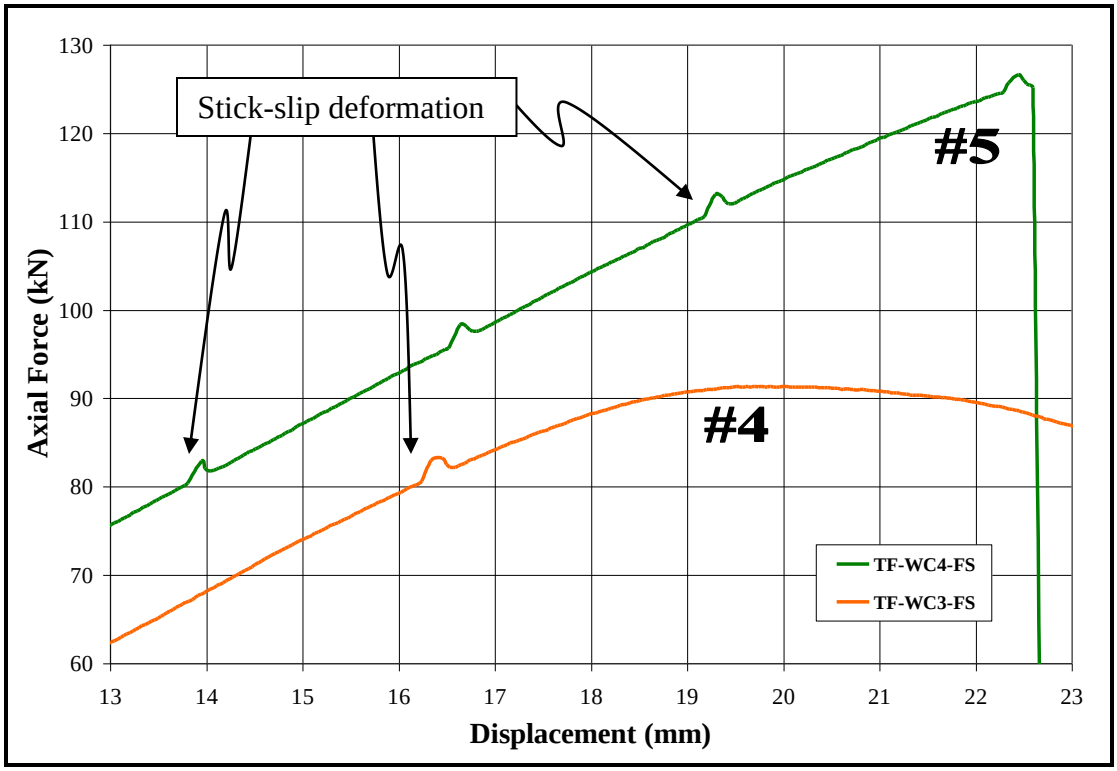

Figure 4.72: Second occurrence of stick-slip mechanism

The occurrences of stick-slip were identified based on the magnitude of the fluctuations that were noted on the force versus displacement plots. As can be seen in Figures 4.71 and 4.72, the magnitude of the oscillations remained constant with increasing axial load.

In addition to the stick-slip, another unusual trend appeared on the force vs. displacement plots of both samples. This phenomenon was a sudden drop in the axial load that cannot be attributed to stick-slip. As can be seen in Figures 4.73, the loads applied to both TF-WC3-FS and TF-WC4-FS abruptly decreased after 7 to 10 mm of displacement and then immediately continued to increase at the same rate as before, but from the point to which the load had fallen. Stick-slip, however, is characterized by an abrupt load increase which quickly returns to a value equal to or slightly greater than the value at which the spike occurred, before loading continues (see Figures 4.71 and 4.72). Despite the fact that both specimens experienced the same amount of displacement, TF-WC3-FS experienced a much greater load decrease (~24 kN) than TF-WC4-FS (~9 kN). This is likely due to the fact that at the load drop point the TF-WC3-FS sample was at a much greater load than TF-WC4-FS.

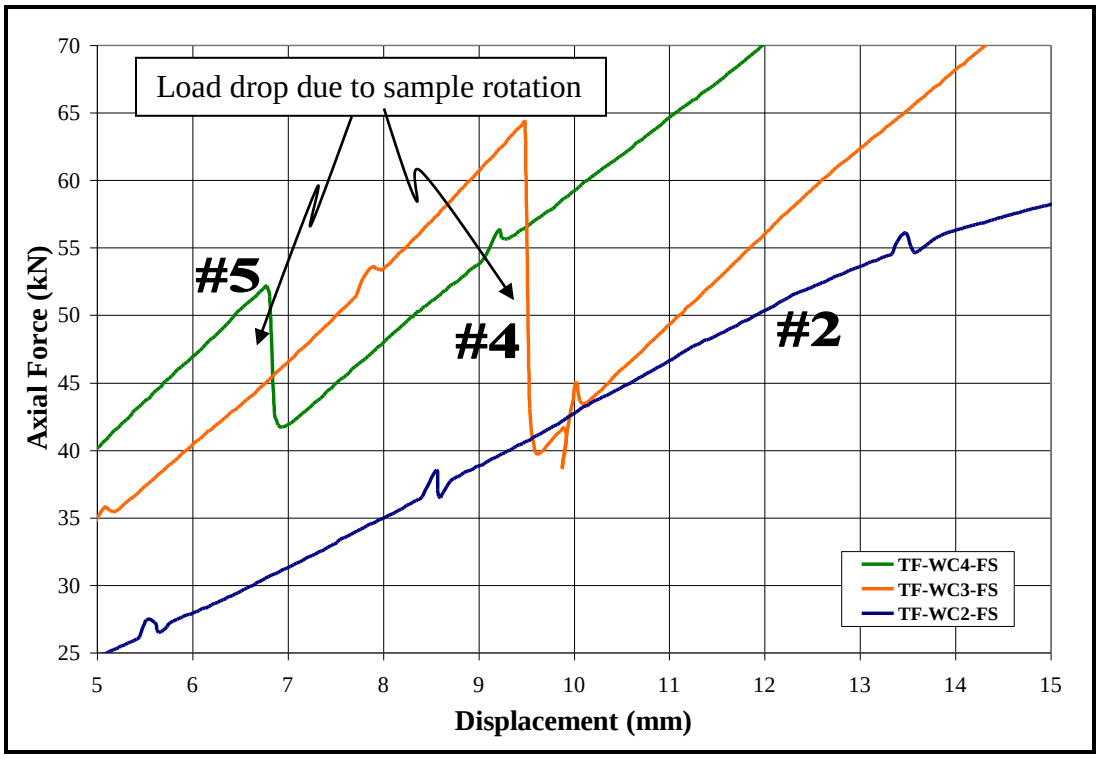

Figure 4.73: Load drop due to sample rotation

In addition to the observations from the force vs. displacement plots, a visual inspection of the rotation markings on the upper tensile lug and coupling can also differentiate this occurrence from stick slip. Around the time that this decrease in force occurred, the black markings that were painted on the upper tensile lug and coupling had separated by about 40 to 45 degrees (see Figure 4.74).

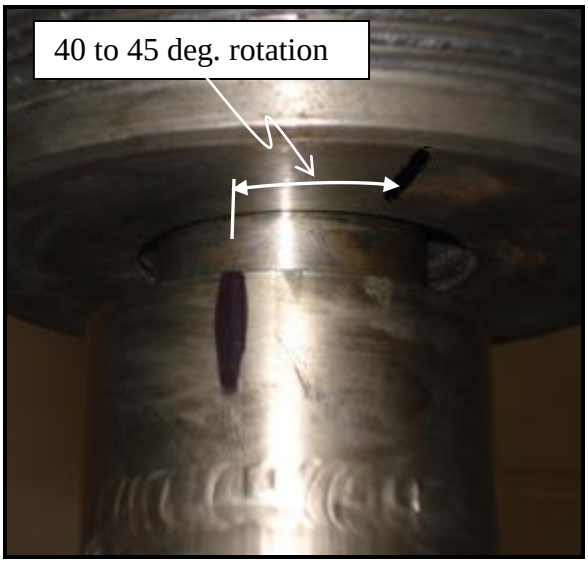

Figure 4.74: Sample rotation responsible for load drop with respect to fixed coupling

Examination of the force vs. displacement plots at the time that this drop in force occurred revealed that both specimens experienced a vertical displacement of about 0.2 mm (0.0079 in.). When we consider that the tensile lug has a thread pattern of 1 in. – 14, meaning it has 14 threads per one inch of length, the 0.2 mm of vertical displacement equates to a rotation of roughly 0.11 threads. A complete rotation around 1 thread is equal to 360 degrees. Therefore a rotation of 0.11 threads would correspond to a rotation of 39.7 degrees. Factoring in the stretch of the cable at these elevated loads, the estimated 40 to 45 degree rotation of the sample with respect to the upper coupling can be attributed to the abrupt reduction in load experienced by both specimens. Installing jam nuts at the upper coupling to prevent rotation of the upper portion of the sample will provide further insight into mechanical behavior of the grip design.

4.1.4. Fatigue Testing

Based on the results of the modified grip design, a series of tests on the fifth, sixth, and seventh full scale TF press-fit grip sleeves were performed. Due to the success of the previous tests (see Section 4.1.3), this final group of samples were constructed to the same specifications as TF-WC4-FS, tested with the same apparatus, and followed the

same tensile testing procedure. Despite the fact that tensile testing provided a good representation of the strength of this grip sleeve configuration, there was still some concern as to how it would perform in the real world. When the actual 800 m long cable is pulled, the grip sleeve is expected to experience a more varied loading pattern than what was created during the monotonic tensile tests. Therefore, these three specimens were subjected to 1000 cycles of loading from 600 to 6000 pounds before tensile loading them to failure.

Based on an observation made during the previous tests, it was observed that due to its helical coil pack geometry, the exposed portion of the cable between the grip sleeves had a natural tendency to untwist during loading (refer to Section 4.1.3). This untwisting caused the upper tensile lug to unscrew itself from the threaded attachment stud, which led to an abrupt drop in load. To prevent this unscrewing, a jam nut was incorporated into the design of the upper coupling. After the specimen was attached, this jam nut was tightened down against the tensile lug to prevent the sample from unscrewing (see Figure 4.75). Additionally, the bottom tensile lug of each sample was tightened down until it was flush with the lower coupling (see Figure 4.76). By restricting the motion of both grip sleeves, any rotation that occurred would be internal to the specimen and concentrated on the exposed portion of the cable.

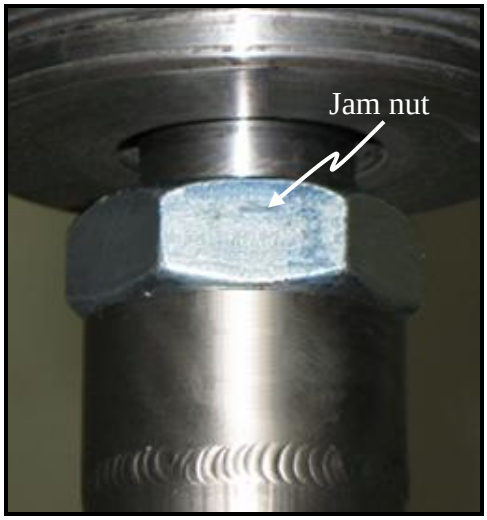

Figure 4.75: Jam nut installed against upper tensile lug to prevent rotation

Figure 4.76: Lower tensile lug tightened flush with coupling to prevent rotation

As was done in previous tests, a series of markings were painted onto each specimen in order to monitor rotation. In addition to the standard markings (vertical line on upper tensile lug and horizontal line on bottom of upper coupling), a second vertical line that corresponded with the original markings was painted on the side of the jam nut (see Figure 4.77). Based on the misalignment between these markings during the loading, the effectiveness of the jam nut could be evaluated.

Figure 4.77: Reference marks to monitor sample rotation

Due to the variable loading that the grip sleeve is likely to experience during actual usage, it was recommended that the final three samples be fatigue tested before loading them to failure in tension. Based on the success of a Russian team who performed this same task with a pulling force of roughly 26.7 kN (6,000 lbs.), the requirements for the fatigue test specified 1,000 cycles within a 3 hour time period over a load ranging from 0 to 3 tons. The fatigue test for the TF grip sleeves were performed using the same Interlaken series 3300 universal testing machine that had been used to conduct all of the previous pull tests. However, unlike the tensile tests which required the machine be operated in displacement control mode, fatigue testing was performed in load control mode. It is important to note that due to some software restrictions, slight modifications had to be made to the recommended testing parameters. The requirements called for 1000

cycles over a 3 hour time period, or a frequency of 0.0926 Hz. For simplicity, a frequency of 0.1 Hz was used instead. Secondly, the specimen was to be subjected to a cyclic load of 0 to 3 tons. Due to a restriction of the test software, the minimum load had to be greater than or equal to 10% of the maximum load. Therefore, the specimen was subjected to a cyclic load ranging from 600 to 6,000 lbs. Lastly, the loading pattern was based on a sinusoidal waveform.

Based on the data collected during the fatigue tests, a series of plots were created to display the force and displacement versus time for the TF-WC5-FS, TF-WC6-FS, and TF-WC7-FS samples. When analyzing this data, it is important to keep in mind that all three samples were identical. Therefore, any deviations observed in the data were an indication of some physical occurrence caused by the cyclic loading rather than the result of a variation between the specimens. Due to the large amount of data collected during each test, it was difficult to evaluate the entire test period at once. Instead, the data was separated into three specific time periods (beginning, middle, and end) and in intervals lasting 100 seconds. A comparison of the axial force and displacement versus time for all three specimen at all three time intervals are displayed below in Figures 4.78 through 4.86.

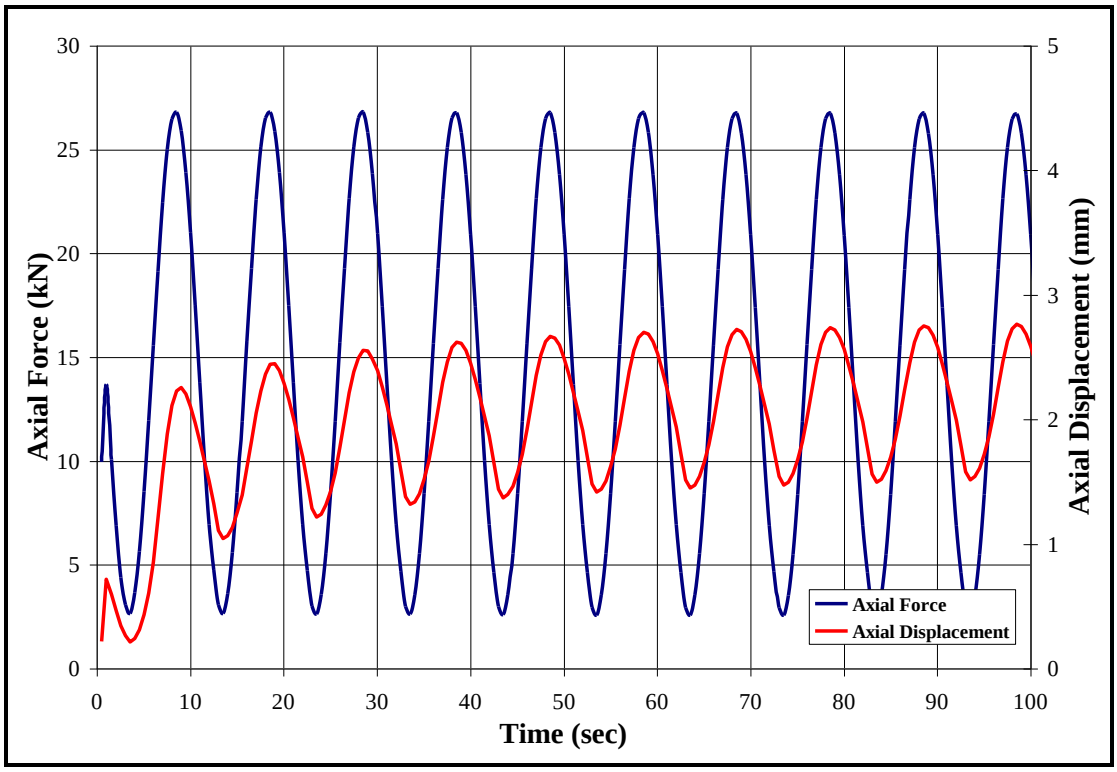

Figure 4.78: Initial 100 sec. interval of TF-WC5-FS fatigue test

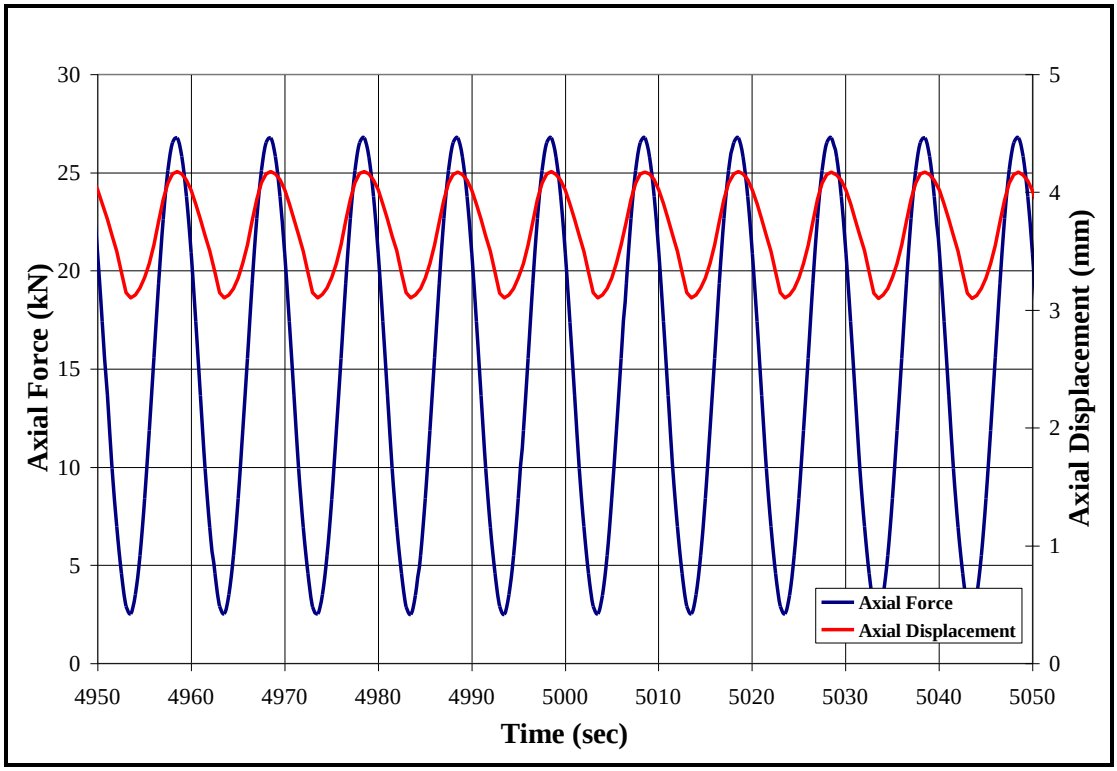

Figure 4.79: Intermediate 100 sec. interval of TF-WC5-FS fatigue test

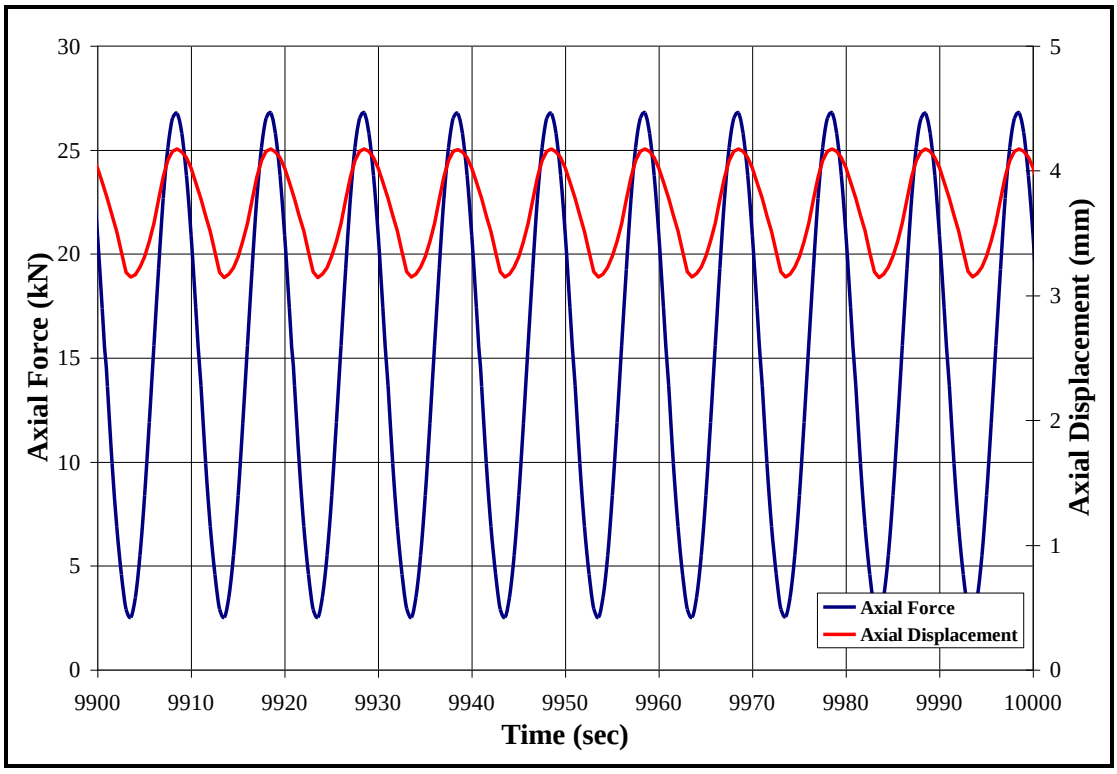

Figure 4.80: Final 100 sec. interval of TF-WC5-FS fatigue test

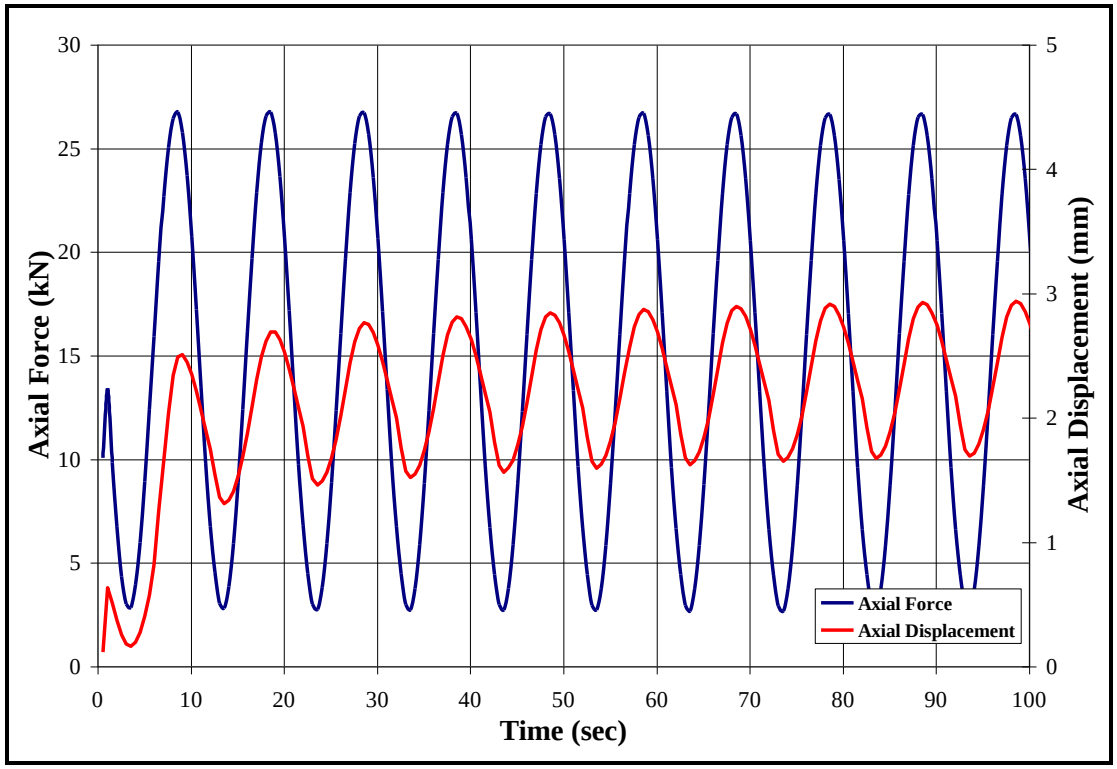

Figure 4.81: Initial 100 sec. interval of TF-WC6-FS fatigue test

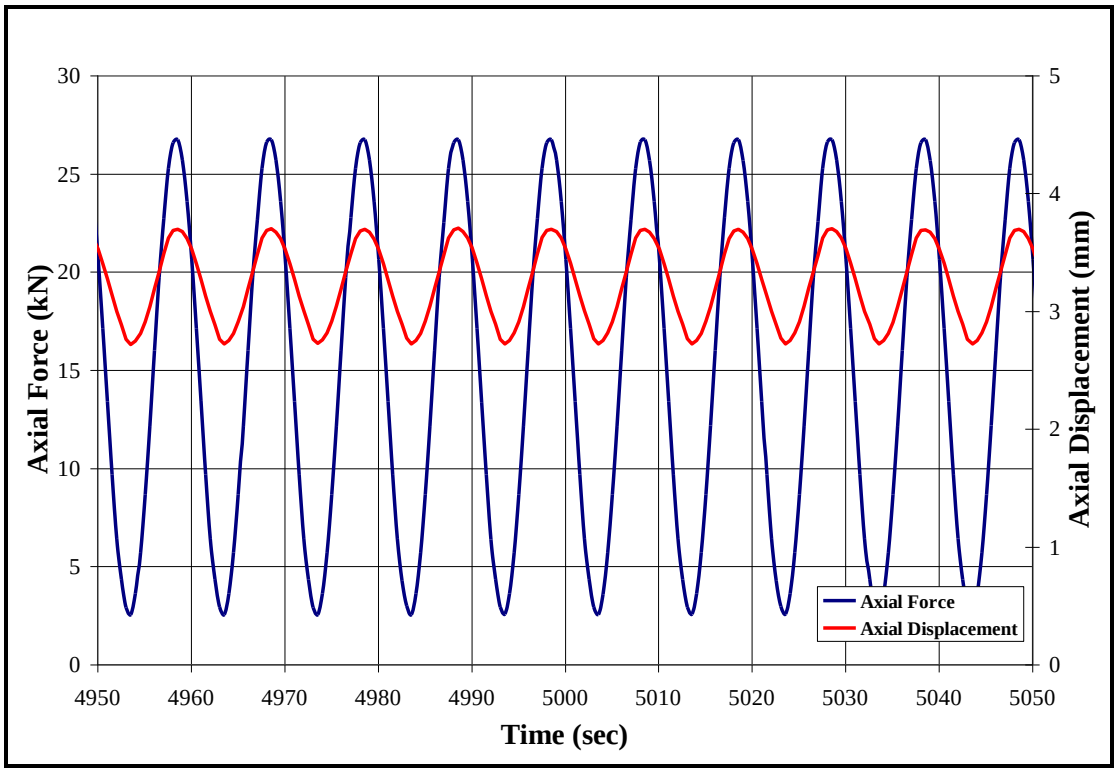

Figure 4.82: Intermediate 100 sec. interval of TF-WC6-FS fatigue test

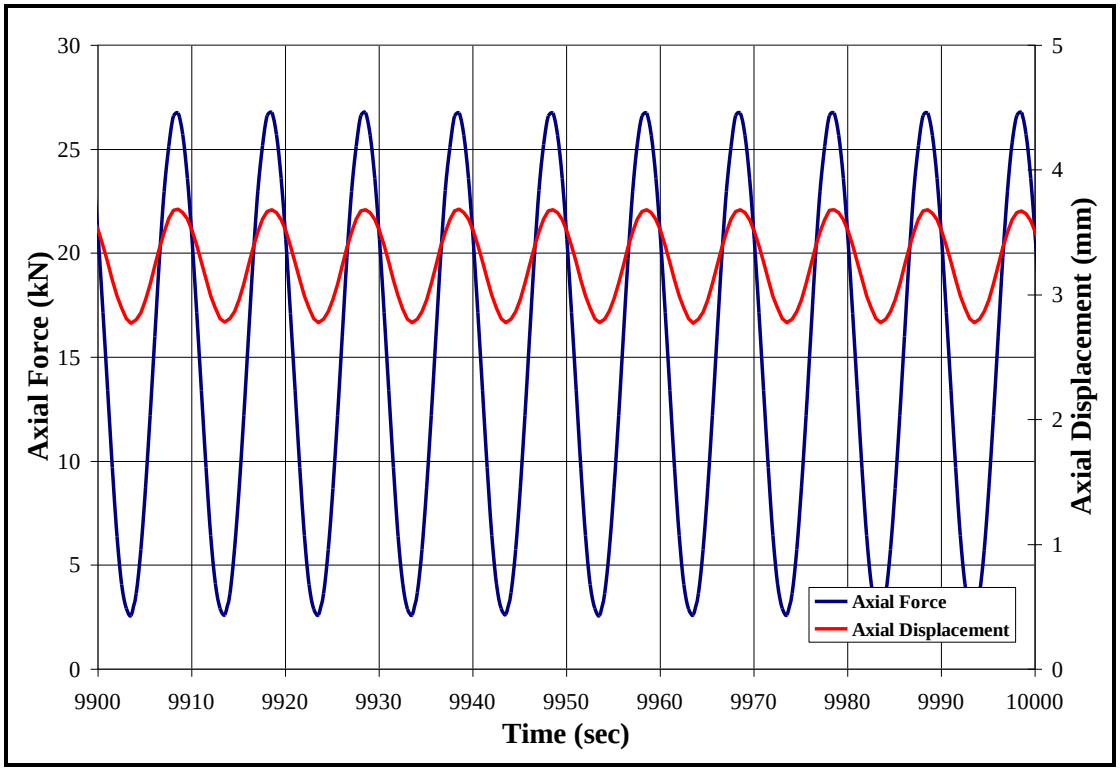

Figure 4.83: Final 100 sec. interval of TF-WC6-FS fatigue test

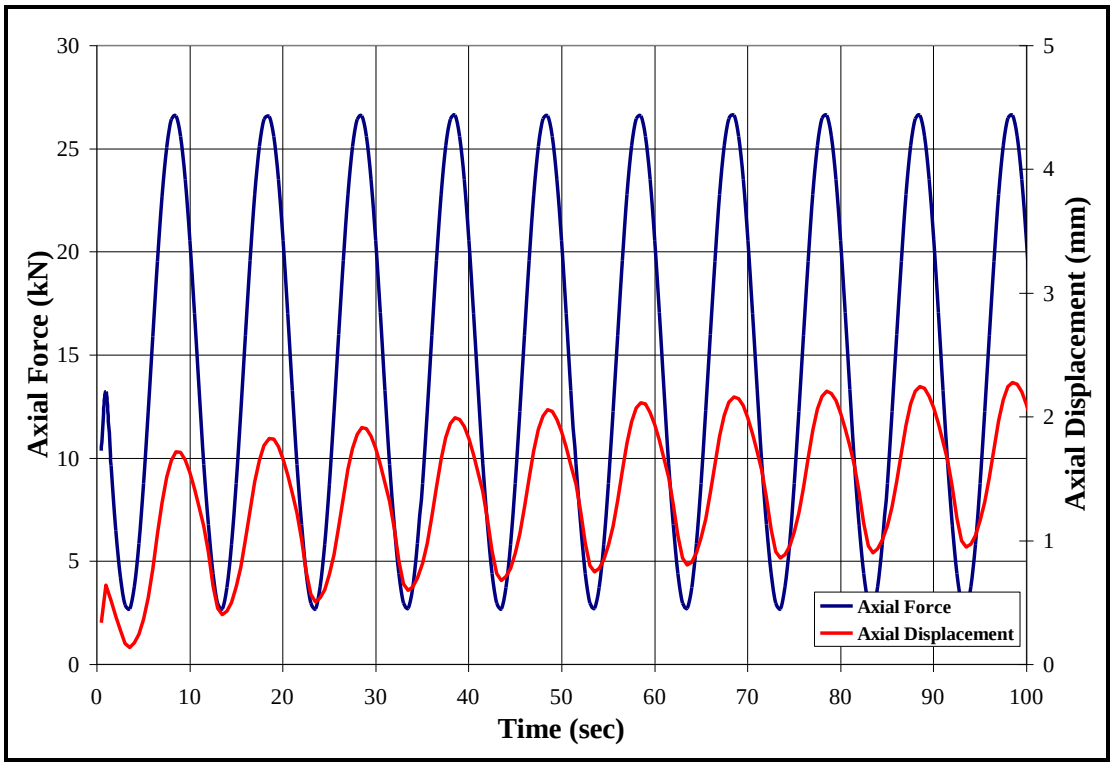

Figure 4.84: Initial 100 sec. interval of TF-WC7-FS fatigue test

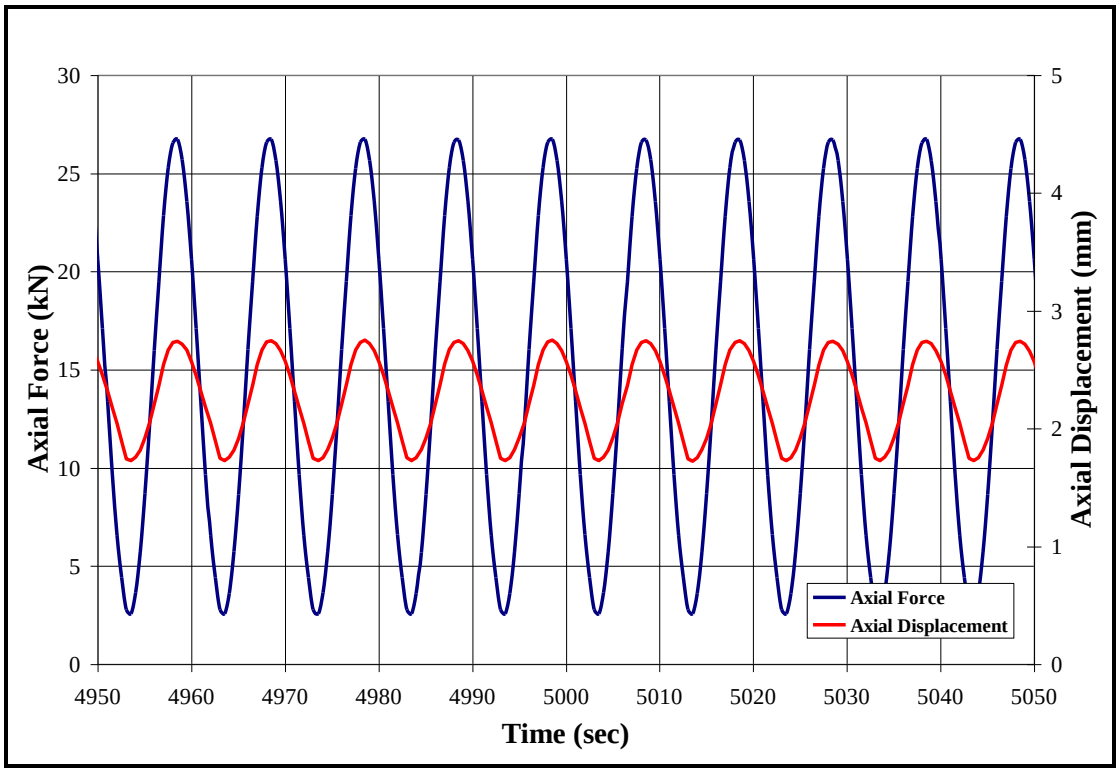

Figure 4.85: Intermediate 100 sec. interval of TF-WC7-FS fatigue test

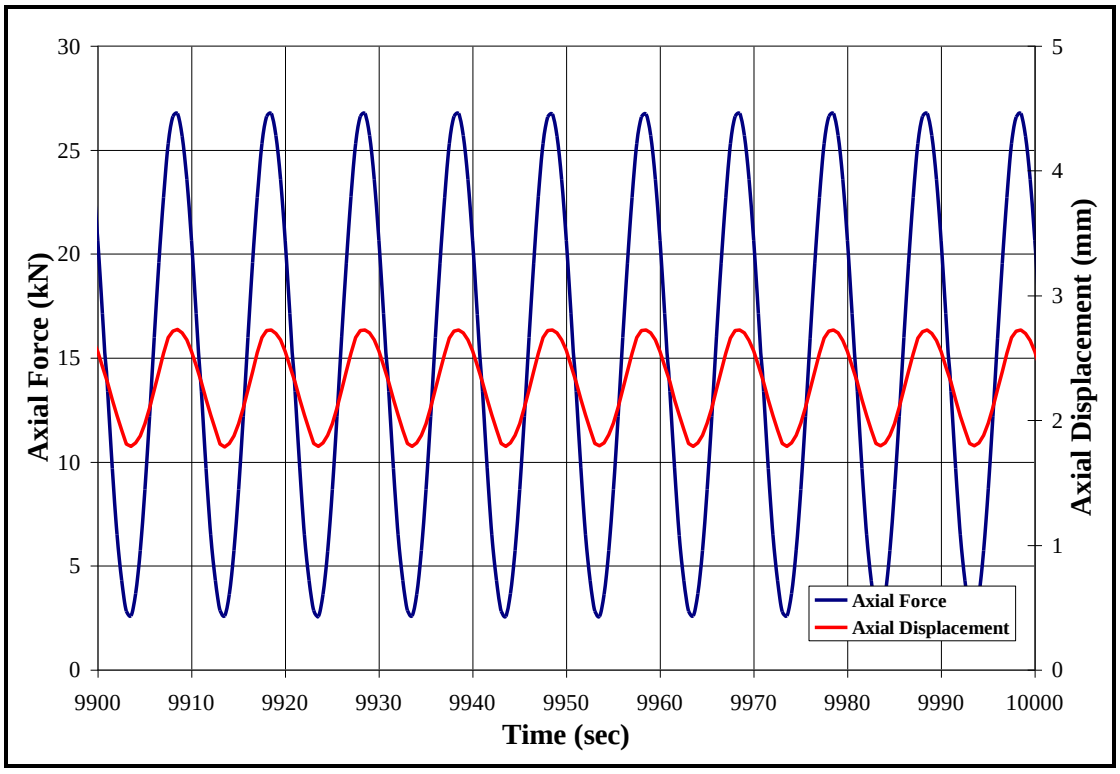

Figure 4.86: Final 100 sec. interval of TF-WC7-FS fatigue test

A close examination of Figures 4.78 – 4.86 reveals several interesting trends that occurred during the fatigue tests; the first being an increase in displacement with increasing number of cycles. As these figures show, the largest increase in displacement occurred for all three specimens during the first time interval. In order to more clearly investigate this trend, an additional set of plots that specifically focus on the first 6,000 seconds or 556 cycles (see Figures 4.87 – 4.89) were created.

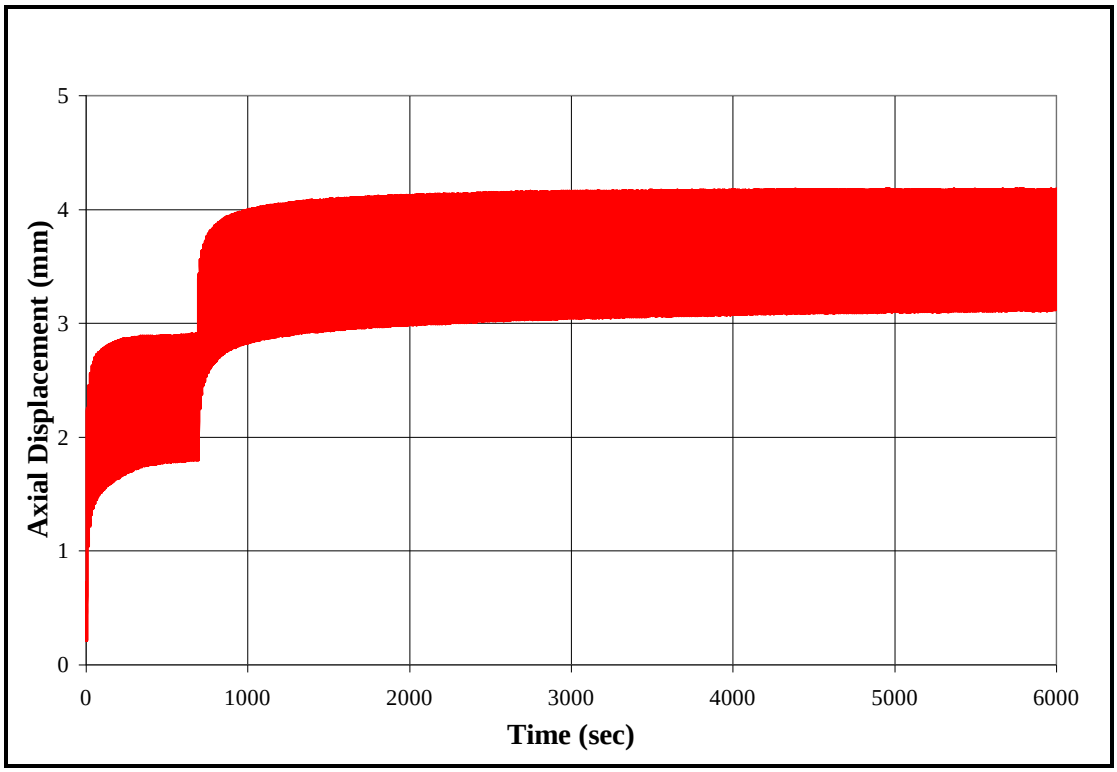

Figure 4.87: TF-WC5-FS displacement increase with increasing time/# cycles

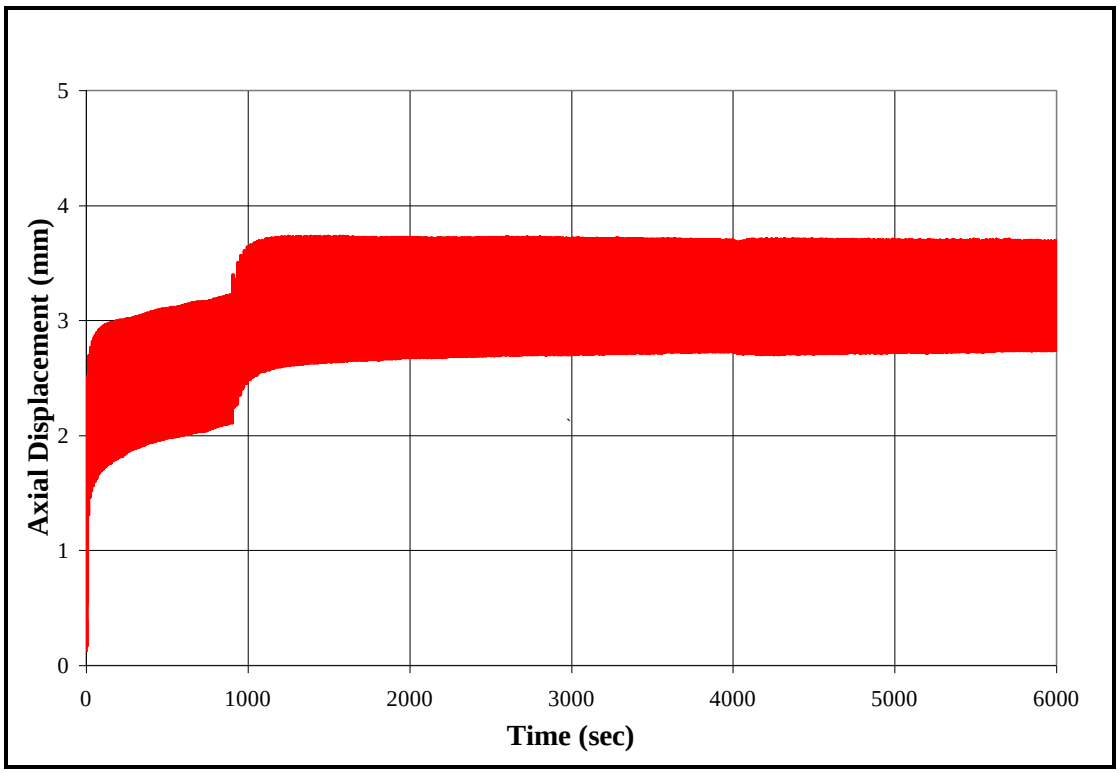

Figure 4.88: TF-WC6-FS displacement increase with increasing time/# cycles

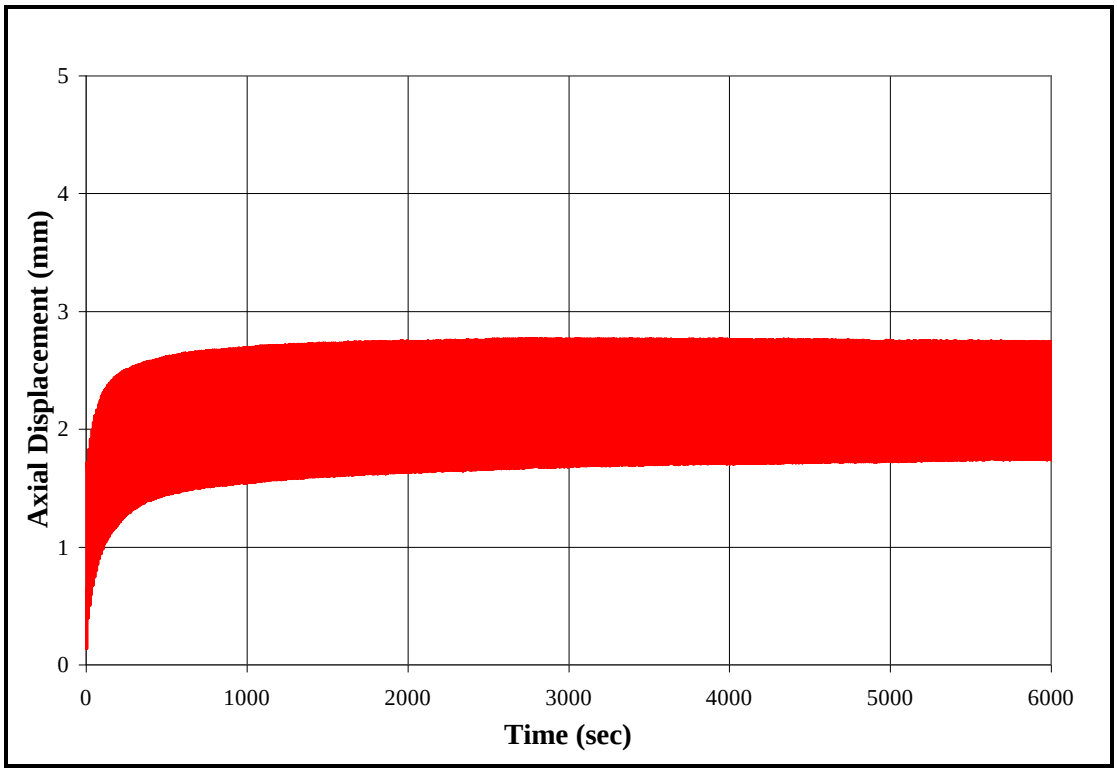

Figure 4.89: TF-WC7-FS displacement increase with increasing time/# cycles

As can be seen in Figures 4.87 – 4.89, not only did each sample achieve a slightly different maximum average displacement, they also occurred at different times. This increase in displacement with increasing cycles is likely the elongation of the cable resulting from a combination of cable stretch, sleeve slippage, and slack within the grip sleeves being removed (see Figures 4.90 and 4.91). It was also noted that the gap between the accent bands occurred during the cyclic loading, but did not appear to increase during the tensile loading to failure.

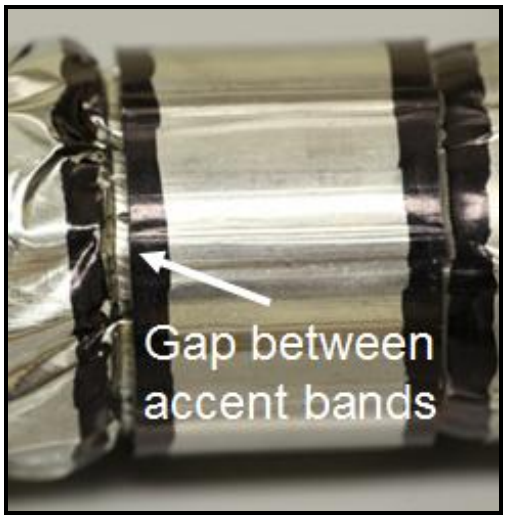

Figure 4.90: Gap between accent bands after fatigue testing

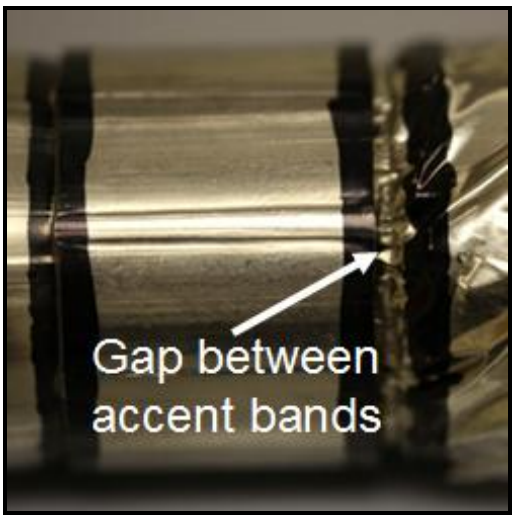

Figure 4.91: Gap between accent bands after fatigue testing

Additionally, the behavior of each specimen as it approached its maximum mean displacement was slightly different. As can be seen in Figures 4.87 – 4.89, TF-WC5-FS and TF-WC6-FS experienced rapid increases in mean displacement (see Figures 4.87 and 4.88), whereas TF-WC7-FS maintained a gradual increase in mean displacement (see Figure 4.89). We can attribute these rapid increased in displacement of TF-WC5-FS and TF-WC6-FS to a stick slip mechanism.

Despite the fact that each of the three samples experienced different displacement at different rates, it's important to note that peak to peak amplitude for all three samples remained constant at about 1.25 mm. Also the slope of the load versus displacement data for each sample was the same during the cyclic loading; providing a good indication of repeatability.

After each fatigue test was concluded, the machine was reconfigured and tensile testing immediately began. Based on the force and displacement data collected during the tensile loading to failure, a series of plots were created to evaluate the performance of the TF-WC5-FS, TF-WC6-FS, and TF-WC7-FS samples as compared to the TF-WC4-FS sample. Note that sample TF-WC4-FS was not subjected to fatigue testing prior to tensile testing, nor did it utilize a jam nut to prevent rotation of its upper grip sleeve. Because TF-WC4-FS was the only dissimilar sample, it can be thought of as a baseline configuration, to which the effects of the modifications made to the subsequent samples

can be evaluated. A comparison of the axial force versus time and axial force versus displacement for all four configurations are displayed below in Figures 4.92 and 4.93.

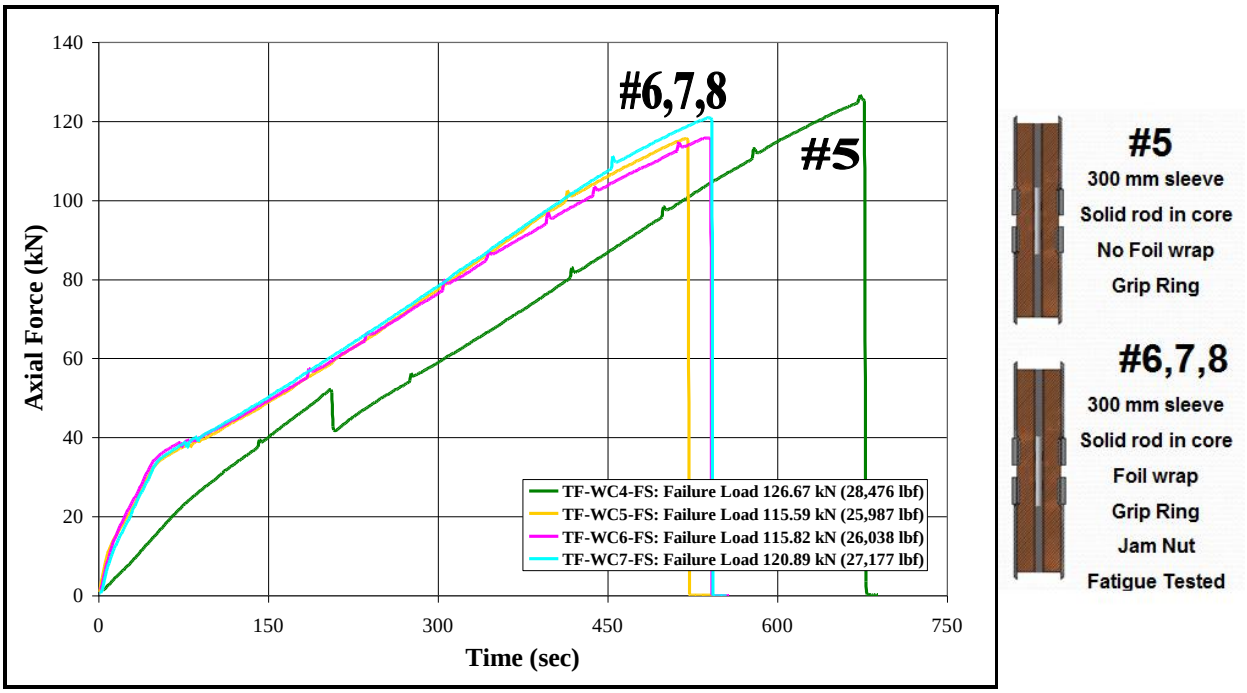

Figure 4.92: Axial force vs. time for TF-WC4, TF-WC5, TF-WC6, and TF-WC7

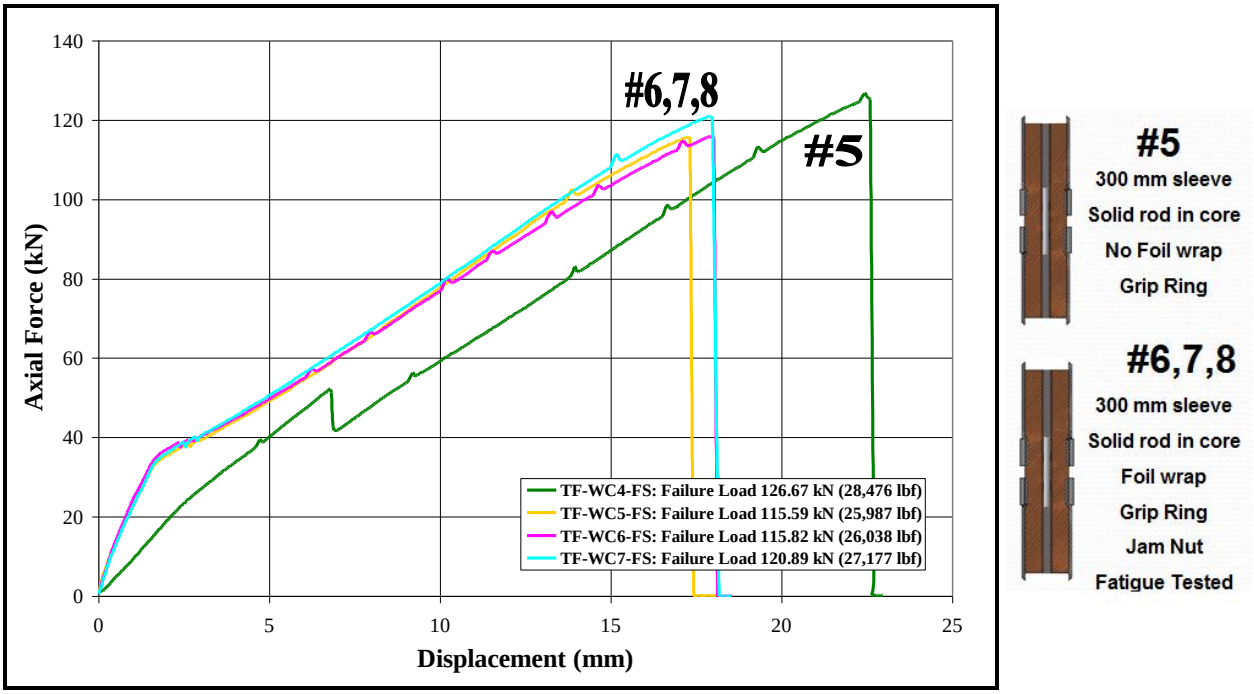

Figure 4.93: Axial force vs. displacement for TF-WC4, TF-WC5, TF-WC6, and TF-WC7

As can be seen in Figures 4.92 and 4.93, TF-WC4-FS, TF-WC5-FS, TF-WC6-FS, and TF-WC7-FS reached loads of 126.67 kN (28,475.77 lbf), 115.59 kN (25,986.7 lbf), 115.821 kN (26,037.53 lbf), and 120.889 kN (27,177.01 lbf) respectively, before failure. Based on these results, several conclusions can be made.

1. All three of the samples that were fatigue tested failed at loads that were an average of 9.237 kN (2,076.5 lbf) lower than similar samples that were not fatigue tested.
2. In addition to fatigue testing, these three samples were also tensile loaded to failure with a jam nut that prevented them from untwisting. The samples that were restricted from motion with jam nuts failed at lower values. It is, however, not clear if the decrease in maximum load in specimens TF-WC5-FS, TF-WC6-FS, and TF-WC7-FS compared to specimen TF-WC4-FS occurred due to cyclic loading or due the use of jam nut.
3. Another interesting observation was the "knee" in the force vs. displacement curve that occurred at a load of approximately 34 kN and 1.8 mm of displacement. This "knee" occurred only in TF-WC5-FS, TF-WC6-FS, and TF-WC7-FS samples, which were also the only specimens that were fatigue tested and utilized jam nuts. Because these samples experienced two major changes (fatigue testing and jam nuts) compared to other similar samples, it is difficult to say which modification caused this behavior. Tensile testing an additional sample that utilizes a jam nut but was not subjected to fatigue testing would help explain this occurrence.

   A possible explanation is that this "knee" occurred at the yield point of one of the materials. As was stated above, this "knee" appeared at a load of around 34 kN. Based on a mechanics of materials calculation, the normal stress in the copper strands, stainless steel core tube, and stainless steel sleeve at 34 kN of applied force were found to be 34.91 MPa, 57.58 MPa, 57.58 MPa, respectively. According to their stress-strain curves, these materials have yield strengths of 70 MPa, 290 MPa, and 170 MPa, respectively, which

are well above the calculated stresses for these components at the time this trend occurred. Based on these results, it can be concluded that this "knee" cannot be attributed to yielding of the sample.

As was previously discussed, the specimen had a tendency to untwist during loading. In an effort to restrict this motion, a jam nut was added to the upper coupling and the lower tensile lug was tightened until it was flush with the lower coupling. Despite the fact that these features restricted the motion of the grip sleeves, a great deal of untwisting still occurred in the exposed region of cable. As can be seen in the Figures 4.94 – 4.96, the rotation of these regions of exposed cable, and thus the protective foil wrap, caused a distortion and rotation of the specimen identification tags (note the movement of letters "C 5", "C 6" and "C 7" in Figures 4.94 – 4.96). It is important to note that all these photos were taken after the specimens failed and there was no load on the specimens.

Figure 4.94: Rotation of foil wrap on TF-WC5-FS sample

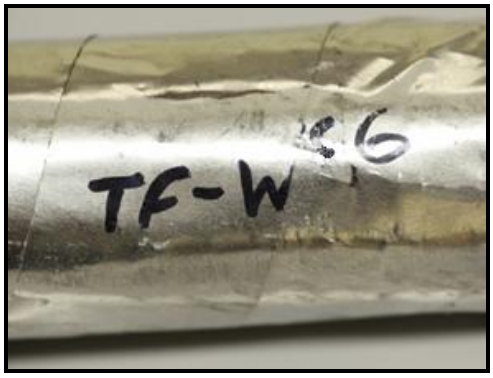

Figure 4.95: Rotation of foil wrap on TF-WC6-FS sample

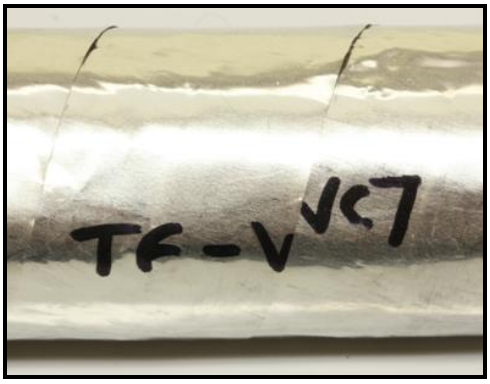

Figure 4.96: Rotation of foil wrap on TF-WC7-FS sample

Another indication that the exposed portion of the cable had attempted to twist were the folds in the protective foil wrap near the strand/sleeve interface at each end (see Figures 4.97 and 4.98). It is important to note that the folds in the foil follow a counterclockwise orientation; the same direction that the cable naturally untwists. For clarification, a picture showing a sample that did not experience this same folding of the foil wrap is shown in Figure 4.99.

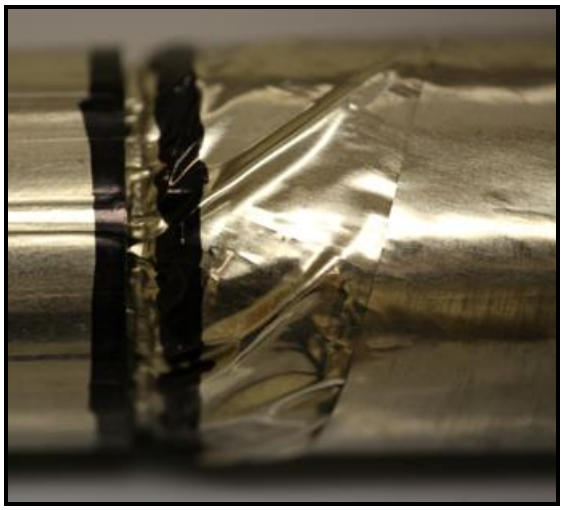

Figure 4.97: Folding of foil wrap due to cable rotation

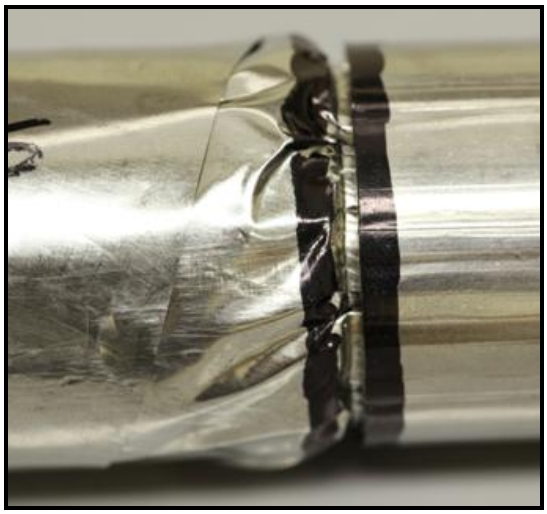

Figure 4.98: Folding of foil wrap due to cable rotation

Figure 4.99: Lack of foil wrap folding due to lack of cable rotation

A great deal of additional information about the way in which each grip sleeve failed can be obtained by looking at the slope of the force vs. displacement curves. As can be seen in Figure 4.93, the slopes for TF-WC5-FS, TF-WC6-FS, and TF-WC7-FS after the 'knee' remained constant until their failure loads were reached. This was an indication that a catastrophic failure, rather than progressive failure due to slippage, had occurred. This drastic failure was actually caused by a seam weld fracture between the tensile lug and grip sleeve body (see Figure 4.100 – 4.105).

Figure 4.100: TF-WC4-FS seam weld fracture

Figure 4.101: TF-WC4-FS seam weld fracture

Figure 4.102: TF-WC6-FS seam weld fracture

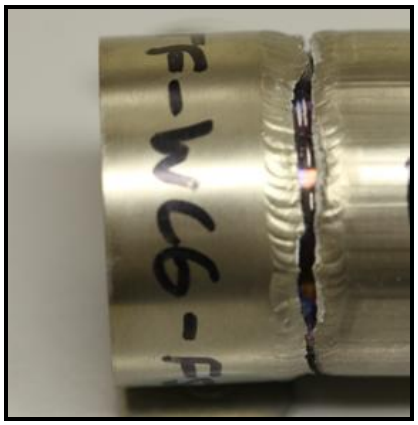

Figure 4.103: TF-WC6-FS seam weld fracture

Figure 4.104: TF-WC7-FS seam weld fracture

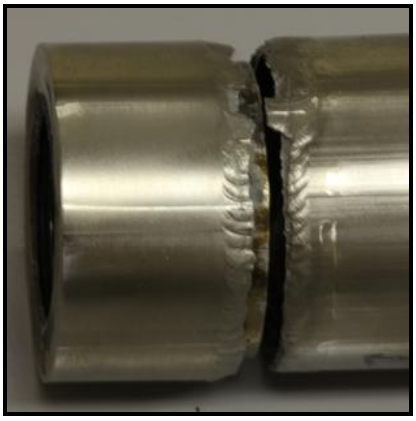

Figure 4.105: TF-WC7-FS seam weld fracture

It is interesting to note that of the six full scale samples that were tested, four broke at seam welds. The most plausible explanation for the weld failure at the lower sleeve is the natural tendency of the twisted cable to untwist when pulled. This specimen twisting is a mechanism by which the internal torque is relieved. Before any efforts were made to restrict the rotation of the grip sleeve, every specimen had a tendency to rotate in a counterclockwise direction when tensile tested. Due to the thread orientation of the tensile lugs that attach the sample to the testing apparatus, this counterclockwise rotation caused the upper tensile lug to unscrew while the lower tensile lug remained stationary (refer Section 4.1.3.). When a jam nut was added to the top and the lower lug was tightened until it was flush with the lower coupling, the grip sleeves remained stationary but this tendency to rotate did not go away. By fixing these ends, a torsional load was created. It is believed that this torsion on the lower grip sleeve is what actually caused the weld failures.

In order to investigate this theory, the torque generated by the untwisting of the cable was calculated, and was then used to determine the shear stress experienced by the lower grip sleeve. By comparing the shear stress on the grip sleeve with the shear strength of the filler material used to create the weld, it would be possible to see if failure due to torsion was feasible.

Based on the rotation of the samples that did not utilize jam nuts, an average rotation at the upper grip sleeve of 180 degrees (π radians) was observed. Utilizing a

standard Mechanics of Materials approach, this amount of rotation was found to produce a torque of approximately 28.98 kN·m on the lower grip sleeve with a corresponding shear stress of approximately 550.65 MPa. Due to the fact that this methodology was based on the assumption that the copper cable was actually a solid tubular shaft, this value is likely higher than the actual shear stress. In order to improve upon the accuracy of this calculation, a second torque value was determined using a Mechanics of Wire Rope approach. With this method, the moment produced by the cable could be determined based on the load applied to the cable, the winding radius of the cable, the number of layers that comprise the cable, the number of strands in each layer, and the lay angle of the strands in the cable [42]. For a single layer 6 strand rope with a failure load of 121 kN (the average load supported by the four samples that experienced weld failures), the torque produced by the unwinding of the cable was approximately 17.18 kN·m. Utilizing the same Mechanics of Materials approach as before, the shear stress based on this torque was calculated to be approximately 326.42 MPa. Despite the fact that this approach accounted for the 6 strands that comprise the cable, there was no consideration for the number of individual wires that make up the strands or the material properties of the cable in the torque equation. Therefore, this shear stress is still likely to be different than the actual number.

The weld joints used to connect the tensile lugs and grip sleeves on the test samples were Gas Tungsten Arc Welded (GTAW or TIG) welded using 304 Stainless Steel filler metal. This particular filler metal possesses a shear strength of 186 MPa and a tensile strength of 500 MPa [43]. A comparison of these values with those calculated above shows that the shear stress produced by the cable torque exceeds the shear strength of the weld joint, but not its tensile strength. Based on this comparison, it is very probable that the failure of the TF-WC4-FS, TF-WC5-FS, TF-WC6-FS, and TF-WC7-FS samples was due to torsion.

Another factor to consider when evaluating these results is the existence of a stick-slip mechanism (see Sections 4.1.2. and 4.1.3.) that occurred during the tensile loading. One distinct case of this stick-slip mechanism was observed on the force versus

displacement plot for the TF-WC4-FS, TF-WC5-FS, TF-WC6-FS, and TF-WC7-FS samples (see Figure 4.106).

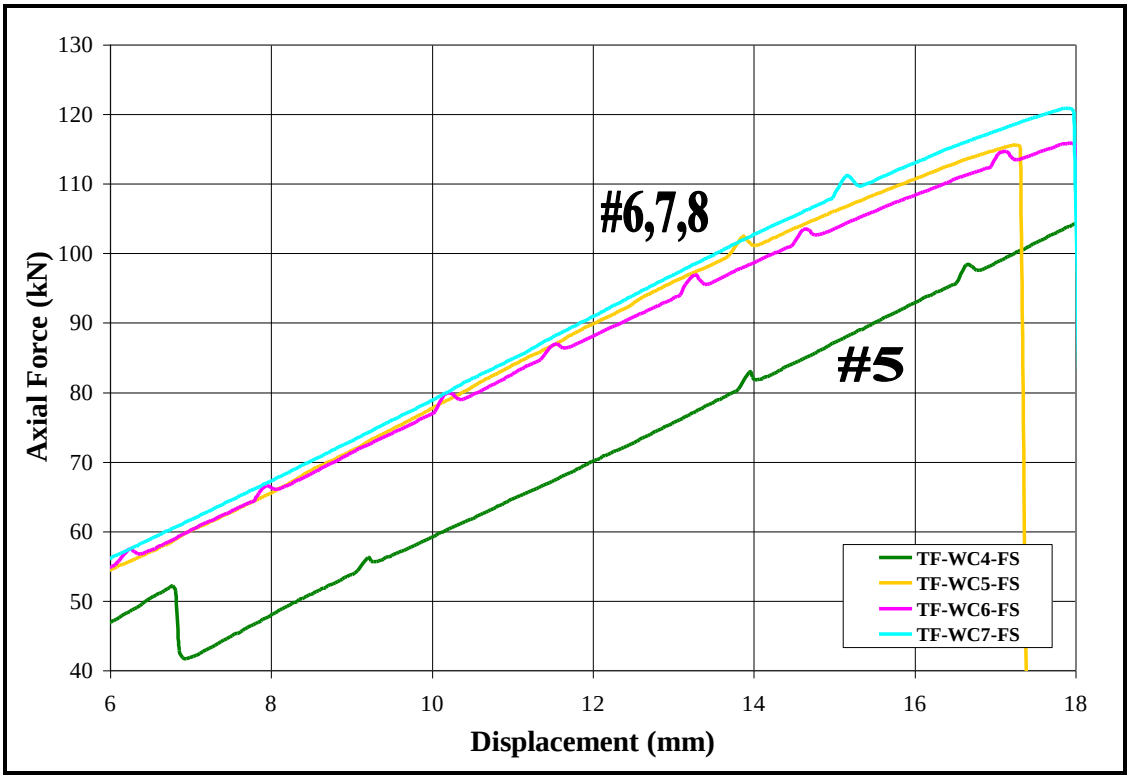

Figure 4.106: Comparison of stick slip experienced by TF-WC4, TF-WC5, TF-WC6, and TF-WC7

The occurrence of stick-slip was identified based on the magnitude of the fluctuations that were observed on the force versus displacement plot. As can be seen in Figure 4.106, the magnitude of the oscillations remained constant with increasing axial load for all four samples, and occurred at roughly the same load/displacement/time. This is an indication that fatigue testing had no effect on this behavior.

In addition to the stick-slip mechanism, another unusual trend appeared on the force vs. displacement plots of both TF-WC3-FS and TF-WC4-FS samples. This phenomenon was characterized by a sudden drop in the axial load that was not indicative of stick-slip. Based on a visual observation as well as a numerical calculation, it was determined that this abrupt load decrease was the result of the upper tensile lug unscrewing from the coupling as the specimen began to untwist (see Section 4.1.3.). In an

attempt to combat this problem, jam nuts were installed against the upper tensile lug to prevent this unwanted action (refer to Figure 4.77). As can be seen in Figures 4.106, this phenomenon did not occur with TF-WC5-FS, TF-WC6-FS, or TF-WC7-FS.

4.2. Finite Element Analysis Results

Despite the fact that they were simplified in a variety of ways, the FEA models that were used to evaluate the deformation behavior of the cable were still extremely complex. Additionally, the Comsol Multiphysics modeling environment is difficult for an inexperienced user to master. As a result, accurate FEA results could not be obtained. Due to these inaccuracies, FEA results will not be included in this thesis. However, the process that was used to develop the FEA models was accurate and could potentially be helpful for someone else who chooses to perform a similar analysis in the future. Therefore, the methodology will still be included.

4.3. Welding Metallurgy Results

In addition to the deformation behavior of the cable, there are several characteristics of the weld joints that indicate grip sleeve failure due to torsion. Based on the angle of their fracture surfaces, it can be concluded that the welds failed in shear rather than tension. As can be seen in Figure 4.107, the fracture face is oriented at an angle of approximately 45°, which is indicative of shear fracture [41]. The surface of a tensile fracture would appear to be flat, or oriented at a 90° angle. Additionally, we can see from figure 4.107 that it was the weld itself that broke and not the grip sleeve as there is no sleeve material at the fracture surface. Since the shear strength of the weld filler material is less than its tensile strength, this is another indication of shear failure.

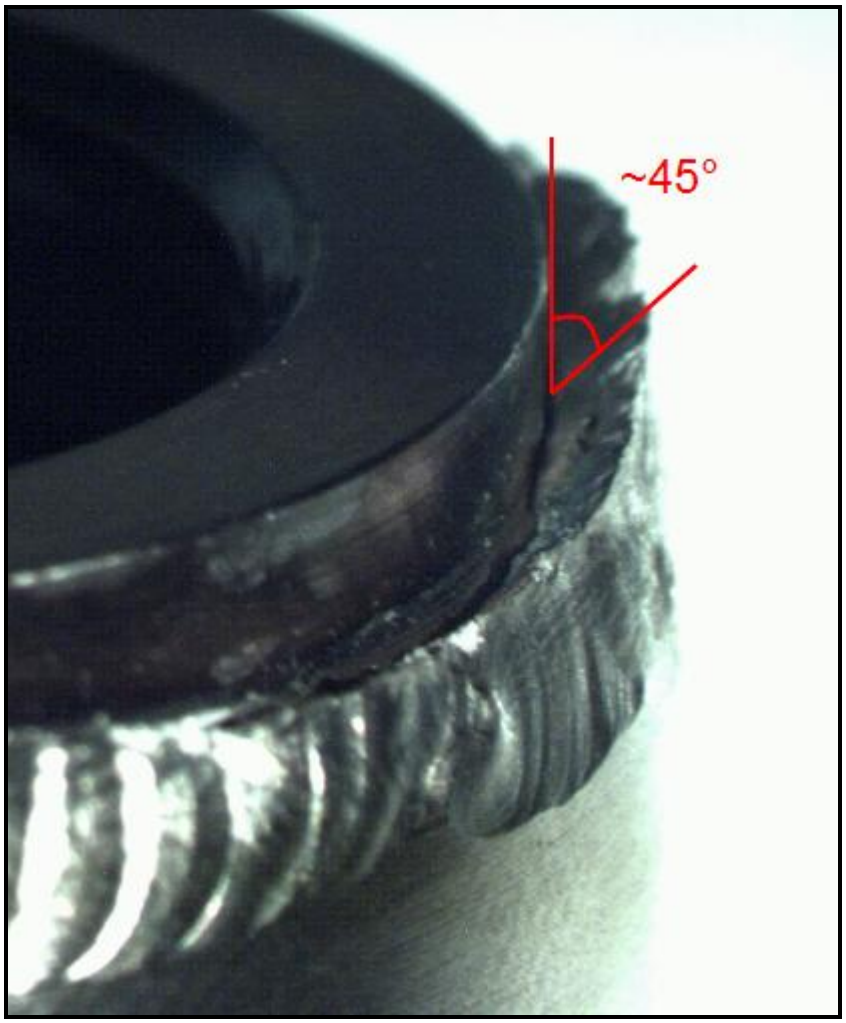

Figure 4.107: Seam weld fracture showing 45° angle of fracture face

Chapter 5
Conclusions and Recommendations

5.1. Conclusions

In order to evaluate the effectiveness of the TF press-fit grip sleeve, a total of eight tests were performed on six different grip sleeve configurations. Based on the tensile loading to failure of the preliminary sleeves, it was observed that a ~70mm grip sleeve with a solid core and no protective foil failed at a load of 81.28 kN (18,273.15 lbf) by sleeve slippage. By increasing the grip sleeve length to 300mm, adding a solid rod to the core tube, and leaving the protective foil wrap in place, the failure load under tensile loading increased to 86.69 kN (19,489.62 lbf) with failure due to sleeve slippage. Utilizing this same construction, with the exception of the removal of the protective foil wrap, the failure load under tensile loading increased to 91.35 kN (20,536.41 lbf) through failure due to sleeve slippage. Through slight modifications to the grip design which included the addition of a reinforcement grip ring to each grip sleeve, the failure load increased to 126.67 kN (28,475.77 lbf) under tensile loading, with failure due to a seam weld fracture at the lower tensile lug. Having surpassed the physical limitations of the grip sleeve attachment, three final samples were created. The only difference between these was that the foil wrap was not removed (due to its negligible contribution to failure load), a jam nut was placed against the upper coupling, and these samples were also fatigue tested prior to tensile loading to failure. Based on these results, it was observed that a 300mm TF press-fit grip sleeve with a 25.4mm wide reinforcement grip ring is capable of supporting a 116 kN (26,000 lbf) to 126.5 kN (28,500 lbf) tensile load, with little to no adverse effects from fatigue testing. Since this failure load exceeds the 8,000 lbf load used by a Russian team to perform this same task, it can be concluded that the press-fit grip design is capable of performing the required cable pull with a generous safety factor.

5.2. Recommendations

Despite our conclusion that the press-fit grip sleeve is an effective means of pulling TF cable through conduit, there were still several observations made during the test results that could not be fully explained; the main one being the failure of the seam weld that joined the lower tensile lug and grip sleeve. Because two major changes were made to the configuration before these tests were performed (fatigue testing and jam nut), it is not possible to attribute this occurrence to either modification. In order to figure out what was responsible for the weld failure, several additional tests need to be performed. Two samples should be pulled to failure with a jam nut but without being fatigue tested and two samples should be fatigue tested and pulled to failure without a jam nut.

Another trend that should be investigated is the "knee" on the force vs. displacement plots of the TF-WC5-FS, TF-WC6-FS, and TF-WC7-FS samples. As was previously described, these samples received two modifications that were not tested individually. Therefore, testing these modifications separately should make it possible to identify which one caused it.

Future testing recommendations

1) A series of additional tensile tests should be performed on a variety of sizes of samples. For example, this research focused on 300mm grip sleeves. In order to broaden the application of this grip sleeve design, grip sleeves of 100mm and 200mm lengths should be tested as well. Based on the results of these tests, it might be possible to develop some sort of linear trend that could be used to help a user of this design predict what size grip sleeve would be needed to support a desired load.
2) A more accurate FEA model should be created to obtain better insight into the deformation behavior of the cable. A truly accurate model could be used to evaluate the relationship between lay length and torque and even wire/strand lay direction and torque. Additionally, an accurate FEA model that agreed with the experimental test results could also be used to help a user predict what grip sleeve length would be required to achieve a desired failure load.

References

1. BP. (2006). [Statistical Review of World Energy 2009]. Retrieved from http://www.bp.com/statisticalreview. 21 July, 2010.

2. Energy Information Administration. (2009). [Emissions of Greenhouse Gases in the United States 2008]. Retrieved from http://www.eia.doe.gov/oiaf/1605/ggrpt/pdf/0573%282008%29.pdf. 18 October, 2010.

3. ITER. [Plasma Confinement]. Retrieved from http://www.iter.org/sci/plasmaconfinement. 13 July, 2010.

4. Associated Plasma Laboratory. [Plasma Confinement]. Retrieved from http://www.plasma.inpe.br/LAP_Portal/LAP_Site/Text/Plasma_Confinement.htm. 13, Jule 2010.

5. ITER. [Small quantities of fuel]. Retrieved from http://www.iter.org/sci/fusionfuels. 13 July, 2010.

6. ITER. [20th Century Fusion]. Retrieved from http://www.iter.org/sci/beyonditer. 11 July, 2010.

7. ITER. [ITER: the world's largest tokomak]. Retrieved from http://www.iter.org/mach. 13 July, 2010.

8. [Nuclear Fission vs. Nuclear Fusion]. Retrieved from http://www.diffen.com/difference/Nuclear_Fission_vs_Nuclear_Fusion. 14 August, 2010

9. ITER. Image taken from http://www.iter.org/industry. 13 July, 2010.

10. The Institute of Physics blog. (2010). [Physics around the UK]. Retrieved from http://www.iopblog.org/2010-schools-lecture-part-5/. 14 August, 2010.

11. JET. Image taken from http://www.jet.efda.org/focus-on/plasma-heating-current-drive/ohmic-heating/. 14 August, 2010.

12. ITER. [Magnets]. Retrieved from http://www.iter.org/mach/magnets. 11 July, 2010.

13. ITER. Image taken from http://www.iter.org/mach/magnets. 13 July, 2010.

14. ITER. [Toroidal Field System]. Retrieved from http://www.iter.org/mach/magnets. 11 July, 2010

15. Chan, Kevin. ITER. Personal communication. May 2010 – October 2010.

16. Washington State Department of Labor and Industries. Image taken from http://www.lni.wa.gov/wisha/rules/construction/HTML/296-155L_2.htm. 14 August, 2010

17. Wikipedia: Wire Rope. Image taken from http://en.wikipedia.org/wiki/File:Wire_rope_with_thimble_and_ferrule.jpg. 2 September, 2010.

18. Far Reach Voyages. Image taken from http://www.farreachvoyages.com/projects/standingrigging.html. 2 September, 2010.

19. The Yacht Shop. Image taken from http://www.theyachtshop.co.uk/items/rope~twine~chain-and-wire/wire-rope/rope-grips/bulldog-grip-12mm-galvanised-h02811-detail.htm. 2 September, 2010.

20. Image taken from http://www.tpub.com/content/construction/14251/css/14251_139.htm. 5 September, 2010

21. Noble and Son Ltd. Image taken from http://www.nobles.com.au/products.aspx?doc_id=2827. 5 September, 2010.

22. Gunnebo Industries. Image taken from http://www.gunneboindustries.com/en/Lifting/Products/Steel-wire-ropes/Steel-wire-rope-components/Open-spelter-socket/. 2 September, 2010.

23. Integrated Publishing. [Construction: Basket Socket]. Retrieved from http://www.tpub.com/content/construction/14251/css/14251_140.htm. 4 September, 2010

24. McMaster-Carr. Image taken from http://www.mcmaster.com/#catalog/116/1406/=98ibf4. 4 September, 2010

25. ThomasNet News. Image taken from http://news.thomasnet.com/fullstory/Wire-Rope-Fittings-eliminate-need-for-swage-press-479682. 4 September, 2010

26. Wire Rope Specialists. Image taken from http://www.wireropespecialists.com/wirerope.htm. 4 September, 2010

27. Costello, George A. Theory of Wire Rope. Springer – Verlag. New York, New York. 1997. 1-3.

28. I and I Sing Inc. Image taken from http://www.iandisling.com/wire_rope_by_the_foot.htm. 4 September, 2010.

29. Integrated Publishing. Image taken from http://www.tpub.com/content/aviation/14018/css/14018_142.htm. 4 September, 2010.

30. Casar. Image taken from http://www.fastlift.co.za/pdf/CASAR%20-%20Rotation%20characteristics%20of%20steel%20wire%20rope.pdf. 4 September, 2010.

31. Chaplin, C.R. et al. (1999). [Tension-torsion fatigue effects in wire rope]. Retrieved from http://www.bgisl.com/RRR_OE_Twist_article_OIPEEC_1999.pdf

32. Chaplin, C.R., [Torsional failure of a wire rope during mooring line installation in deep water], Failure Analysis Case Studies II. Jones, D.R.H., Pergamon 2001. 49.

33. Hanes Supply, Inc. [Wire Rope 101]. Retrieved from http://www.hanessupply.com/content/catalog/001/001-0001.pdf. 2 September, 2010.

34. CarlStahl. Image taken from http://www.carlstahlevita.co.uk/Category.aspx?category=18. 2 September, 2010.

35. MITCalc. [Interference Fit]. Retrieved from http://www.mitcalc.com/doc/shaftconf/help/en/shaftconf.htm. 17 September, 2010.

36. Laboratory of Physics of Granular Plant Materials. [Wall Friction: Frictional Vibrations]. Retrieved from http://lgm.ipan.lublin.pl/eng/research.html. 17 September, 2010.

37. International Journal of Mechanical Sciences, Volume 29, Issue 9. (1987). Pages 605-619. [The response of wire rope to axial tensile loads- Part 1. Experimental results and theoretical predictions.

38. Images provided by Steve Kenney of ITER

39. COMSOL Solid Mechanics Module Documentation

40. Costello, George A. (2003). [Mechanics of Wire Rope]. Retrieved from http://www.ideals.illinois.edu/bitstream/handle/2142/286/1018.pdf?sequence=1. 21 September, 2010.

41. Lundin, Carl. University of Tennessee. Personal Communication. September 2010.

42. Feyrer, Klaus. [Wire Ropes: Tension, Endurance, Reliability]. Springer. New York. 2007. 64-104.

43. The University of Bolton. [Mechanical Properties of Metals]. Retrieved from http://www.ami.ac.uk/courses/topics/0123_mpm/index.html. 19 October, 2010.

Appendix

Appendix A

As was described earlier, a variety of micrographs were created that focus on several critical locations around the sample. The locations of interest were the interface between the sleeve and strands, and three radial locations between the sleeve/strand interface and the core of the sample. These same areas were observed at four different locations around the circumference of the sample, each 90 degrees apart. A schematic was created to illustrate the locations of interest (See Figure A1). In the schematic, NSEW refer to the region, I refers to the strand/sleeve interface, and 123 refers to the various radial locations; 1 being closest to the outside, and 3 being closest to the center or core of the sample. The micrographs are identified based on this system. For example, a photo of the TF-WOC1 sample at the 2nd radial position in the north quadrant will be labeled TF-WOC1-N2.

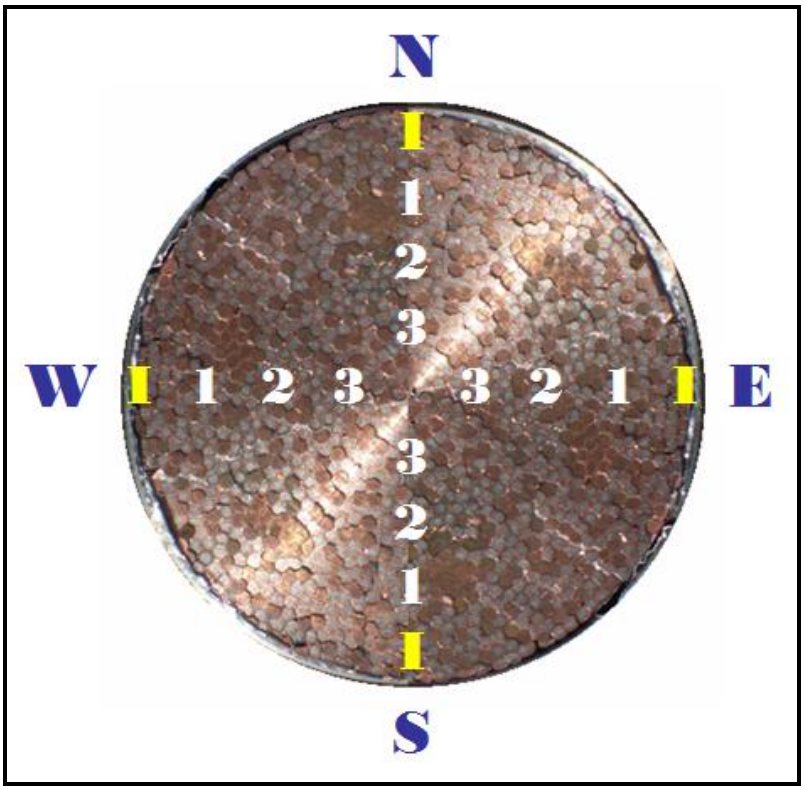

Figure A1: Legend for micrograph pictures

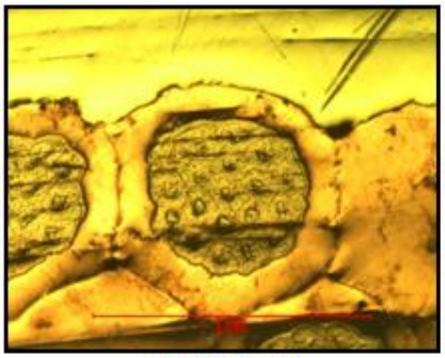

TF-WC1-NI

North Location Sleeve/Sample interface

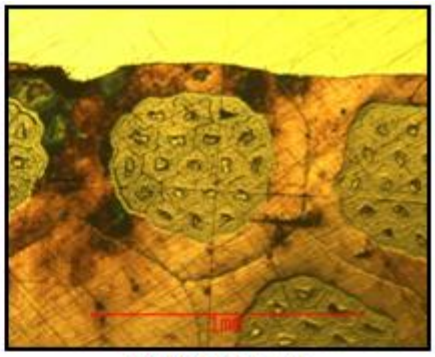

TF-WOC1-NI

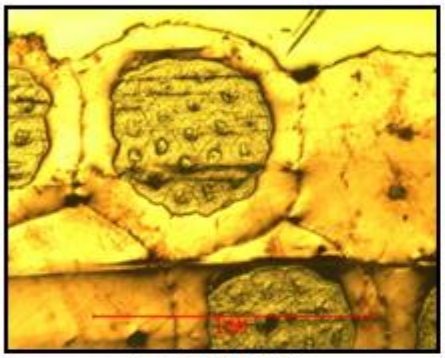

TF-WC1-N1

North Location Position 1

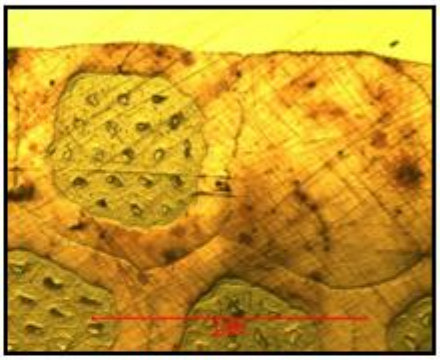

TF-WOC1-N1

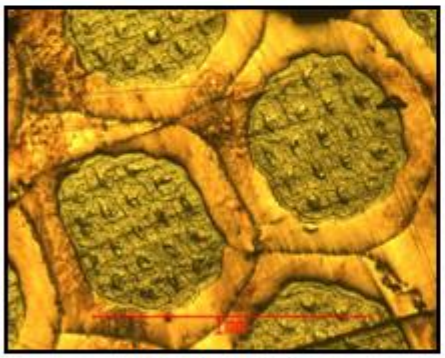

TF-WC1-N2

North Location Position 2

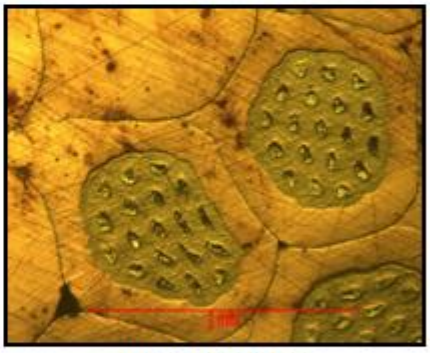

TF-WOC1-N2

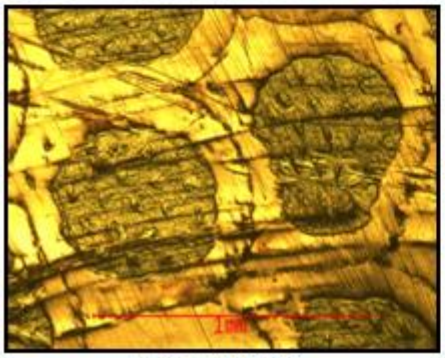

TF-WC1-N3

North Location Position 3

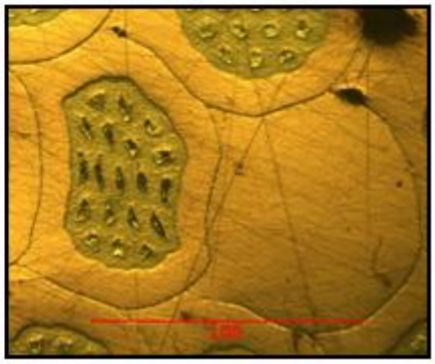

TF-WOC1-N3

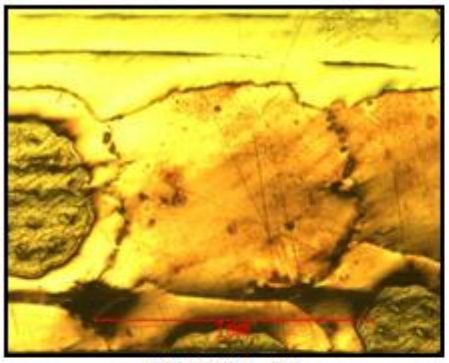

TF-WC1-EI

East Location Sleeve/Sample interface

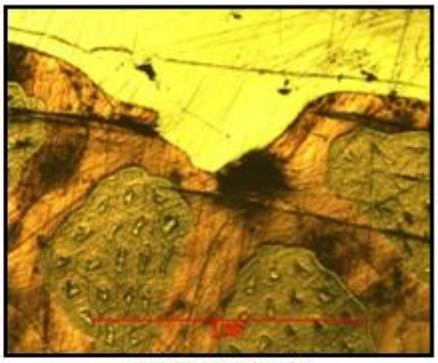

TF-WOC1-EI

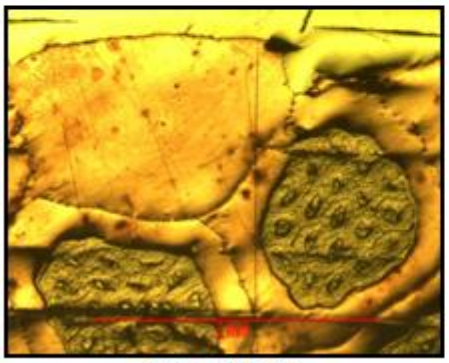

TF-WC1-E1

East Location Position 1

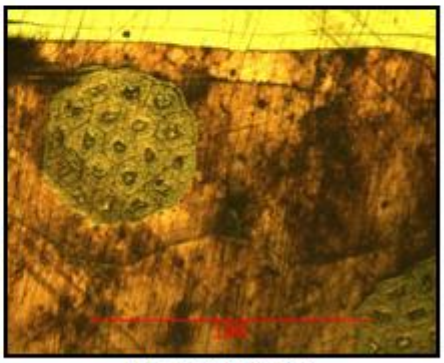

TF-WOC1-E1

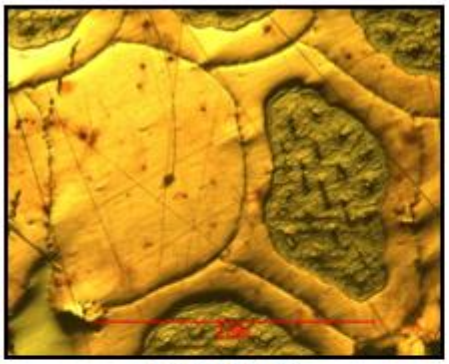

TF-WC1-E2

East Location Position 2

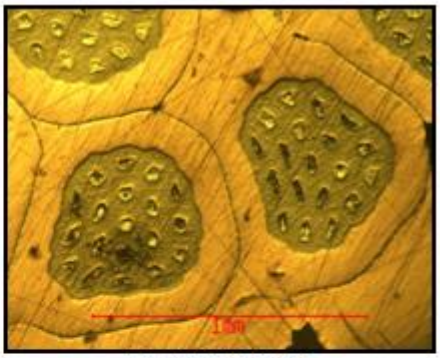

TF-WOC1-E2

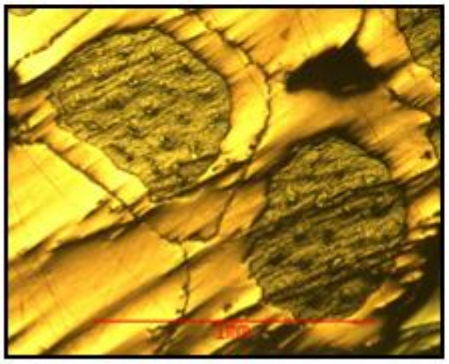

TF-WC1-E3

East Location Position 3

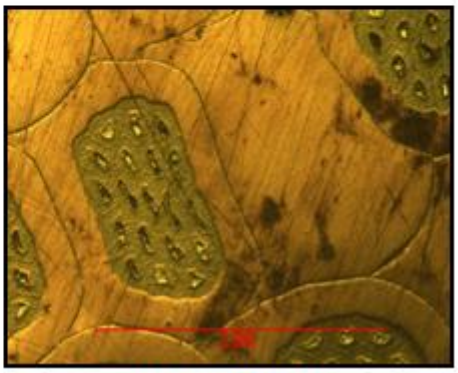

TF-WOC1-E3

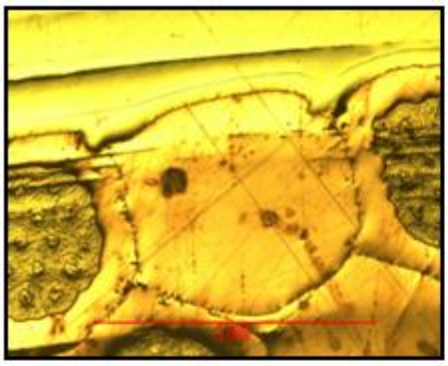

TF-WC1-SI

South Location Sleeve/Sample interface

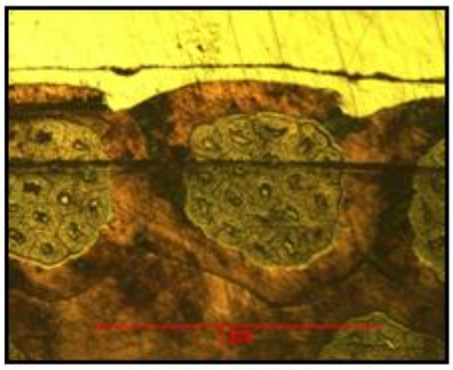

TF-WOC1-SI

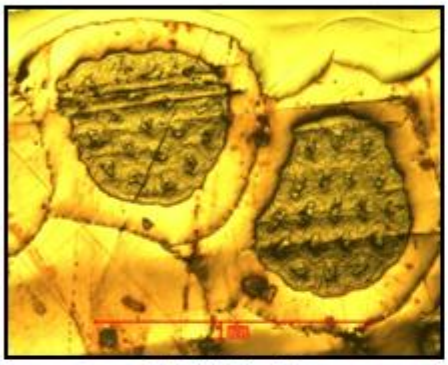

TF-WC1-S1

South Location Position 1

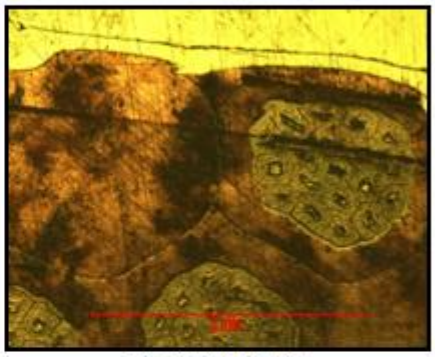

TF-WOC1-S1

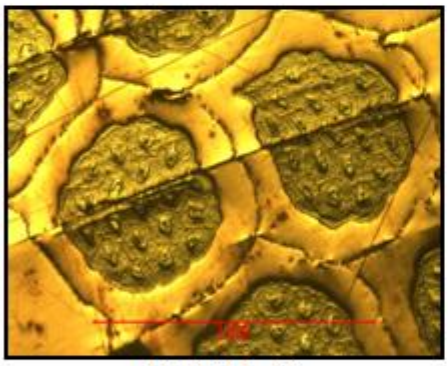

TF-WC1-S2

South Location Position 2

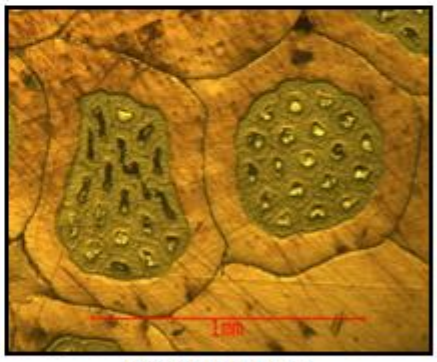

TF-WOC1-S2

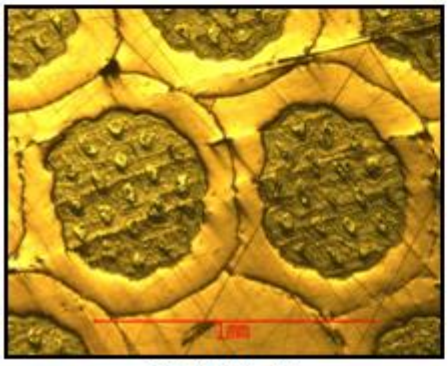

TF-WC1-S3

South Location Position 3

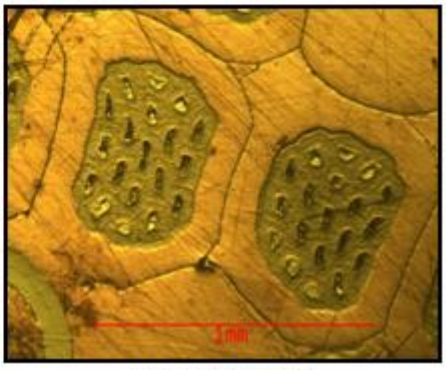

TF-WOC1-S3

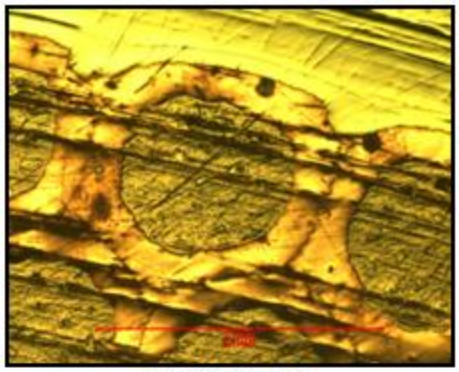

TF-WC1-WI

West Location Sleeve/Sample interface

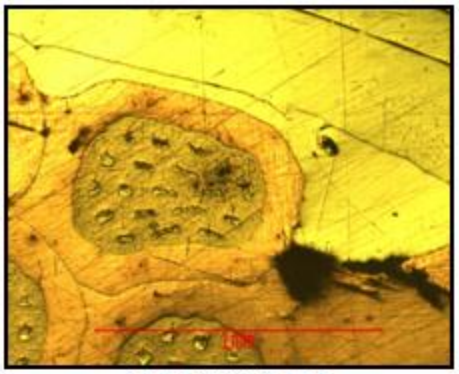

TF-WOC1-WI

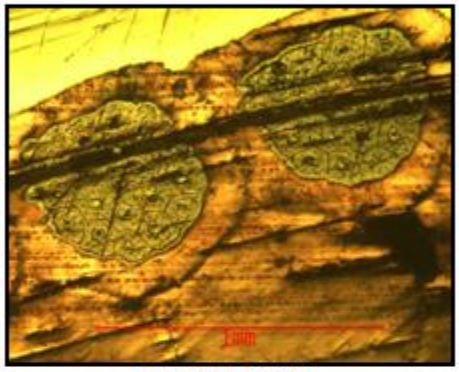

TF-WC1-W1

West Location Position 1

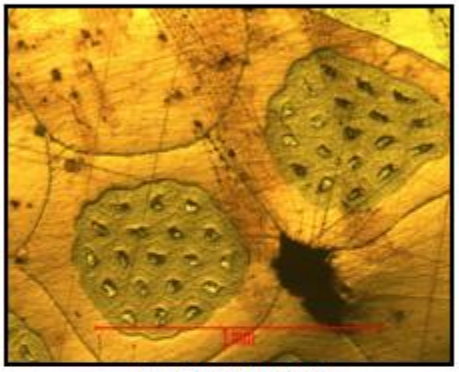

TF-WOC1-W1

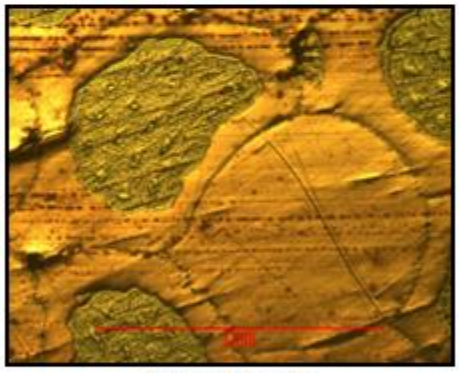

TF-WC1-W2

West Location Position 2

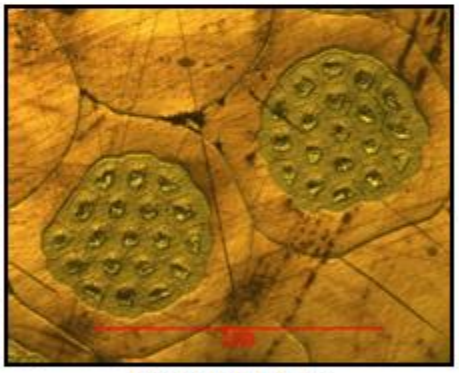

TF-WOC1-W2

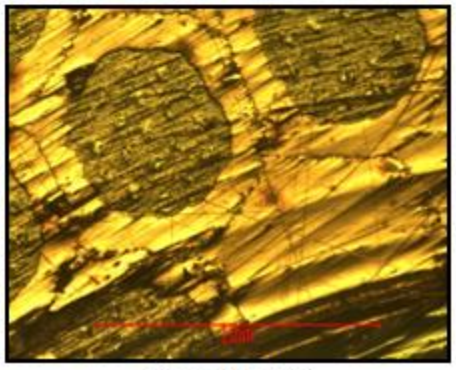

TF-WC1-W3

West Location Position 3

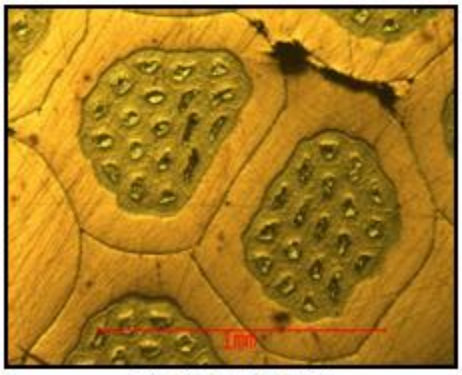

TF-WOC1-W3

Appendix B

Lower: 6,800 lbf

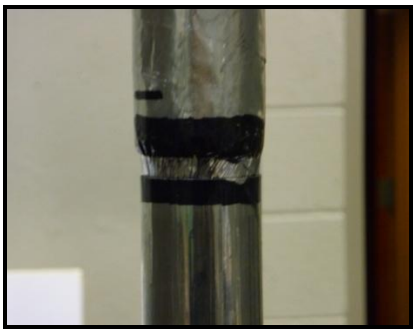

Lower: 16,250 lbf

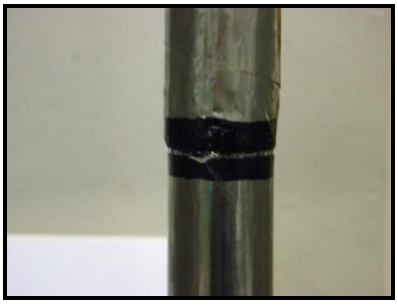

Lower: 11,500 lbf

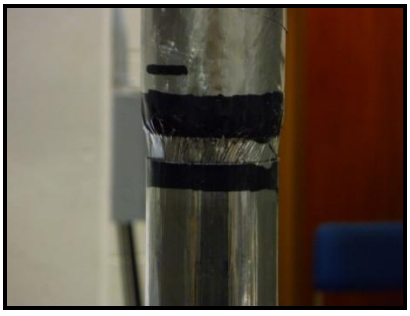

Lower: 17,125 lbf

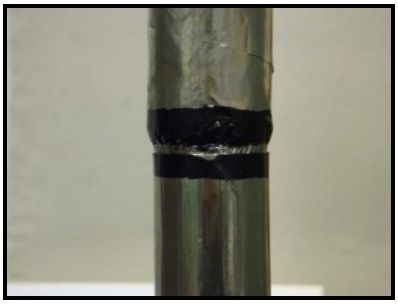

Lower: 12,800 lbf

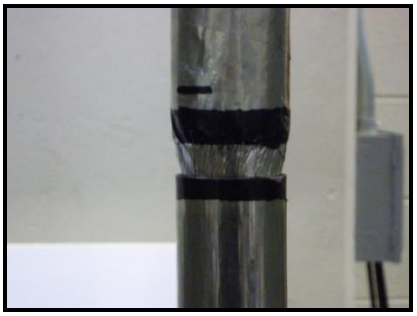

Lower: 18,750 lbf

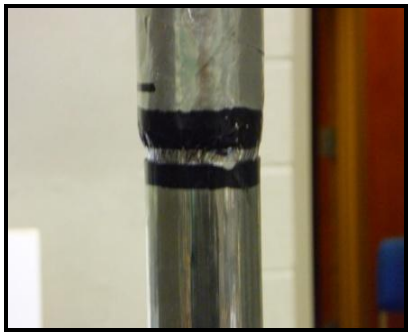

Lower: 13,800 lbf

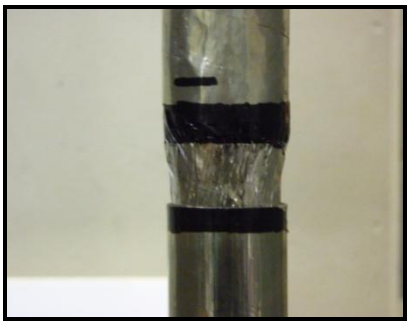

Lower: 19,000 lbf

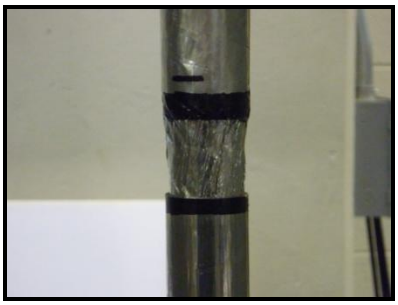

Lower: 18,750 lbf

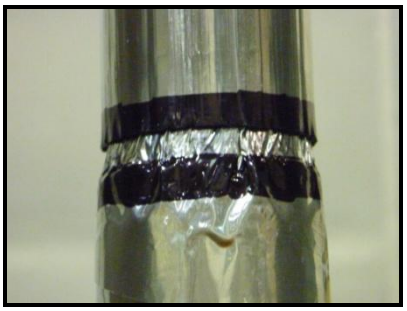

Upper: 15,350 lbf

Lower: 18,100 lbf

Upper: 16,250 lbf

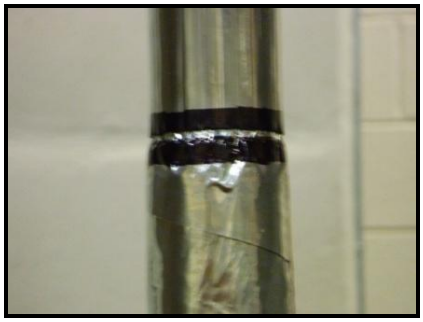

Upper: 12,500 lbf

Upper: 17,500 lbf

Upper: 13,250 lbf

Upper: 18,050 lbf

Upper: 18,300 lbf

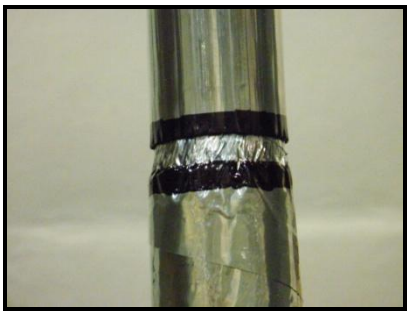

Upper: 19,200 lbf

VITA

Paul Michael Hayes was born on May 24, 1985 in Knoxville, Tennessee. He was raised in Knoxville, Tennessee where he attended Cedar Bluff Primary, Middle, and Intermediate for grades K-8, and went to high school at Bearden High School. He graduated in 2003 and began college that fall at the University of Tennessee in Knoxville. After pursuing a Logistics degree for two years, he changed majors to Mechanical Engineering and graduated in May of 2009 with his Bachelor of Science in Mechanical Engineering. During his undergraduate studies, Paul worked at Imagepoint, Inc. as an engineering designer. He began his graduate studies in May 2009 in Mechanical Engineering with a concentration on machine design. He worked as a research assistant to Dr. Madhu S. Madhukar at the Magnet Development Laboratory in collaboration with the University of Tennessee and the Oak Ridge National Laboratory. He will be graduating in December 2010 with his Masters of Science in Mechanical Engineering and will begin working in January 2011 for DCP Midstream as a project engineer in Houston, Texas.